INVESTIGATION OF THE ATMOSPHERIC OZONE FORMATION POTENTIAL OF METHYL PIVALATE

Report to
ExxonMobil Chemical Company

by

William P. L. Carter, Dongmin Luo, and Irina L. Malkina

November 17, 2000

College of Engineering
Center for Environmental Research and Technology
University of California
Riverside, California 92521

00-AP-RT2R-001-FR

ABSTRACT

A series of environmental chamber experiments and computer model calculations were carried out to assess the atmospheric ozone formation potentials of methyl pivalate. The experiments consisted of determining the effects of this compound on NO oxidation, ozone formation, OH radical levels, and other measures of reactivity when added to varying simulated model photochemical smog systems. Methyl pivalate was found to slightly enhance O_3 formation under conditions most representative of the atmosphere, but to inhibit radical levels and inhibit O_3 in experiments that are sensitive to effects on radical levels. A mechanism for the atmospheric reaction for methyl pivalate was developed that is consistent with available laboratory data and current estimation methods, and that could simulate the results of these experiments after only minor adjustments of the overall nitrate yield to within its range of uncertainty. This mechanism was then incorporated in the overall SAPRC-99 mechanism and used to predict the atmospheric ozone impacts of this compound under various atmospheric conditions. The ozone formation potentials of methyl pivalate on a mass basis was found to be about 10-20% that of the mixture used to represent reactive VOC emissions from all sources. Its ozone formation potentials were found to be very similar to those of ethane, the compound used by the EPA as the basis for determining exemptions of compounds from regulation as ozone precursors.

ACKNOWLEDGEMENTS

The authors acknowledge Mr. Dennis Fitz for assistance in administering this program, Mr. Kurt Bumiller with assistance in carrying out the environmental chamber experiments, and Dr. Roger Atkinson for helpful discussions.

Although this work was funded by ExxonMobil Chemical Company, the opinions and conclusions expressed in this report are entirely those of the primary author, Dr. William P. L. Carter. Mention of trade names or commercial products do not constitute endorsement or recommendation for use.

TABLE OF CONTENTS

LIST OF TABLES

LIST OF FIGURES

INTRODUCTION

Ozone in photochemical smog is formed from the gas-phase reactions of volatile organic compounds (VOCs) and oxides of nitrogen (NO_x) in sunlight. Although Houston and Los Angeles currently have the worst ozone problems in the United States, other areas of the country also have episodes where ozone exceeds the federal air quality standard. Ozone control strategies in the past have focused primarily on VOC controls, though the importance of NO_x control has become recognized in recent years. VOC and NO_x controls have differing effects on ozone formation. NO_x is required for ozone formation, and if the levels of NO_x are low compared to the levels of reactive VOCs, then changing VOC emissions will have relatively little effect on ozone. Since NO_x is removed from the atmosphere more rapidly than VOCs, ozone in areas far downwind from the primary sources tend to be more NO_x limited, and thus less responsive to VOC controls. VOC controls tend to reduce the rate that O_3 is formed when NO_x is present, so VOC controls are the most beneficial in reducing O_3 in the urban source areas, where NO_x is relatively plentiful, and where O_3 yields are determined primarily by how rapidly it is being formed. Because of this, any comprehensive ozone control strategy should involve reduction of emissions of both NO_x and VOCs.

Many different types of VOCs are emitted into the atmosphere, each reacting at different rates and having different mechanisms for their reactions. Because of this, they can differ significantly in their effects on ozone formation, or their “reactivity”. Some compounds, such as CFCs, do not react in the lower atmosphere at all, and thus make no contribution to ground-level ozone formation. Others, such as methane, react and contribute to ozone formation, but react so slowly that their practical effect on ozone formation in urban atmospheres is negligible. Obviously, it does not make sense to regulate such compounds as ozone precursors. In recognition of this, the EPA has exempted certain compounds from such regulations on the basis of having “negligible” effects on ozone formation. Although the EPA has no formal policy on what constitutes “negligible” reactivity, in practice it has used the ozone formation potential of ethane as the standard in this regard. Therefore, the ozone formation potential of a compound relative to ethane is of particular interest when assessing whether it might be a likely candidate for exemption from regulation as an ozone precursor.

Many VOCs that would not be judged to have “negligible” reactivity under the current criterion might still have much lower ozone formation potential than average, and substituting emissions of highly reactive VOCs with such moderate-to-low reactivity VOCs would be expected to result in air quality improvements. Although the current EPA policies do not encourage such substitutions, it has been proposed to implement reactivity-based policies on a voluntary basis in consumer product regulations in California (CARB, 1999), and the EPA is currently re-evaluating its reactivity-based VOC policies (Dimitriades, 1999, RRWG, 1999). Mc.Bride et al (1997) showed that adopting reactivity-based VOC control policies could result in significant cost savings in ozone reduction strategies, though a number of difficult policy and enforcement issues need to be resolved (RRWG, 1999). Although regulatory approaches that appropriately deal with differences in VOC reactivity are still evolving, it is clear that producers of solvent VOCs will need to know how their VOCs might be classified under any such system, so they can appropriately adapt to reactivity-based policies once they are implemented. This requires an ability to reliably estimated the ozone impacts of the VOCs of interest.

Methyl pivalate, $CH_3OC(O)C(CH_3)_3$, is a compound produced by ExxonMobil Chemical Company that has a potential market for many solvent applications. If this compound were to be shown to have sufficiently low ozone reactivity that it can be exempted from regulation as an ozone precursor, its market as a replacement solvent would be significantly enhanced. An initial modeling assessment suggested that this might be the case (Carter, unpublished results). Because of this Exxon Chemical Company (now ExxonMobil) contracted the College of Engineering Center for Environmental Research and Technology (CE-CERT) to carry out the experimental and modeling study needed to provide more definitive evidence in this regard. This involves conducting environmental chamber experiments to determine the effects of the compound on O_3 formation and other measures of air quality under various conditions, and then using the results to determine if current estimated mechanisms for this compound can appropriately predict its atmospheric impact. Once its predictive capability is established, the mechanism can then be used in model calculations to determine its ozone impacts under various atmospheric conditions. The results can then be compared for the ozone impacts calculated for ethane under those same conditions, to determine if methyl pivalate has sufficiently low ozone impact under the standards currently used by the EPA to be exempted from regulation as an ozone precursor. The results of this study are documented in this report.

EXPERIMENTAL AND DATA ANALYSIS METHODS

Overall Experimental Approach

Most of the environmental chamber experiments for this program consisted of measurements of "incremental reactivities" of methyl pivalate under various conditions. These involve two types of irradiations of model photochemical smog mixtures. The first is a "base case" experiment where a mixture of reactive organic gases (ROGs) representing those present in polluted atmospheres (the "ROG surrogate") is irradiated in the presence of oxides of nitrogen (NO_x) in air. The second is the "test" experiment that consists of repeating the base case irradiation except that the VOC whose reactivity is being assessed is also added. The differences between the results of these experiments provide a measure of the atmospheric impact of the test compound, and the difference relative to the amount added is a measure of its reactivity. To provide data concerning the reactivities of the test compound under varying atmospheric conditions, three types of base case experiments were carried out:

<u>Mini-Surrogate Experiments</u>. This base case employs a simplified ROG surrogate and relatively low ROG/NO_x ratios. Low ROG/NO_x ratios represent "maximum incremental reactivity" (MIR) conditions, which are most sensitive to VOC effects. This is useful because it provides a sensitive test for the model, and also because it is most important that the model correctly predict a VOC's reactivity under conditions where the atmosphere is most sensitive to the VOCs. The ROG mini-surrogate mixture employed consisted of ethene, n-hexane, and m-xylene. It consists of the following average initial concentrations (in ppm): NO: 0.30, NO_2: 0.10, n-hexane: 0.50, ethene: 0.85, and m-xylene: 0.14. This surrogate was employed in our previous studies (Carter et al, 1993; 1995a-c, 1997, 2000a), and was found to provide a more sensitive test of the mechanism than the more complex surrogates that more closely represent atmospheric conditions (Carter et al, 1995b). This high sensitivity to mechanistic differences makes the mini-surrogate experiments most useful for mechanism evaluation.

<u>Full Surrogate Experiments</u>. This base case employed a more complex ROG surrogate under somewhat higher, though still relatively low, ROG/NO_x conditions. While less sensitive to the mechanism employed, experiments with a more representative ROG surrogate are needed to evaluate the mechanism under conditions that more closely resembling the atmosphere. The ROG surrogate employed was the same as the 8-component "lumped molecule" surrogate employed in our previous study (Carter et al. 1995b. Calculations have indicated that use of this 8-component mixture will give essentially the same results in incremental reactivity experiments as actual ambient mixtures (Carter et al. 1995b). It consists of the following average initial concentrations, in ppm: NO: 0.25, NO_2: 0.05, n-butane: 0.40, n-octane: 0.10, ethene: 0.07, propene: 0.06, trans-2-butene: 0.06, toluene: 0.09, m-xylene 0.09, and formaldehyde: 0.10.

<u>Full Surrogate, low NO_x Experiments</u>. This base case employing the same 8-component "lumped molecule" surrogate as the full surrogate experiments described above, except that lower NO_x levels (higher

ROG/NO_x ratios) were employed to represent NO_x-limited conditions. Such experiments are necessary to assess the ability of the model to properly simulate reactivities under conditions where NO_x is low. The initial ROG and NO_x reactant concentrations were comparable to those employed in our previous studies (Carter et al. 1995b, 1997, 2000a). The initial concentrations are the same as above except for 0.06 ppm of NO and 0.03 ppm of NO_2.

An appropriate set of control and characterization experiments necessary for assuring data quality and characterizing the conditions of the runs for mechanism evaluation were also carried out. These are discussed where relevant in the results or modeling methods sections (see also Carter et al, 1995c, 2000a).

Environmental Chamber

All experiments for this program were carried out using the CE-CERT "Dividable Teflon Chamber" (DTC) with a blacklight light source. This consists of two ~6000-liter 2-mil heat-sealed FEP Teflon reaction bags located adjacent to each other and fitted inside an 8' x 8' x 8' framework, and which uses two diametrically opposed banks of 32 Sylvania 40-W BL black lights as the light source. The lighting system in the DTC was found to provide so much intensity that only half the lights were used for irradiation. The air conditioner for the chamber room was turned on before and during the experiments. Four air blowers that are located in the bottom of the chamber were used to help cool the chamber as well as mix the contents of the chamber. The CE-CERT DTC is very similar to the SAPRC DTC which is described in detail elsewhere (Carter et al, 1995b,c).

The blacklight light source has the advantage of being relatively inexpensive to operate and provides a reasonably good simulation of natural sunlight in the region of the spectrum that is important in affecting most photolysis reactions of importance for non-aromatic VOCs (Carter et al, 1995c,d). This is therefore appropriate for studies of reactivities of compounds, such as methyl pivalate, which are not photoreactive or believed to form significant yields of photoreactive products whose action spectra are not well characterized.

The DTC is designed to allow simultaneous irradiations of experiments with and without added test reactants under the same reaction conditions. Since the chambers are actually two adjacent FEP Teflon reaction bags, two mixtures can be simultaneously irradiated using the same light source and with the same temperature control system. These two reaction bags are referred to as the two "sides" of the chambers (Side A and Side B) in the subsequent discussion. The sides are interconnected with two ports, each with a box fan, which rapidly exchange their contents to assure that base case reactants have equal concentrations in both sides. In addition, a fan is located in each of the reaction bags to rapidly mix the reactants within each chamber. The ports connecting the two reactors can then be closed to allow separate injections on each side, and separate monitoring of each side.

Experimental Procedures

The reaction bags were flushed with dry air produced by an AADCO air purification system for 14 hours (6pm-8am) on the nights before experiments. The continuous monitors were connected prior to reactant injection and the data system began logging data from the continuous monitoring systems. The reactants were injected as described below (see also Carter et al, 1993, 1995c). The common reactants were injected in both sides simultaneously using a three-way (one inlet and two outlets connected to side A and B respectively) bulb of 2 liters in the injection line and were well mixed before the chamber was divided. The contents of each side were blown into the other using two box fans located between them. Fans were used to mix the reactants in the chamber during the injection period, but these were turned off prior to the irradiation. The sides were then separated by closing the ports that connected them, after turning all the fans off to allow their pressures to equalize. After that, reactants for specific sides (the test compound in the case of reactivity experiments) were injected and mixed. After the run, the contents of the chamber were emptied by allowing the bags to collapse, and then the chamber was flushed with purified air. The contents of the reactors were vented into a fume hood.

The procedures for injecting the various types of reactants were as follows. The NO and NO_2 were prepared for injection using a high vacuum rack. Known pressures of NO, measured with MKS Baratron capacitance manometers, were expanded into Pyrex bulbs with known volumes, which were then filled with nitrogen (for NO) or oxygen (for NO_2). The contents of the bulbs were then flushed into the chamber with nitrogen. The gaseous reactants were prepared for injection either using a high vacuum rack or a gas-tight syringes whose amounts were calculated to achieve the desired concentrations in the chamber. Sufficiently volatile liquid reactants (which included methyl pivalate and liquid surrogate components used in this study) were injected using a micro syringe into a 1-liter Pyrex bulb equipped with stopcocks on each end and a port for the injection of the liquid. Then one end of the bulb was attached to the injection port of the chamber and the other to a nitrogen source. The stopcocks were then opened, and the contents of the bulb were flushed into the chamber with a combination of nitrogen and heat gun for approximately 5 minutes. Formaldehyde was prepared in a vacuum rack system by heating paraformaldehyde in an evacuated bulb until the pressure corresponded to the desired amount of formaldehyde. The bulb was then closed and detached from the vacuum system and its contents were flushed into the chamber with dry air through the injection port.

Analytical Methods

Ozone and nitrogen oxides (NO_x) were continuously monitored using commercially available continuous analyzers with Teflon sample lines inserted directly into the chambers. The sampling lines from each side of the chamber were connected to solenoids that switched from side to side every 10 minutes, so the instruments alternately collected data from each side. Ozone was monitored using a Dasibi 1003-AH UV photometric ozone analyzer and NO and total oxides of nitrogen (including organic nitrates and perhaps HNO_3) were monitored using a Teco Model 42 chemiluminescent NO/NO_x monitor. The output of these instruments, along with that from the temperature sensors and the formaldehyde instrument, were attached to a computer data acquisition system, which recorded the data at 10 minutes intervals for ozone, NOx and temperature (and at 15 minutes for formaldehyde), using 30 second averaging times. This yielded a sampling interval of 20 minutes for taking data from each side.

The Teco instrument and Dasibi CO analyzer were calibrated prior to each experiment using a certified NO and CO source and CSI 1700 gas-phase titration calibrator. The Dasibi ozone analyzer was calibrated against a transfer standard ozone analyzer using transfer standard method in an interval of three months and was checked with CSI ozone generator for each experiment to assure that the instrument worked properly. The details were discussed elsewhere (Carter et al, 1995c)

Organic reactants other than formaldehyde were measured by gas chromatography with FID detection as described elsewhere (Carter et al. 1993; 1995c). GC samples were taken for analysis at intervals from 20 minutes to 30 minutes either using 100 ml gas-tight glass syringes or by collecting the 100 ml sample from the chamber onto Tenax-GC solid adsorbent cartridge. These samples were taken from ports directly connected to the chamber after injection and before irradiation and at regular intervals after irradiation was started. The sampling method employed for injecting the sample onto the GC column depended on the volatility or “stickiness” of the compound. For analysis of the more volatile species, which includes methyl pivalate and all the other organic compounds monitored in this study, the contents of the syringe were flushed through a 10 ml and 5 ml stainless steel or 1/8' Teflon tube loop and subsequently injected onto the column by turning a gas sample valve.

The calibrations for the GC analyses for most compounds were carried out by sampling from chambers or vessels of known volume into which known amounts of the reactants were injected, as described previously (Carter et al, 1995c).

Formaldehyde was monitored using an adaptation of the diffusion scrubber method developed by Dasgupta et al (1988, 1990), as described by Carter et al (1995c). It was calibrated using a formaldehyde diffusion tube whose weight loss was monitored over time. The system cycled between zero, calibrate, and sample modes to correct for zero and span drifts.

Characterization Methods

Temperature

Three temperature thermocouples were used to monitor the chamber temperature, two of which were located in the sampling line of continuous analyzers to monitor the temperature in each side. The third one was located in the outlet of the air conditioning system used to control the chamber temperature. The temperature range in these experiments was typically 25-30 C.

Blacklight Light Source

The light intensity in the DTC chamber was monitored by periodic NO_2 actinometry experiments utilizing the quartz tube method of Zafonte et al (1977), with the data analysis method modified as discussed by Carter et al. (1995c). The results of these experiments were tracked over time, and there was a gradual decrease in light intensity over time during most of the operational lifetime of this chamber. The actinometry results around the time of these experiments were fit reasonably well by a straight line up to run DTC704, and this was used to determine the NO_2 photolysis rates used for modeling those runs. This line yielded an NO_2 photolysis rate of 0.163 min^{-1} for DTC694, the first DTC run for this project, and 0.161 min^{-1} for run DTC704. For runs after DTC704 the results of the actinometry experiments did not indicate a significant decline in light intensity and NO_2 photolysis rate used for modeling was the average of the experimental measurements for this period, which was 0.161min^{-1}.

The spectrum of the blacklight light source is periodically measured using a LiCor LI-1200 spectroradiometer, and found to be essentially the same as the general blacklight spectrum recommended by Carter et al (1995c) for use in modeling blacklight chamber experiments

Dilution

The dilution of the chambers due to sampling is expected to be small because the flexible reaction bags can collapse as samples are withdrawn for analysis. Also, the chambers were designed to operate under slightly positive pressure, so any small leaks would result in reducing the bag volume rather than diluting the contents of the chamber. Information concerning dilution in an experiment can be obtained from relative rates of decay of added VOCs that react with OH radicals with differing rate constants (Carter et al. 1993; 1995c). Most experiments had a more reactive compound such as m-xylene and n-octane present either as a reactant or added in trace amounts to monitor OH radical levels. Trace amounts (~0.1 ppm) of n-butane were also added to experiments if needed to provide a less reactive compound for monitoring dilution. In addition, specific dilution check experiments such as CO dark decay measurements were periodically carried out. Based on these results, the dilution rate was found to be negligible in this chamber during this period, being less than 0.3% per hour in all runs, and usually less than 0.1% per hour.

Reactivity Data Analysis Methods

As indicated above, most of the experiments for this program consisted of simultaneous irradiation of a “base case” reactive organic gas (ROG) surrogate - NO_x mixture in one of the dual reaction chambers, together with an irradiation, in the other reactor, of the same mixture with the test compound added. The results are analyzed to yield two measures of VOC reactivity: the effect of the added VOC on the amount of NO reacted plus the amount of ozone formed, and integrated OH radical levels. These are discussed in more detail below.

The first measure of reactivity is the effect of the VOC on the change in the quantity $[O_3]$-[NO], or $\Delta([O_3]$-[NO]). As discussed elsewhere (e.g., Johnson, 1983; Carter and Atkinson, 1987; Carter and Lurmann, 1990, 1991, Carter et al, 1993, 1995a), this gives a direct measure of the amount of conversion of NO to NO_2 by peroxy radicals formed in the photooxidation reactions, which is the process that is directly responsible for ozone formation in the atmosphere. (Johnson calls it "smog produced" or "SP".) The incremental reactivity of the VOC relative to this quantity, which is calculated for each hour of the experiment, is given by

$$\mathrm{IR}[\Delta([\mathrm{O}_3]-[\mathrm{NO}])_t^{\mathrm{VOC}}] = \frac{\Delta([\mathrm{O}_3]-[\mathrm{NO}])_t^{\mathrm{Test}} - \Delta([\mathrm{O}_3]-[\mathrm{NO}])_t^{\mathrm{Base}}}{[\mathrm{VOC}]_0} \qquad \text{(I)}$$

where $\Delta([O3]\text{-}[NO])_t^{Test}$ is the $\Delta([O_3]$-[NO]) measured at time t from the experiment where the test VOC was added, $\Delta([O3]\text{-}[NO])_t^{Base}$ is the corresponding value from the corresponding base case run, and $[VOC]_0$ is the amount of test VOC added. An estimated uncertainty for IR[$\Delta([O_3]$-[NO])] is derived based on assuming an ~3% uncertainty or imprecision in the measured $\Delta([O_3]$-[NO]) values. This is consistent with the results of the side equivalency test, where equivalent base case mixtures are irradiated on each side of the chamber.

Note that reactivity relative to Δ([O3]-[NO]) is essentially the same as reactivity relative to O_3 in experiments where O_3 levels are high, because under such conditions $[NO]_t^{base}$. $[NO]_t^{test}$. 0, so a change in Δ([O3]-[NO]) caused by the test compound is due to the change in O_3 alone. However, Δ([O3]-[NO]) reactivity has the advantage that it provides a useful measure of the effect of the VOC on processes responsible for O_3 formation even in experiments where O_3 formation is suppressed by relatively high NO levels.

The second measure of reactivity is the effect of the VOC on integrated hydroxyl (OH) radical concentrations in the experiment, which is abbreviated as "IntOH" in the subsequent discussion. This is an important factor affecting reactivity because radical levels affect how rapidly all VOCs present, including the base ROG components, react to form ozone. If a compound is present in the experiment that reacts primarily with OH radicals, then the IntOH at time t can be estimated from

$$\mathrm{IntOH}_t = \frac{\ln([\mathrm{tracer}]_0/[\mathrm{tracer}]_t) - \mathrm{D}t}{\mathrm{kOH}^{\mathrm{tracer}}} \qquad \text{(II)}$$

where $[tracer]_0$ and $[tracer]_t$ are the initial and time=t concentrations of the tracer compound, kOH^{tracer} its OH rate constant, and D is the dilution rate in the experiments. The latter was found to be small and was neglected in our analysis. The concentration of tracer at each hourly interval was determined by linear interpolation of the experimentally measured values. M-xylene was used as the OH tracer in these experiments because it is a surrogate component present in all experiments, its OH rate constant is known (the value used was 2.36×10^{-11} cm^3 $molec^{-1}$ s^{-1} [Atkinson, 1989]), and it reacts relatively rapidly.

The effect of the VOC on OH radicals can thus be measured by its IntOH incremental reactivity, which is defined as

$$\mathrm{IR[IntOH]_t} = \frac{\mathrm{IntOH_t^{Test}} - \mathrm{IntOH_t^{Base}}}{\mathrm{[VOC]_0}} \qquad \text{(III)}$$

where $\mathrm{IntOH^{Test}}$ and $\mathrm{IntOH^{Base}}$ are the IntOH values measured at time t in the added VOC and the base case experiment, respectively. The results are reported in units of 10^6 min. The uncertainties in IntOH and IR[IntOH] are estimated based on assuming an ~2% imprecision in the measurements of the m-xylene concentrations. This is consistent with the observed precision of results of replicate analyses of this compound.

CHEMICAL MECHANISMS AND MODELING METHODS

Chemical Mechanism

General Atmospheric Photooxidation Mechanism

The chemical mechanism used in the environmental chamber and atmospheric model simulations in this study is the SAPRC-99 mechanism that is documented in detail by Carter (2000). This mechanism represents a complete update of the SAPRC-90 mechanism of Carter (1990), and incorporates recent reactivity data from a wide variety of VOCs, including those discussed in this report. This includes assignments for ~400 types of VOCs, and can be used to estimate reactivities for ~550 VOC categories. A condensed version, developed for use in regional models, is used to represent base case emissions in the atmospheric reactivity simulations discussed in this report. A feature of this mechanism is the use of a computerized system to estimate and generate complete reaction schemes for most non-aromatic hydrocarbons and oxygenates in the presence of NO_x, from which condensed mechanisms for the model can be derived. The SAPRC-99 mechanism was evaluated against the results of almost 1700 environmental chamber experiments carried out at the University of California at Riverside, including experiments to test ozone reactivity predictions for over 80 types of VOCs. This also includes experiments discussed in this report.

A listing of the mechanism as used in the model simulations in this report is given in Appendix A. This consists of the "base mechanism" representing the reactions of the inorganics and common organic products, the reactions of the specific VOCs used in the environmental chamber experiments, and the reactions of the lumped model species used when representing base case VOCs in the ambient reactivity simulations. The report of Carter (2000) should be consulted for a more detailed discussion of these portions of the mechanism. The mechanism used for methyl pivalate discussed below. Note that although the report of Carter (2000) included a mechanism for methyl pivalate, some minor modifications were made to the methyl pivalate mechanism used this work because of new data and other considerations.

Atmospheric Reactions of Methyl Pivalate

The major gas-phase atmospheric loss process for methyl pivalate and other esters is expected to be reaction with OH radicals. Based on available information for related compounds, reaction of esters with NO_3 radicals (Atkinson, 1991) and O_3 (Atkinson and Carter, 1984; Atkinson, 1994) are expected to be unimportant. The possibility of photolysis can be ruled out on the basis of the absorption cross section data given by Calvert and Pitts (1977), and absorption cross section measurements made by Wallington et al (2000) for methyl pivalate.

The rate constant for the reaction of OH radicals with methyl pivalate has recently been measured by Orkin and co-workers (Wallington et al, 2000), and a non-Arrhenius temperature dependence was observed. The rate constants as a function of temperature were as follows:

Temperature (^oK)	k (10^{-12} cm^3 $molec^{-1}$ s^{-1})
250	1.39 ± 0.02
272	1.21 ± 0.02
298	1.18 ± 0.02
330	1.23 ± 0.01
370	1.37 ± 0.02

where the error bars reflect the precision of the data and do not include an estimated systematic uncertainty of 4%. The reason for this complex temperature dependence is uncertain, but it should be noted that a similar non-Arrhenius temperature dependence has been observed for the reaction of OH radicals with acetone (Wollenhaupt et al, 2000). Wallington et al (2000) attribute this to possible complex formation between the OH radical and the carbonyl group. In any case, the temperature variation in the 272-330 K range is small (less than 3% variation between minimum and maximum), and for this work we ignore the small temperature dependence in the ambient temperature range and use the 298 K value of

$$k\ (OH + \text{methyl pivalate}) = 1.18 \times 10^{-12}\ cm^3\ molec^{-1}\ s^{-1}.$$

No other measurements of this rate constant have been reported in the literature, though a qualitative measurement of ~1.3×10^{-12} cm^3 $molec^{-1}$ s^{-1} made in our laboratory using a relative rate technique (unpublished results from our laboratory) is consistent with this. This is about 60% higher than the rate constant estimated using the group additivity methods of Kwok and Atkinson (1995), though this is within the uncertainty range of this estimation method.

The products of the reactions of OH radicals with methyl pivalate have recently been determined by Wallington et al (2000), who observed acetone formation in 51 ± 6% yields. Methyl nitrite was used as the radical source, so the formaldehyde yield could not be determined because it is also formed from methyl nitrite. Essentially the same acetone yield (54 ± 4%) was observed in the reactions of Cl atoms with methyl pivalate in the presence of NO_x, where the mechanisms is expected to be similar. Formaldehyde, CO, CO_2, and $CH_3C(O)OONO_2$ were also observed to be formed in the product study of the Cl reaction in the presence of NO_x, but quantitative yields were not given. In addition, an upper limit of 7% was given for the formation of methyl pyruvate, $CH_3C(O)C(O)OCH_3$, and infrared bands corresponding to unidentified organic nitrate products were observed. Based on literature IR absorption cross sections for other organic nitrates, Wallington et al (2000) estimated an approximate 25% yield of unidentified organic nitrate products.

The expected mechanism for the reactions of OH radicals with methyl pivalate are shown on Table 1, which also gives the branching ratios and relative contributions of each reaction that are used as the basis for the mechanism derived for the model calculations in this work. Footnotes indicate the

Table 1. Detailed mechanism for the reactions of methyl pivalate with OH radicals in the presence of NO_x. Predicted products are shown in bold font.

	Reaction with OH [a]	Notes [b]	Branching [c]	
			Rxn	Total
	$CH_3C(CH_3)(CH_3)C(O)OCH_3$			
1	$+ OH \rightarrow H_2O + CH_3C(CH_3)(CH_2\cdot)C(O)OCH_3$	1	75%	75%
2	$+ OH \rightarrow H_2O + CH_3C(CH_3)(CH_3)C(O)OCH_2\cdot$	1	25%	25%
	<u>Radicals formed from reaction at t-butyl end</u>			
3	$CH_3C(CH_3)(CH_2\cdot)C(O)OCH_3 + O_2 \rightarrow CH_3C(CH_3)(CH_2OO\cdot)C(O)OCH_3$			75%
	$CH_3C(CH_3)(CH_2OO\cdot)C(O)OCH_3$			
4	$+ NO \rightarrow \mathbf{CH_3OC(O)C(CH_3)(CH_3)CH_2ONO_2}$	2	13%	10%
5	$+ NO \rightarrow NO_2 + CH_3C(CH_3)(CH_2O\cdot)C(O)OCH_3$	2	87%	65%
	$CH_3C(CH_3)(CH_2O\cdot)C(O)OCH_3$			
6	$+ O_2 \rightarrow \mathbf{CH_3C(CH_3)(CHO)C(O)OCH_3} + HO_2\cdot$	3	5%	3%
7	$\rightarrow \mathbf{HCHO} + CH_3C(\cdot)(CH_3)C(O)OCH_3$	3	95%	62%
8	$CH_3C(\cdot)(CH_3)C(O)OCH_3 + O_2 \rightarrow CH_3C(OO\cdot)(CH_3)C(O)OCH_3$			62%
	$CH_3C(OO\cdot)(CH_3)C(O)OCH_3$			
9	$+ NO \rightarrow \mathbf{CH_3C(CH_3)(ONO_2)C(O)OCH_3}$	4	6%	4%
10	$+ NO \rightarrow NO_2 + CH_3C(O\cdot)(CH_3)C(O)OCH_3$	4	94%	58%
	$CH_3C(O\cdot)(CH_3)C(O)OCH_3$			
11	$\rightarrow \mathbf{CH_3C(O)CH_3} + CH_3OC(O)\cdot$	3	86%	50%
12	$\rightarrow CH_3C(CH_3)(OH)C(O)OCH_2\cdot$	3	14%	8%
13	$CH_3OC(O)\cdot + O_2 \rightarrow CH_3OC(O)OO\cdot$			50%
	$CH_3OC(O)OO\cdot$			
14	$+ NO_2 \rightarrow \mathbf{CH_3OC(O)OONO_2}$	5	[d]	$\leq$50%
15	$+ NO \rightarrow NO_2 + CH_3OC(O)O\cdot$	5	[d]	$\leq$50%
16	$CH_3OC(O)OONO_2 \rightarrow CH_3OC(O)OO\cdot + NO_2$	5		$\leq$50%
17	$CH_3OC(O)O\cdot \rightarrow CO_2 + CH_3O\cdot$	6		$\leq$50%
18	$CH_3O\cdot + O_2 \rightarrow HCHO + HO_2$			$\leq$50%
19	$CH_3C(CH_3)(OH)C(O)OCH_2\cdot + O_2 \rightarrow CH_3C(CH_3)(OH)C(O)OCH_2OO\cdot$			8%
	$CH_3C(CH_3)(OH)C(O)OCH_2OO\cdot$			
20	$+ NO \rightarrow NO_2 + CH_3C(CH_3)(OH)C(O)OCH_2O\cdot$	7	94%	8%
21	$+ NO \rightarrow CH_3C(CH_3)(OH)C(O)OCH_2ONO_2$	7	6%	$<$1%
	$CH_3C(CH_3)(OH)C(O)OCH_2O\cdot$			
21	$+ O_2 \rightarrow \mathbf{CH_3C(CH_3)(OH)C(O)OCHO} + HO_2\cdot$	3	34%	3%
22	$\rightarrow \mathbf{CH_3C(CH_3)(OH)C(O)OH} + HCO\cdot$	8	66%	5%
23	$HCO\cdot + O_2 \rightarrow CO + HO_2\cdot$			19%
	<u>Radicals formed from reaction at methoxy end</u>			
24	$CH_3C(CH_3)(CH_3)C(O)OCH_2\cdot + O_2 \rightarrow CH_3C(CH_3)(CH_3)C(O)OCH_2OO\cdot$			25%
	$CH_3C(CH_3)(CH_3)C(O)OCH_2OO\cdot$			
25	$+ NO \rightarrow \mathbf{CH_3C(CH_3)(CH_3)C(O)OCH_2ONO_2}$	2	13%	3%
26	$+ NO \rightarrow NO_2 + CH_3C(CH_3)(CH_3)C(O)OCH_2O\cdot$		87%	22%

Table 1 (continued)

Reaction with OH [a]		Notes [b]	Branching [c] Rxn	Total
	$CH_3C(CH_3)(CH_3)C(O)OCH_2O\cdot$			
27	$+ O_2 \rightarrow$ **$CH_3C(CH_3)(CH_3)C(O)OCHO$** $+ HO_2\cdot$	3	34%	7%
28	$\rightarrow$ **$CH_3C(CH_3)(CH_3)C(O)OH$** $+ HCO\cdot$	8	66%	14%

[a] Predicted stable organic products are shown in bold font.

[b] Documentation notes for branching ratios are as follows. See Carter (2000) for details concerning the estimation methods.

1 Branching ratio derived to give a predicted acetone yield that agrees with the measured yield of Wallington et al (unpublished results, 2000), as discussed in the text. This is not significantly different from the estimated 70% branching ratio derived using the group additivity method of Kwok and Atkinson (1995).

2 The branching ratio for nitrate formation (nitrate yield) is estimated to be 10% using the procedures of Carter (2000), based on yields derived for other compounds. However, best fits to the chamber data obtained in this project are obtained if the nitrate yields for the initially formed peroxy radicals are adjusted upwards to 13% (see text).

3 Rate constants for alkoxy radical reactions estimated as discussed by Carter (2000).

4 Nitrate yield for this reaction adjusted to fit environmental chamber reactivity data for methyl isobutyrate (Carter 2000; Carter et al, 2000a).

5 Assumed to react with the same rate constants as higher acyl peroxy radicals and PAN analogue (e.g., $C_2H_4C(O)OONO_2$ and PPN). Lumped with the RCO-O2. or PAN2 model species when implemented in the SAPRC-99 mechanism.

6 This decomposition is assumed to be fast.

7 Nitrate yield estimated from nitrate yields derived for other compounds as discussed by Carter (2000).

8 The data used by Carter (2000) to estimate rate constants for "ester rearrangement" reactions had an error, so the estimation method for these reactions is revised for this work. The rate constant for this ester rearrangement reaction is estimated to be $8.0 \times 10^{10} \exp(-8.49 \text{ kcal mol}^{-1}/RT) = 5.24 \times 10^4$ s^{-1} at 300K. The A factor assumed to be approximately the same as assumed for 1,4-H-shift isomerizations, based on expected similarities in transition states, and is the same as used by Carter (2000) The activation energies are assumed to be linearly dependent on the heat of reaction, where $Ea = EaA + EaB \times \Delta H_r$, and EaA = 9.11 and EaB = 0.20 were derived to be consistent with OH + methyl acetate product yields reported by Christensen et al (2000), OH +ethyl acetate yields of Tuazon et al (1998), and results of modeling n-butyl acetate reactivity chamber experiments. Carter (2000) had an error in the assumed product yields for the OH + methyl acetate reaction, and thus the EaA and EaB parameters used there are somewhat different. The effect of this correction on estimated branching ratios for most compounds is minor, but is non-negligible for methyl pivalate.

[c] Predicted branching ratios. The "Rxn" column shows the importance of the reaction relative to the competing reactions of the species or radical. The "Total" column shows the importance of the reaction relative to the overall process.

[d] The relative importances of these reactions depend on [NO]/[NO_2] ratio.

derivations of the branching ratios that are used. It can be seen that the predicted products, shown in bold font on the table, are consistent with the product data of Wallington et al (2000).

As indicated on Table 1, most branching ratios were estimated using the mechanism estimation procedures associated with the SAPRC-99 mechanism as documented by Carter (2000). Since the report of Carter (2000) describes these estimation procedures in detail, they are not discussed further here. However, as indicated on Footnote 8 on the table, Carter (2000) had a minor error in the estimates of ester rearrangement rate constants that affects estimates for compounds such as this, and that is corrected in this work.[1] In addition, as also noted in the footnote, two adjustments were made to the estimated mechanism based on data obtained by Wallington et al (2000) and this work.

Model simulations of some of the environmental reactivity experiments are highly sensitive to the assumed nitrate yields in the reactions of peroxy radicals with NO (e.g., the ratios of rate constants for Reactions 4 and 5 and 25 and 26 on Table 1), and estimates of these rate constant ratios are highly uncertain (Carter, 2000). Therefore, for most compounds for which environmental chamber data are available and where the simulations are sensitive to these yields, the nitrate yields for the peroxy radicals formed in the initial reactions are generally adjusted to optimize the fits of model predictions to the data. As shown in the Results section, better fits to the data are obtained if nitrate yields in the reactions of NO with the initially formed peroxy radicals (i.e., Reactions 4 and 25) are assumed to be ~13% instead of the initially estimated ~10%. This is well within the ±60% uncertainty of the SAPRC-99 nitrate yield estimation method.

The mechanism derived using the SAPRC-99 estimation procedures (Carter, 2000), corrected as indicated in Footnote 8, and with the nitrate yields adjusted as indicated above, predicts that the total acetone yield of 46%. This is within the stated error limits of the 51±6% yield of Wallington et al (2000), and is in remarkably good agreement with these data given the number of uncertain rate constant estimates involved. This includes the estimate for the branching ratio for the initial OH reaction derived using the group additivity method of Kwok and Atkinson (1995). However, that estimate is clearly uncertain because this procedure gives a total rate constant that is low by 60%. Therefore, it is not inappropriate to adjust that ratio slightly so the model prediction better matches the observed acetone yields. As indicated in Footnote 1 to Table 1, this is done by assuming that reaction at the t-butyl end is slightly faster than estimated using the group additivity methods, and occurs 75% of the time rather than 70% of the time. This gives an acetone yield of ~50%, corresponding to the data of Wallington et al (2000).

In terms of model species used in the SAPRC-99 mechanism (Carter, 2000), the overall process for the reactions shown on Table 3 can be represented as follows:

---

[1] The error was due to using an incorrect branching ratio for the products of the methyl acetate + OH reactions when deriving the estimate. This significantly affects only estimates for methyl esters, where

$$OH + \text{Methyl Pivalate} \rightarrow 0.328\ RO2\text{-}R. + 0.175\ RO2\text{-}N. + 1.198\ R2O2. + 0.497\ RCO\text{-}O2. + 0.194\ CO + 0.619\ HCHO + 0.034\ RCHO + 0.497\ ACET + 0.100\ MEK + 0.194\ RCO\text{-}OH$$

Here the RO2-R. represents the formation of peroxy radicals that react to convert NO to NO_2 and form HO_2, RO2-N. represents the formation of peroxy radicals that react with NO to form organic nitrates, R2O2. represents extra NO to NO_2 conversions caused by peroxy radicals formed in multi-step mechanisms, RCO-O2. represents the lumped higher acyl peroxy radical [used for $CH_3OC(O)OO\cdot$ in this case], HCHO represents formaldehyde, RCHO represents the lumped higher aldehyde species [used for $CH_3C(CH_3)(CHO)C(O)OCH_3$], ACET represents acetone, MEK represents the lumped lower reactivity oxygenated product (used for $CH_3C(CH_3)(CH_3)C(O)OCHO$ and $CH_3C(CH_3)(OH)C(O)OCHO$), and RCO-OH represents the lumped higher organic acid (used for $CH_3C(CH_3)(CH_3)C(O)OH$ and $CH_3C(CH_3)(OH)C(O)OH$).

Modeling Methods

Environmental Chamber Simulations

The ability of the chemical mechanisms to appropriately simulate the atmospheric impacts of methyl pivalate was evaluated by conducting model simulations of the environmental chamber experiments carried out for this study. This requires including in the model appropriate representations of chamber-dependent effects such as wall reactions and characteristics of the light source. The methods used are based on those discussed in detail by Carter and Lurmann (1990, 1991), updated as discussed by Carter et al. (1995c; 1997, 2000a). The photolysis rates were derived from results of NO_2 actinometry experiments and measurements of the relative spectra of the light source. The thermal rate constants were calculated using the temperatures measured during the experiments, with the small variations in temperature with time during the experiment being taken into account. The computer programs and modeling methods employed are discussed in more detail elsewhere (Carter et al, 1995c). The specific values of the chamber-dependent parameters used in the model simulations of the experiments for this study are given in Table A-4 in Appendix A.

In the case of the methyl pivalate all model calculations used the mechanism discussed in the previous section, except for those showing the effects of using different overall methyl nitrate yields.

Atmospheric Reactivity Simulations

To estimate its effect on ozone formation under conditions more representative of polluted urban atmospheres, incremental reactivities, defined as the change in O_3 caused by adding small amounts of the compound to the emissions, were calculated for methyl pivalate, as well as for ethane and several other representative compounds. The scenarios employed are discussed in more detail later in this report, and are the same as used in our previous studies (Carter 1994a,b, 2000). The, software, and calculation

---

reactions forming this radical tend to be relatively unimportant except for the few relatively slowly reacting methyl esters such as methyl acetate and methyl pivalate.

procedures are as described by Carter (1994b), and were exactly the same as used by Carter (2000) when calculating the reactivity scale for the SAPRC-99 mechanism. The mechanism used is given in Appendix A.

EXPERIMENTAL RESULTS AND MECHANISM EVALUATION

Summary of Experiments and Characterization Results

Table 2 gives a chronological listing of all the experiments carried out for this program. These consisted primarily of the experiments with methyl pivalate, which are discussed in the next section. In addition to these, several characterization runs were carried out to determine the chamber-dependent inputs needed for the model simulations of the experiments. Table 2 summarizes the purposes and relevant results from these runs.

As indicated on Table 2, the results of most of these experiments were as expected based on our previous experience with these and similar chambers in our laboratories (Carter et al, 1995c and references therein; Carter et al, 2000a), and indicated no special problems with characterizing run conditions for mechanism evaluation. See Carter et al (2000a) for more discussion of the characterization results for these chambers during this time period, particularly with respect to light intensity and the chamber radical source. As noted on the table, some experiments were carried out following experiments where small amounts (usually less than 100 ppb) of nitrous acid was injected into the chamber, and there was initially some concern that this might affect some experiments. However, no unusual results were found in characterization tests such as n-butane - NO_x irradiations (which are sensitive to the chamber radical source) that followed such experiments.

A potentially more serious problem was a lack of side equivalency observed in the side equivalency test experiment DTC709 carried out around the end of this project. In this experiment, the same low NO_x mini-surrogate mixture was irradiated on both sides of the chamber. As indicated in Table 2, somewhat less O_3 was observed on Side B than Side A, and also the O_3 decayed more rapidly on that side once the O_3 maximum was reached. The $\Delta([O_3]\text{-}[NO])$ data and the $\Delta([O_3]\text{-}[NO])$ differences between the two sides for that experiment are shown on Figure 1. To show the bias this might introduce on the experimentally $\Delta([O_3]\text{-}[NO])$ incremental reactivities, the $\Delta([O_3]\text{-}[NO])$ differences between the two sides are also shown for the low NO_x full surrogate runs where methyl pivalate was added. It can be seen that the bias introduced is relatively small for DTC702 but may be a non-negligible factor for run DTC700, where the amount of methyl pivalate added was smaller. However, except for the last two hours of the experiment, the side differences were within the error bars given for the $\Delta([O_3]\text{-}[NO])$ incremental reactivity data. The relatively small side equivalency is not sufficient to affect the results in terms of whether the addition of methyl pivalate in these experiments enhances or inhibits $\Delta([O_3]\text{-}[NO])$ levels.

Figure 1 also shows the side differences in the IntOH data derived from the m-xylene consumption rate measurements in this side equivalency test run and also in the comparable runs with methyl pivalate added. In this case, the side equivalency appears to be reasonably good, with the IntOH changes being much less than in the added methyl pivalate runs, and within the estimated error limits.

Table 2. Chronological listing of the environmental chamber experiments carried out for this program.

Run ID	Date	Title	Comments
DTC673	6/22/98	NO_2 Actinometry	NO_2 photolysis rate measured using the quartz tube method was 0.156 min^{-1}, in good agreement with the trend observed with the other such runs.
DTC682	7/8/98	Ozone and CO dark Decay	Control run to check for leaks and measure the O_3 wall decay rate. Essentially no CO decay was observed, indicating negligible leakage. The O_3 decay rates were 1.4 x 10^{-4} min^{--1} on Side A and 1.6 x 10^{-4} min^{--1} on Side B, in excellent agreement with the value of 1.5 x 10^{-4} min^{--1} that is used when modeling these DTC runs.
DTC683	7/9/98	Propene - NO_x	Standard propene - NO_x control run for comparison with other such runs in this and other chambers. Results in normal range.
DTC684	7/13/98	NO_2 Actinometry	NO_2 photolysis rate measured using the quartz tube method was 0.160 min^{-1}, in good agreement with the trend observed with the other such runs.
	7/20 - 7/31/98	Runs for another program	Runs were carried out for other programs that involved injections of sub-ppm amounts of HONO in the chamber. Tests carried out in separate experiments indicate that this shouldn't affect the results of subsequent experiments.
	8/4 - 8/7/98	Runs for another program	
DTC694	8/12/98	Mini-Surrogate + Methyl Pivalate	Mini-surrogate reactivity experiment with 11 ppm methyl pivalate added to Side A. Results on Table 3 and Figure 2.
DTC695	8/13/98	Full Surrogate + Methyl Pivalate	High NO_x full surrogate reactivity experiment with 12 ppm methyl pivalate added to Side B. Results on Table 3 and Figure 2.
	8/14 - 8/19/98	Runs for other program	A run was carried out for another programs that involved injections of sub-ppm amounts of HONO in the chamber., following reactivity experiments for other programs.
DTC699	8/20/98	n-Butane - NO_x	Characterization run to measure the chamber radical source. The NO oxidation rates were consistent with those predicted by the standard chamber model, but the rate on Side B was slightly higher than that on Side A.
DTC700	8/21/98	Low NO_x Full Surrogate + Methyl Pivalate (A)	Low NO_x full surrogate reactivity experiment with 19 ppm methyl pivalate added to Side A. Results on Table 3 and Figure 2.
DTC701	8/26/98	Mini-Surrogate + Methyl Pivalate	Mini-surrogate reactivity experiment with 16 ppm methyl pivalate added to Side B. Results on Table 3 and Figure 2.
DTC702	8/27/98	Full Surrogate + Methyl Pivalate	High NO_x full surrogate reactivity experiment with 19 ppm methyl pivalate added to Side A. Results on Table 3 and Figure 2.
	8/28/98	Runs for another program	

Table 2 (continued)

Run ID	Date	Title	Comments
DTC704	8/31/98	NO_2 Actinometry	NO_2 photolysis rate measured using the quartz tube method was 0.165 min^{-1}, in good agreement with the trend observed with the other such runs.
	9/1/98	Run for another program	
DTC706	9/2/98	Propene - NO_x	Standard propene - NO_x control run for comparison with other such runs in this and other chambers. Results in normal range.
DTC707	9/3/98	Low NO_x Full Surrogate + Methyl Pivalate	Low NO_x full surrogate reactivity experiment with 29 ppm methyl pivalate added to Side B. Results on Table 3 and Figure 2.
DTC708	9/4/98	Low NO_x Full Surrogate Side equivalence Test	Irradiation of the same low NO_x full surrogate mixture was carried out in both reactors to determine side equivalency for this type of experiment. The NO oxidation rates and initial O_3 formation rates were the same on both sides, but the maximum ozone was slightly less on Side B, and the O_3 decayed slightly faster on that side once the peak O_3 concentration was reached. The maximum and final O_3 on side A was around 265 ppb, and the maximum O_3 on side B was around 250 ppb after 3 hours, declining to ~230 ppb at the end of the 6-hour run. N-Butane data suggest a slightly higher than normal leak rate on Side B, but it was still less than 1% per hour.
DTC709	9/8/98	Ozone and CO dark Decay	Control run to check for leaks and measure the O_3 wall decay rate just before replacing the reaction bag. Essentially no CO decay was observed, indicating negligible leakage. The O_3 decay rates were 1.2 x 10^{-4} min^{--1} on Side A and 2.1 x 10^{-4} min^{--1} in Side B, in fair agreement with the value of 1.5 x 10^{-4} min^{--1} that is used when modeling these DTC runs. The higher decay rate in Side B is consistent with the results of run DTC708. However, changing the O_3 wall loss rate within this range does not significantly affect results of model simulations of this run.
DTC710	10/19/98	n-Butane - NO_x	Run to measure the rate of the chamber radical source, as discussed by Carter et al (1995c). Results are well simulated using the standard chamber model assigned to this series of experiments, and good side equivalency was obtained.
DTC736	11/30/98	NO_2 Actinometry	NO_2 photolysis rate measured using the quartz tube method was 0.162 min^{-1}, suggesting that the light intensity is becoming approximately constant during this period.

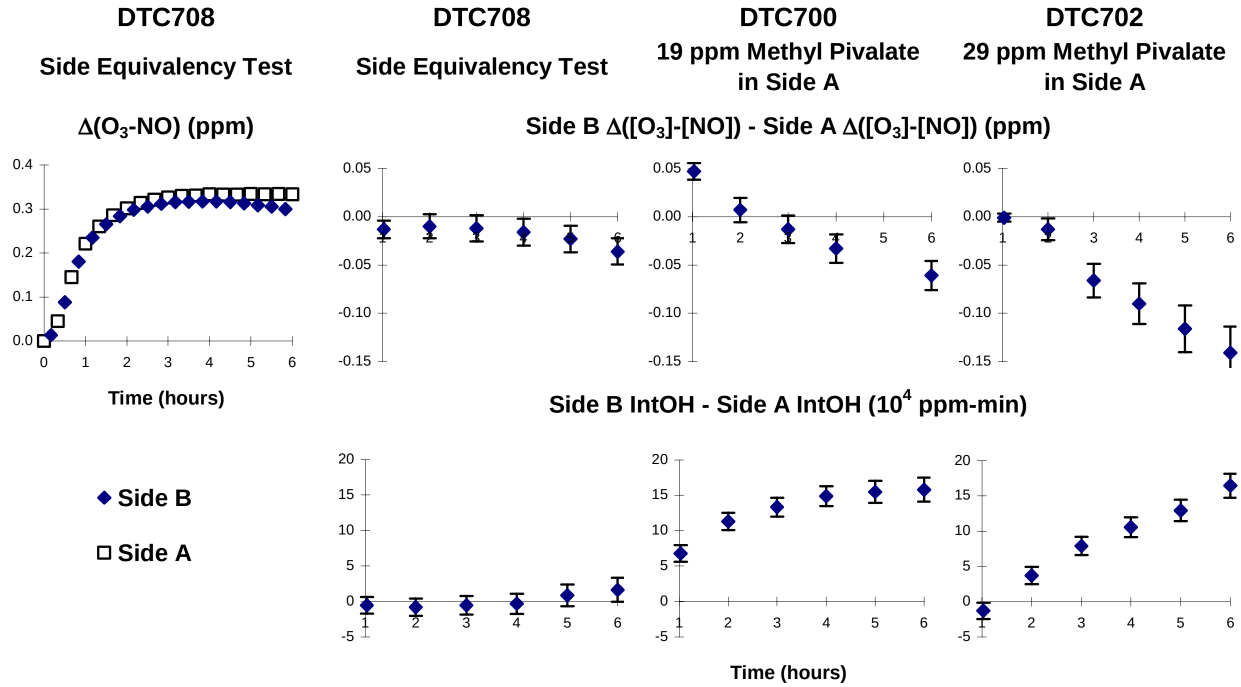

Figure 1. Selected results of the low NO_x mini-surrogate side equivalency test experiment, and comparison with comparable data obtained in low NO_x mini-surrogate experiments with added methyl pivalate.

Table 3. Summary of conditions and selected results of the environmental chamber reactivity experiments with methyl pivalate.

Run	Test VOC (ppm)	NO_x (ppm)	Surg. (ppm C)	Δ([O3]-[NO]) (ppm) 2nd Hour Base	Test	IR [a]	6th Hour Base	Test	IR [a]	5th Hour IntOH (10^{-6} min) Base	Test	IR [a]
Mini-Surrogate												
DTC694A	10.5	0.40	5.98	0.11	0.08	-2.8e-3	0.55	0.38	-1.6e-2	12.5	4.0	-0.8
DTC701B	16.5	0.39	5.60	0.11	0.07	-2.4e-3	0.56	0.31	-1.5e-2	11.1	3.9	-0.4
High NO_x Full Surrogate												
DTC695B	12.3	0.31	4.77	0.29	0.28	-4.1e-4	0.63	0.69	5.4e-3	18.8	4.4	-1.2
DTC702A	20.4	0.32	4.48	0.26	0.27	6.4e-4	0.57	0.71	6.9e-3	20.7	7.7	-0.6
Low NO_x Full Surrogate												
DTC700A	19.0	0.11	4.40	0.30	0.30	-3.7e-4	0.33	0.39	3.2e-3	21.3	5.8	-0.8
DTC707B	29.2	0.11	4.05	0.30	0.27	-1.2e-3	0.35	0.38	1.1e-3	23.6	3.9	-0.7

[a] IR = Incremental Reactivity = ([Test] - [Base]) / [Methyl Pivalate]

Methyl Pivalate Reactivity Experiments

Six incremental reactivity experiments were carried out with methyl pivalate, two for each of the three types of base mixtures. The results are summarized on Table 3 and concentration-time plots of the major reactivity results are shown on Figure 2. Results of model calculations are also shown in the figure.

The results show that the effects of methyl pivalate on NO oxidation and O_3 formation rates depend on the conditions of the experiments. It has a significant inhibiting effect on Δ([O3]-[NO]) in the mini-surrogate experiments and to a lesser extent inhibits it during the initial periods of the low NO_x full surrogate runs. On the other hand it has relatively small but positive effects on O_3 throughout most of the higher NO_x full surrogate runs and the latter periods of the low NO_x full surrogate experiments. It inhibits OH radical levels under all conditions, with the effects of this radical inhibition increasing during the course of the experiments. The magnitudes of the incremental reactivities are relatively low because of the relatively low OH radical rate constant for this compound.

The radical inhibition effects of methyl pivalate addition can be attributed to radical termination by the reactions of the peroxy radicals with NO forming organic nitrate and also to radical termination caused by the formation of the PAN analogue $CH_3OC(O)OONO_2$. Note that the relative importance of nitrate formation in terms of the total methyl pivalate oxidation process is independent of reaction conditions as long as sufficient NO_x is present in the system that reaction with NO is the dominant loss process for peroxy radicals, while the relative importance of PAN analogue formation depends on the $[NO_2]/[NO]$ ratio which depends on reaction conditions.

The fact methyl pivalate inhibits $\Delta([O_3]-[NO])$ in the mini-surrogate runs while having positive effects on $\Delta([O_3]-[NO])$ during most periods in the full surrogate experiments is fairly common for VOCs with sufficiently large radical sinks in their mechanism. It is attributed to the fact that mini-surrogate experiments tend to be more sensitive to aspects of the mechanism concerning radical initiation and termination, while the full surrogate runs are relatively more sensitive to the positive effects of NO to NO_2 conversions caused by the peroxy radicals formed when the VOC reacts. The latter stages of the low NO_x full surrogate runs are also sensitive to NO_x sinks in the VOC's mechanism, which if sufficiently large would cause negative ozone reactivities under those conditions. Apparently in the case of methyl pivalate the radical sinks are not sufficient to overcome the positive effects of the direct NO to NO_2 conversions in under most conditions in the full surrogate runs. Similarly, the NO_x sink caused by the formation of the PAN analogue is also not sufficient to overcome the positive effect of the NO to NO_2 conversions in the low NO_x full surrogate runs.

Consistent with the predicted and observed products in the reactions of OH with methyl pivalate, the addition of methyl pivalate in the reactivity experiments causes the formation of acetone (which is not formed in the base case experiments), and an increase in the formaldehyde levels in the full surrogate experiments. On the other hand, the methyl pivalate reduces the rate of formaldehyde formation in the mini-surrogate runs. This is attributed to the inhibiting effect of methyl pivalate on radical levels, which

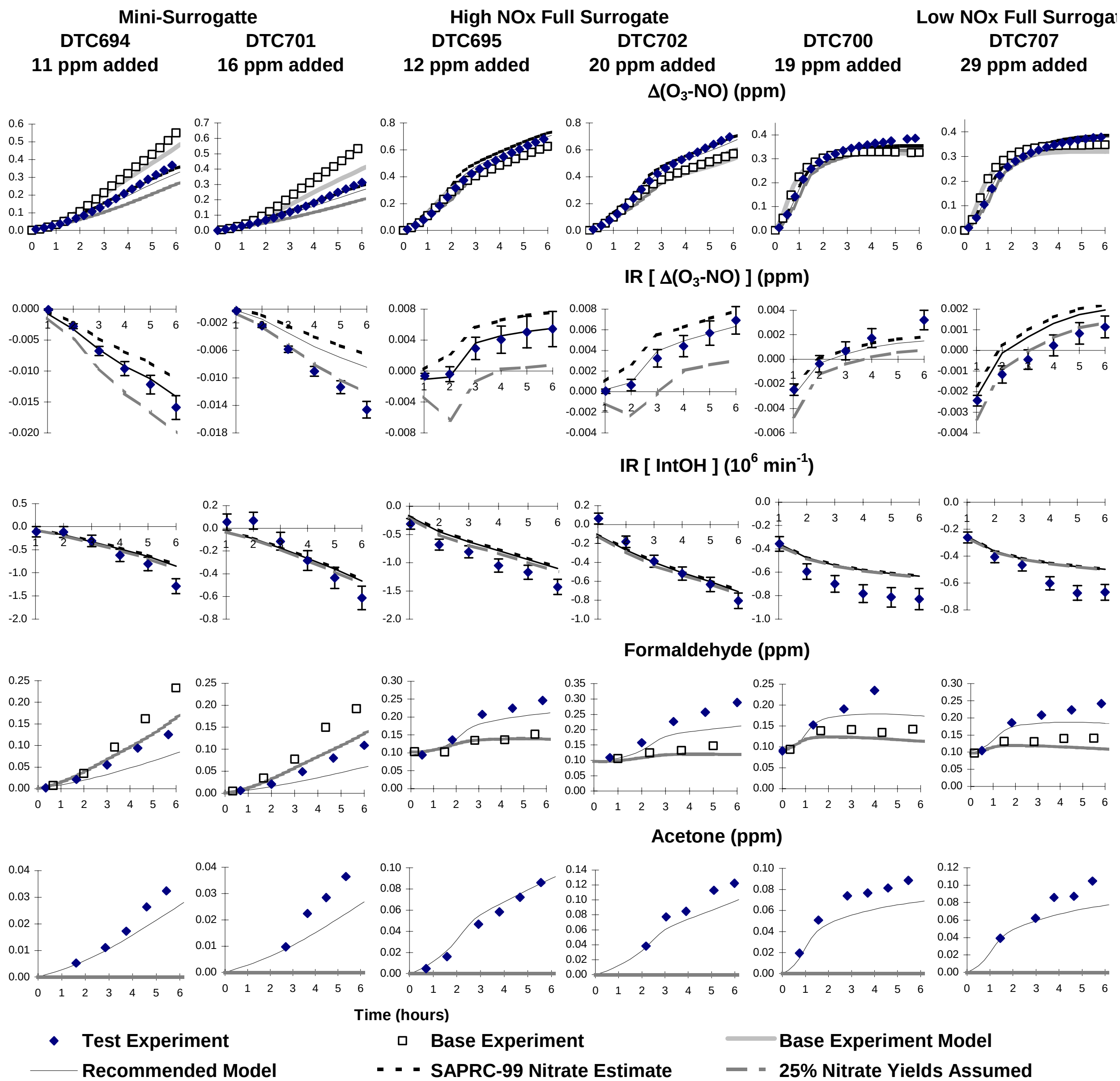

Figure 2. Selected experimental and calculated results of the incremental reactivity experiments with methyl pivalate. (Effects of nitrate yield variation are not shown for simulated formaldehyde and acetaldehyde data.)

would reduce the rate of formaldehyde formation from ethylene, a major component of the mini-surrogate. In the case of the mini-surrogate experiments this effect is enough to offset the formaldehyde formed from methyl pivalate's direct reactions. In the case of the full surrogate runs, the effects on overall radical levels are relatively less important, and also the formaldehyde formation from the base case surrogate components is relatively less important compared to the initial formaldehyde and the formaldehyde formed from the added methyl pivalate.

The results of model simulations using the methyl pivalate mechanism discussed in the previous section are also shown on Figure 2. Three sets of calculations are shown, one (lines with darker, shorter dashes) using the alkyl nitrate yields derived using the SAPRC-99 estimation methods, one (lines with lighter longer dashes) using the ~25% yield as estimated from the nitrate IR bands in the product study of Wallington et al (2000), and one (solid lines) using the nitrate yields judged to give the best overall fits to the data. The figure shows that the nitrate yields as derived using the SAPRC-99 estimation methods has a consistent bias towards underpredicting the inhibition or overpredicting the positive effects of methyl pivalate on $\Delta([O_3]\text{-}[NO])$. This is removed by the relatively minor adjustment of increasing the nitrate yields from the initially formed radicals from 10% to 13%. Although using the high ~25% overall nitrate yield suggested by the data of Wallington et al (2000) gives better fits to the results of run DTC701, the results of the other experiments are poorly simulated with this model. Given the uncertainties in making quantitative yield estimates from IR bands without authentic calibration standards, the overall nitrate yields found to give the best fits to the data in this work are probably not outside uncertainty range of the yields derived by Wallington et al (2000).

The mechanism with the adjusted nitrate yields gives reasonably good simulations of the results of the reactivity experiments in this work. The one exception is run DTC701 where the inhibition of $\Delta([O_3]\text{-}[NO])$ is somewhat underestimated. However, the $\Delta([O_3]\text{-}[NO])$ in the base case experiment for that run is also underpredicted by the model (the results of mini-surrogate experiments tend to be more sensitive to the variable chamber radical source), and this may bias the simulation of the $\Delta([O_3]\text{-}[NO])$ reactivities. Overall the model gives a good prediction of how the $\Delta([O_3]\text{-}[NO])$ reactivities of methyl pivalate are affected by changes in chemical conditions.

The mechanism also gives reasonably good simulations of the effects of methyl pivalate on formaldehyde and acetone yields, and correctly predicts that it suppresses formaldehyde in the mini-surrogate runs while enhancing it in the other experiments. It appears to have a bias towards underpredicting the yields of these compounds, though this may not be outside of experimental uncertainty. Note that the amount of methyl pivalate that reacts could not be experimentally determined because the fraction reacted is relatively low, and if the model is underestimating the amount of methyl pivalate reacting it would underestimate the yields of its products.

The mechanism gives good predictions of the IntOH reactivities of methyl pivalate, except for the low NO_x full surrogate runs where the inhibition of IntOH reactivity is underpredicted. However, the inhibitions of IntOH reactivities in low NO_x full surrogate runs are underpredicted for almost all VOCs, even compounds with relatively simple mechanisms such as CO (Carter et al, 1995a, 2000). Thus this is more likely due to a problem of the mechanism in simulating the conditions of the base case experiment under low NO_x conditions than necessarily a problem with the VOC whose reactivity is being tested.

ATMOSPHERIC REACTIVITY CALCULATIONS

Incremental reactivities of VOCs have been shown to be highly dependent on environmental conditions, so reactivities measured in environmental chamber experiments cannot necessarily be assumed to be the same as those under atmospheric conditions (Carter and Atkinson, 1989; Carter et al, 1995b). Because of this, the only method available to obtain quantitative estimates of incremental reactivities of VOCs in ambient air pollution episodes is to conduct airshed model simulations of the episodes. Since these simulations cannot be any more reliable than the chemical mechanisms used, the major objective of this program was to assess the reliability of the methyl pivalate mechanism for use in such calculations. As discussed above, the results of the experiments indicate that the mechanism developed in this work serves as an appropriate basis for estimating the effects of this compound on ozone under atmospheric conditions. The atmospheric reactivity estimates based on this mechanism are discussed in this section.

Note that Carter (2000) already gives reactivity estimates for the methyl pivalate, calculated using the same (SAPRC-99) mechanism. However, some updates were made to the methyl pivalate mechanism in the process of preparing this report that were not incorporated in the mechanism used by Carter (2000), so the reactivities calculated for this compound will be slightly different. The effect of this change is relatively minor, as can be seen in the results presented below.

Scenarios Used for Reactivity Assessment

The set of airshed scenarios employed to assess the reactivities for this study is the same as those used for calculating the MIR and other reactivity scales in our previous work (Carter, 1994a), and also in the update using the SAPRC-99 mechanism (Carter, 2000). These scenarios, and the reasons for using them, are briefly described below.

The objective is to use a set of scenarios that represents, as much as possible, a comprehensive distribution of the environmental conditions where unacceptable levels of ozone are formed. Although a set of scenarios has not been developed for the specific purpose of VOC reactivity assessment, the EPA developed an extensive set of scenarios for conducting analyses of effects of ROG and NO_x controls on ozone formation using the EKMA modeling approach (Gipson et al. 1981; Gipson and Freas, 1983; EPA, 1984; Gery et al. 1987; Baugues, 1990). The EKMA approach involves the use of single-cell box models to simulate how the ozone formation in one day episodes is affected by changes in ROG and NO_x inputs. Although single-cell models cannot represent realistic pollution episodes in great detail, they can represent dynamic injection of pollutants, time-varying changes of inversion heights, entrainment of pollutants from aloft as the inversion height rises, and time-varying photolysis rates, temperatures, and humidities (Gipson and Freas, 1981; EPA, 1984; Gipson, 1984; Hogo and Gery, 1988). Thus, they can be used to simulate a wide range of the chemical conditions which affect ozone formation from ROG and NO_x, and which affect VOC reactivity. Therefore, at least to the extent they are suitable for their intended purpose, an appropriate set of EKMA scenarios should also be suitable for assessing reactivities over a wide range of conditions.

Base Case Scenarios

The set of EKMA scenarios used in this study were developed by the United States EPA for assessing how various ROG and NO_x control strategies would affect ozone nonattainment in various areas of the country (Baugues, 1990). The characteristics of these scenarios and the methods used to derive their input data are described in more detail elsewhere (Baugues, 1990; Carter, 1994b). Briefly, 39 urban areas in the United States were selected based on geographical representativeness of ozone nonattainment areas and data availability, and a representative high ozone episode was selected for each. The initial non-methane organic carbon (NMOC) and NO_x concentrations, the aloft O_3 concentrations, and the mixing height inputs were based on measurement data for the various areas, the hourly emissions in the scenarios were obtained from the National Acid Precipitation Assessment Program emissions inventory (Baugues, 1990), and biogenic emissions were also included. Table 4 gives a summary of the urban areas represented and other selected characteristics of the scenarios.

Several changes to the scenario inputs were made based on discussions with the California ARB staff and others (Carter, 1994a,b). Two percent of the initial NO_x and 0.1% of the emitted NO_x in all the scenarios was assumed to be in the form of HONO. The photolysis rates were calculated using solar light intensities and spectra calculated by Jeffries (1991) for 640 meters, the approximate mid-point of the mixed layer during daylight hours. The composition of the non methane organic pollutants entrained from aloft was based on the analysis of Jeffries et al. (1989). The composition of the initial and emitted reactive organics was derived as discussed below. Complete listings of the input data for the scenarios are given elsewhere (Carter, 1994b).

This set of 39 EKMA scenarios are referred to as “base case” to distinguish them from the scenarios derived from them by adjusting NO_x inputs to yield standard conditions of NO_x availability as discussed below. No claim is made as to the accuracy of these scenarios in representing any real episode, but they are a result of an effort to represent, as accurately as possible given the available data and the limitations of the formulation of the EKMA model, the range of conditions occurring in urban areas throughout the United States. When developing general reactivity scales it is more important that the scenarios employed represent a realistic distribution of chemical conditions than accurately representing the details of any one particular episode.

The Base ROG mixture is the mixture of reactive organic gases used to represent the chemical composition of the initial and emitted anthropogenic reactive organic gases from all sources in the scenarios. Consistent with the approach used in the original EPA scenarios, the same mixture was used for all scenarios. The speciation for this mixture was derived by Croes (1991) based on an analysis of the EPA database (Jeffries et al. 1989) for the hydrocarbons and the 1987 Southern California Air Quality

Table 4. Summary of the conditions of the scenarios used for atmospheric reactivity assessment.

	Scenario	Max O_3 (ppb)	Max 8-Hr Avg O_3 (ppb)	ROG / NO_x	NO_x / MOIR NO_x	Height (kM)	Init., Emit ROG (m. mol m^{-2})	O_3 aloft (ppb)	Integrated OH (ppt-min)
Avg.	MIR	187	119	3.1	1.5	1.8	15	70	128
Cond.	MOIR	239	165	4.5	1.0	1.8	15	70	209
	EBIR	227	172	6.4	0.7	1.8	15	70	210
Base	Atlanta, GA	179	132	7.3	0.7	2.1	12	63	200
Case	Austin, TX	175	144	9.3	0.5	2.1	11	85	179
	Baltimore, MD	334	215	5.2	1.1	1.2	17	84	186
	Baton Rouge, LA	241	173	6.8	0.9	1.0	11	62	186
	Birmingham, AL	244	202	6.9	0.5	1.8	13	81	208
	Boston, MA	197	167	6.5	0.6	2.6	14	105	262
	Charlotte, NC	143	126	7.8	0.3	3.0	7	92	212
	Chicago, IL	278	226	11.6	0.5	1.4	25	40	164
	Cincinnati, OH	205	153	6.4	0.7	2.8	17	70	220
	Cleveland, OH	252	179	6.6	0.9	1.7	16	89	187
	Dallas, TX	208	141	4.7	1.2	2.3	18	75	176
	Denver, CO	204	139	6.3	1.1	3.4	29	57	143
	Detroit, MI	246	177	6.8	0.7	1.8	17	68	235
	El Paso, TX	182	135	6.6	1.0	2.0	12	65	138
	Hartford, CT	172	144	8.4	0.5	2.3	11	78	220
	Houston, TX	312	217	6.1	0.9	1.7	25	65	225
	Indianapolis, IN	212	148	6.6	0.9	1.7	12	52	211
	Jacksonville, FL	155	115	7.6	0.6	1.5	8	40	206
	Kansas City, MO	159	126	7.1	0.6	2.2	9	65	233
	Lake Charles, LA	286	209	7.4	0.6	0.5	7	40	233
	Los Angeles, CA	568	406	7.6	1.0	0.5	23	100	134
	Louisville, KY	212	155	5.5	0.8	2.5	14	75	260
	Memphis, TN	229	180	6.8	0.6	1.8	15	58	249
	Miami, FL	132	111	9.6	0.4	2.7	9	57	181
	Nashville, TN	167	138	8.0	0.4	1.6	7	50	225
	New York, NY	365	294	8.1	0.7	1.5	39	103	159
	Philadelphia, PA	247	169	6.2	0.9	1.8	19	53	227
	Phoenix, AZ	277	193	7.6	1.0	3.3	40	60	153
	Portland, OR	166	126	6.5	0.7	1.6	6	66	233
	Richmond, VA	242	172	6.2	0.8	1.9	16	64	217
	Sacramento, CA	204	142	6.6	0.8	1.1	7	60	209
	St Louis, MO	324	209	6.1	1.1	1.6	26	82	176
	Salt Lake City, UT	186	150	8.5	0.6	2.2	11	85	182
	San Antonio, TX	133	98	3.9	1.0	2.3	6	60	192
	San Diego, CA	193	150	7.1	0.9	0.9	8	90	146
	San Francisco, CA	229	126	4.8	1.8	0.7	25	70	61
	Tampa, FL	230	153	4.4	1.0	1.0	8	68	211
	Tulsa, OK	231	160	5.3	0.9	1.8	15	70	264
	Washington, DC	283	209	5.3	0.8	1.4	13	99	239

Study (SCAQS) database for the oxygenates (Croes et al. 1994; Lurmann and Main. 1992). This mixture consists of 52% (by carbon) alkanes, 15% alkenes, 27% aromatics, 1% formaldehyde, 2% higher aldehydes, 1% ketones, and 2% acetylene. The detailed composition of this mixture is given elsewhere (Carter, 1994b; Carter, 2000).

Adjusted NO_x scenarios

Incremental reactivities in the base case scenarios would be expected to vary widely, since incremental reactivities depend on the ROG/NO_x ratio, and that ratio varies widely among the base case scenarios. To obtain reactivity scales for specified NO_x conditions, separate scenarios, designated MIR (for maximum incremental reactivity), MOIR (for maximum ozone incremental reactivity), and Equal Benefit Incremental Reactivity (EBIR) were developed (Carter, 1994a). In the MIR scenarios, the NO_x inputs were adjusted so the base ROG mixture (and most other VOCs) has its highest incremental reactivity. This is representative of the highest NO_x conditions of relevance to VOC reactivity assessment because at higher NO_x levels O_3 yields become significantly suppressed, but is also the condition where O_3 is most sensitive to VOC emissions. In the MOIR scenarios, the NO_x inputs were adjusted to yield the highest ozone concentration. In the EBIR scenarios, the NO_x inputs were adjusted so that the relative effects of NO_x reductions and total ROG reductions on peak ozone levels were equal. This represents the lowest NO_x condition of relevance for VOC reactivity assessment, because O_3 formation becomes more sensitive to NO_x emissions than VOC emissions at lower NO_x levels. As discussed by Carter (1994a) the MIR and EBIR ROG/NO_x ratios are respectively ~1.5 and ~0.7 times those for the MOIR scenarios in all cases.

NO_x Conditions in the Base Case Scenarios

The variability of ROG/NO_x ratios in the base case scenarios suggests a variability of reactivity characteristics in those scenarios. However, as discussed previously (Carter, 1994a), the ROG/NO_x ratio is also variable in the MIR or MOIR scenarios, despite the fact that the NO_x inputs in these scenarios are adjusted to yield a specified reactivity characteristic. Thus, the ROG/NO_x ratio, by itself, is not necessarily a good predictor of reactivity characteristics of a particular scenario. The NO_x/NO_x^{MOIR} ratio is a much better predictor of this, with values greater than 1 indicating relatively high NO_x conditions where ozone formation is more sensitive to VOCs, and values less than 1 indicating NO_x-limited conditions. NO_x/NO_x^{MOIR} ratios less than 0.7 represent conditions where NO_x control is a more effective ozone control strategy than ROG control (Carter, 1994a). Note that more than half of the base case scenarios represent NO_x-limited conditions, and ~25% of them represent conditions where NO_x control is more beneficial than VOC control. A relatively small number of scenarios represent MIR or near MIR conditions. However, as discussed elsewhere (Carter, 1994a), this set of scenarios is based on near-worst-case conditions for ozone formation in each of the airsheds. Had scenarios representing less-than-worst-case conditions been included, one might expect a larger number of MIR or near MIR scenarios. This is because NO_x is consumed more slowly on days with lower light intensity or temperature, and thus the scenario is less likely to become NO_x-limited.

Quantification of Atmospheric Reactivity

The reactivity of a VOC in an airshed scenario is measured by its incremental reactivity. For ambient scenarios, this is defined as the change in ozone caused by adding the VOC to the emissions, divided by the amount of VOC added, calculated for sufficiently small amounts of added VOC that the incremental reactivity is independent of the amount added[2].

$$\mathrm{IR(VOC, Scenario)} = \lim_{VOC \to 0} \left[\frac{\mathrm{O_3(Scenario\ with\ VOC) - O_3(Base\ Scenario)}}{\mathrm{Amount\ of\ VOC\ Added}} \right] \qquad \text{(IV)}$$

The specific calculation procedure is discussed in detail elsewhere (Carter, 1994a,b).

Incremental reactivities derived as given above tend to vary from scenario to scenario because they differ in their overall sensitivity of O_3 formation to VOCs. These differences can be factored out to some extent by using "relative reactivities", which are defined as ratios of incremental reactivities to the incremental reactivity of the base ROG mixture, which is used to represent emissions of reactive VOCs from all sources.

$$\mathrm{RR(VOC, Scenario)} = \frac{\mathrm{IR(VOC, Scenario)}}{\mathrm{IR\ (Base\ ROG, Scenario)}} \qquad \text{(V)}$$

These relative reactivities can also be thought of as the relative effect on O_3 of controlling emissions of the particular VOC by itself, compared to controlling emissions from all VOC sources equally. Thus, they are more meaningful in terms of control strategy assessment than absolute reactivities, which can vary greatly depending on the episode and local meteorology.

In addition to depending on the VOC and the scenario, the incremental and relative reactivities depend on how the amounts of VOC added are quantified. In this work, this is quantified on a mass basis, since this is how VOCs are regulated, and generally approximates how VOC substitutions are made in practice. Note that relative reactivities will be different if they are quantified on a molar basis, with VOCs with higher molecular weight having higher reactivities on a mole basis than a gram basis.

Relative reactivities can also depend significantly on how ozone impacts are quantified (Carter, 1994a). Two different ozone quantification methods are used in this work, as follows:

"Ozone Yield" reactivities measure the effect of the VOC on the total amount of ozone formed in the scenario at the time of its maximum concentration. Incremental reactivities are quantified as grams O_3 formed per gram VOC added. Most previous recent studies of ozone reactivity (Dodge, 1984; Carter and

[2] Note that this differs from how the term "incremental reactivity" is used in the context of chamber experiments. In that case, the incremental reactivity refers to the relative change observed in the individual experiments, which in general depends on the amount added.

Atkinson, 1987, 1989, Chang and Rudy, 1990; Jeffries and Crouse, 1991) have been based on this quantification method. The MIR, MOIR, and EBIR scales of Carter (1994a) also use this quantification.

"Maximum 8 Hour Average" reactivities measure the effect of the VOC on the average ozone concentration during the 8-hour period when the average ozone concentration was the greatest, which in these one-day scenarios was the last 8 hours of the simulation. This provides a measure of ozone impact that is more closely related to the new Federal ozone standard that is given in terms of an 8 hour average. This quantification is used for relative reactivities in this work.

In previous reports, we have reported reactivities in terms of integrated O_3 over a standard concentration of 0.09 or 0.12 ppm. This provides a measure of the effect of the VOC on exposure to unacceptable levels of ozone. This is replaced by the maximum 8 hour average reactivities because it is more representative of the proposed new Federal ozone standard and because reactivities relative to integrated O_3 over a standard tend to be between those relative to ozone yield and those relative to 8-hour averages. Therefore, presenting both ozone yield and maximum 8-hour average relative reactivities should be sufficient to provide information on how relative reactivities vary with ozone quantification method. Incremental reactivities are quantified as ppm O_3 per milligram VOC emitted per square meter, but maximum 8 hour average reactivities are usually quantified as relative reactivities quantified on a mass basis.

Note that incremental reactivities are calculated for a total of 156 scenarios, consisting of the 39 base case scenarios and the three adjusted NO_x scenarios for each of the 39 base case scenarios. However, the incremental reactivities in the MIR, MOIR, or EBIR) scales are reported as averages of the incremental reactivities in the corresponding adjusted NO_x scenarios, because adjusting the NO_x conditions reduces the scenario variability, and this allows for a derivation single reactivity scales representing each type of NO_x condition. On the other hand, the individual scenario results will be shown for the base case scenarios, to give an indication of the scenario-to-scenario variability of the calculated reactivity results.

Results

Table 5 lists the ozone yield incremental reactivities calculated for methyl pivalate, ethane, acetone and the mixture of emitted reactive organic compounds (the base ROG). The methyl pivalate reactivity results shown are those calculated using the mechanism developed in this work that gave the best fits to the chamber that, and also those as given by Carter (2000) ("SAPRC-99"), which as indicated above was slightly revised in this work. Table 6 gives the ozone yield and maximum 8-hour average reactivities relative to the base ROG for three compounds. Ethane is chosen for comparison because it has been used by the EPA as the informal standard to determine "negligible" reactivity for VOC exemption purposes (Dimitriades, 1999). If a compound does not have a significantly greater impact on ozone than ethane in most or all the scenarios, it might be reasonably be considered for exemption from regulation as

Table 5. Atmospheric incremental reactivities calculated for the base ROG mixture, ethane, methyl pivalate, and acetone.

Scenario		Incremental Reactivities (gm O_3 / gm VOC)				
		Base ROG	Ethane	Methyl Pivalate		Acetone
				This Work	SAPRC-99	
Adj'd NOx	Max React	3.68	0.30	0.39	0.40	0.42
	Max Ozone	1.46	0.20	0.23	0.24	0.17
	Equal Benefit	0.85	0.15	0.15	0.16	0.11
Base Case	Average	1.03	0.15	0.17	0.17	0.13
	St.Dev	0.42	0.04	0.06	0.06	0.05
	ATL GA	0.82	0.13	0.13	0.14	0.10
	AUS TX	0.63	0.12	0.11	0.12	0.08
	BAL MD	1.59	0.20	0.24	0.25	0.19
	BAT LA	0.85	0.11	0.12	0.13	0.10
	BIR AL	0.72	0.16	0.16	0.17	0.11
	BOS MA	0.72	0.14	0.15	0.16	0.09
	CHA NC	0.53	0.11	0.10	0.10	0.08
	CHI IL	0.26	0.07	0.06	0.06	0.05
	CIN OH	1.12	0.20	0.22	0.23	0.13
	CLE OH	1.17	0.15	0.18	0.18	0.14
	DAL TX	2.14	0.23	0.28	0.28	0.23
	DEN CO	1.66	0.15	0.18	0.19	0.20
	DET MI	0.98	0.18	0.20	0.21	0.12
	ELP TX	1.45	0.14	0.16	0.17	0.17
	HAR CT	0.77	0.16	0.15	0.15	0.10
	HOU TX	1.10	0.17	0.20	0.21	0.13
	IND IN	1.24	0.18	0.19	0.20	0.14
	JAC FL	0.67	0.11	0.10	0.10	0.08
	KAN MO	1.07	0.20	0.21	0.22	0.13
	LAK LA	0.42	0.09	0.08	0.09	0.06
	LOS CA	0.76	0.08	0.10	0.10	0.09
	LOU KY	1.24	0.22	0.24	0.25	0.15
	MEM TN	0.76	0.15	0.15	0.16	0.10
	MIA FL	0.49	0.10	0.07	0.07	0.07
	NAS TN	0.67	0.15	0.13	0.14	0.10
	NEW NY	0.39	0.07	0.07	0.07	0.05
	PHI PA	1.08	0.17	0.19	0.20	0.13
	PHO AZ	1.46	0.18	0.21	0.22	0.17
	POR OR	0.96	0.17	0.17	0.17	0.12
	RIC VA	1.06	0.18	0.20	0.21	0.13
	SAC CA	1.22	0.19	0.21	0.21	0.16
	SAI MO	1.38	0.16	0.19	0.20	0.16
	SAL UT	0.90	0.15	0.16	0.17	0.12
	SAN TX	1.62	0.21	0.25	0.26	0.18
	SDO CA	0.85	0.09	0.10	0.11	0.08
	SFO CA	1.87	0.09	0.13	0.13	0.25
	TAM FL	1.52	0.19	0.22	0.23	0.17
	TUL OK	1.17	0.20	0.22	0.23	0.14
	WAS DC	0.99	0.18	0.20	0.21	0.12

Table 6. Atmospheric relative reactivities calculated for ethane, methyl pivalate and acetone..

Scenario		Reactivities relative to the base ROG (mass basis)					
		Ozone Yield			Max 8 Hour Avg		
		Ethane	Me-Pvat	Acetone	Ethane	Me-Pvat	Acetone
Adj'd	MIR	0.08	0.10	0.11	0.07	0.09	0.11
NOx	MOIR	0.13	0.16	0.12	0.08	0.10	0.10
	EBIR	0.17	0.18	0.13	0.10	0.10	0.10
Base	Average	0.16	0.17	0.13	0.10	0.10	0.10
Case	St.Dev	0.04	0.03	0.02	0.02	0.02	0.01
	ATL GA	0.16	0.16	0.13	0.09	0.10	0.10
	AUS TX	0.19	0.18	0.13	0.11	0.10	0.09
	BAL MD	0.12	0.15	0.12	0.08	0.10	0.11
	BAT LA	0.13	0.14	0.12	0.08	0.09	0.10
	BIR AL	0.22	0.22	0.15	0.12	0.12	0.11
	BOS MA	0.20	0.21	0.13	0.13	0.14	0.10
	CHA NC	0.21	0.18	0.14	0.14	0.12	0.10
	CHI IL	0.28	0.22	0.19	0.13	0.10	0.11
	CIN OH	0.18	0.20	0.12	0.10	0.12	0.09
	CLE OH	0.13	0.15	0.12	0.08	0.10	0.10
	DAL TX	0.11	0.13	0.11	0.08	0.09	0.09
	DEN CO	0.09	0.11	0.12	0.06	0.08	0.11
	DET MI	0.18	0.20	0.12	0.10	0.12	0.09
	ELP TX	0.10	0.11	0.12	0.07	0.08	0.10
	HAR CT	0.20	0.19	0.13	0.12	0.12	0.10
	HOU TX	0.16	0.18	0.12	0.09	0.11	0.10
	IND IN	0.14	0.16	0.12	0.09	0.09	0.09
	JAC FL	0.16	0.15	0.13	0.09	0.08	0.10
	KAN MO	0.19	0.20	0.12	0.11	0.12	0.09
	LAK LA	0.22	0.20	0.14	0.11	0.10	0.10
	LOS CA	0.11	0.13	0.12	0.07	0.08	0.10
	LOU KY	0.17	0.19	0.12	0.11	0.12	0.10
	MEM TN	0.20	0.20	0.13	0.11	0.11	0.10
	MIA FL	0.20	0.14	0.15	0.11	0.08	0.10
	NAS TN	0.23	0.20	0.16	0.15	0.12	0.12
	NEW NY	0.17	0.18	0.12	0.08	0.09	0.09
	PHI PA	0.16	0.17	0.12	0.09	0.11	0.10
	PHO AZ	0.12	0.15	0.12	0.08	0.09	0.10
	POR OR	0.17	0.18	0.12	0.11	0.11	0.10
	RIC VA	0.17	0.19	0.12	0.09	0.11	0.10
	SAC CA	0.15	0.17	0.13	0.09	0.10	0.11
	SAI MO	0.11	0.14	0.12	0.07	0.09	0.11
	SAL UT	0.17	0.18	0.14	0.10	0.10	0.10
	SAN TX	0.13	0.15	0.11	0.09	0.11	0.09
	SDO CA	0.11	0.12	0.10	0.08	0.08	0.08
	SFO CA	0.05	0.07	0.14	0.04	0.06	0.13
	TAM FL	0.12	0.14	0.11	0.08	0.09	0.10
	TUL OK	0.17	0.19	0.12	0.10	0.11	0.09
	WAS DC	0.18	0.20	0.12	0.10	0.12	0.10

an ozone precursor. Acetone is also shown for comparison because it is a compound of comparable reactivity that has already been exempted.

Table 5 shows that the change in methyl pivalate's mechanism made in this work relative to the one used by Carter (2000) causes only a small change in its calculated atmospheric reactivity, with the new values being approximately 3% less than those given by Carter (2000). This is well within the uncertainty of any of these reactivity calculations.

The results show that methyl pivalate is a relatively low impact on ozone formation compared to the mixture used to represent reactive VOC emissions from all sources. On a mass basis, its effect on peak O_3 is only 10-20% that of this mixture depending on NO_x conditions, with the lowest relative impacts being in the higher NO_x conditions that are most sensitive to VOC controls. The effect of methyl pivalate on the maximum 8-hour average ozone is about 10% that of the base ROG, with less dependence on NO_x conditions. This means that regulating methyl pivalate emissions is only about 10-20% as effective in reducing ozone as is regulating emissions from all VOC sources.

The results also show that the incremental reactivities of methyl pivalate, acetone, and ethane are very similar. Although the averages for methyl pivalate are slightly higher than those for ethane, the differences are probably not significant given the 30% uncertainty in relative reactivity estimates even for compounds with relatively well established mechanisms, and given the variability of reactivities with environmental conditions. For example, Wang et al (2000) estimate the relative MIR's for methane, n-butane, and methanol are in the 30-35% range, suggesting that the same should be the case for ethane. An indication of the scenario-to-scenario variability of the reactivities of these compounds can be obtained from the reactivity data on Table 5 and Table 6.

Another indication of scenario-to-scenario variability in relative reactivities of methyl pivalate, ethane, and acetone is given on Figure 3, which shows distribution plots of the relative ozone yield and maximum 8-hour average ozone reactivities for the 39 base case scenarios. It is interesting to note that the distributions in relative reactivities for ethane and methyl pivalate are almost exactly the same, while the relative reactivity of acetone is considerably less dependent on scenario conditions. The differences in the average reactivities of ethane and methyl pivalate are quite small compared to the width of the distributions, and the extent of their overlap.

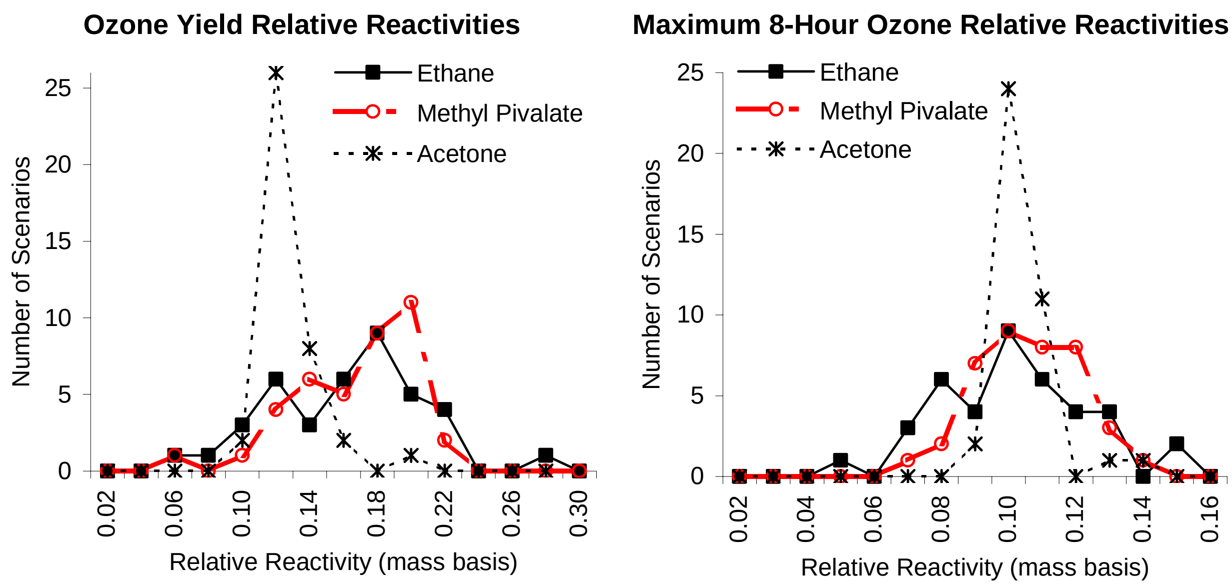

Figure 3. Distribution plots of relative reactivities of ethane, methyl pivalate, and acetone in the base case scenarios.

CONCLUSIONS

The decision whether it is appropriate to regulate a compound as an ozone precursor requires a quantitative assessment of its ozone impacts under a variety of environmental conditions. This involves developing a chemical mechanism for the compound's atmospheric reactions that can be reliably used in airshed models to predict its atmospheric reactivity. Until this study, and that of Wallington et al (2000) there was no experimental information concerning the atmospheric reactions of methyl pivalate, and thus reactivity estimates for this compound were highly uncertain. The study of Wallington et al (2000) provided needed data concerning the atmospheric reaction rate of methyl pivalate, and useful information concerning the products formed in this reaction. The objective of this study was to develop a mechanism for the atmospheric reactions of methyl pivalate that is consistent with these data, and to verify whether this mechanism can accurately predict the ozone impacts of this compound under a variety of environmental conditions. We believe this program was successful in achieving this objective.

The methyl pivalate atmospheric reaction mechanism developed in this work was found to give sufficiently good simulations of the effects of methyl pivalate on NO oxidation, O_3 formation and other manifestations of reactivity that it should serve as a reliable basis for estimating its ozone impacts in the atmosphere. The mechanism is consistent with the kinetic and product data of Wallington et al (2000), and although the mechanism incorporates some uncertain estimates concerning some of its details, the only adjustments made to optimize fits to the chamber data concerned relatively small changes to the overall nitrate yields that are well within the uncertainty of the estimation methods. Therefore, the mechanism is considered to be consistent with our current knowledge of atmospheric chemistry as well as having predictive capability.

Based on this mechanism, the ozone impact of methyl pivalate on a mass basis was calculated to be relatively low, with the impacts on peak ozone being between 10-20% of the mixture representing VOC emissions from all sources, depending on scenario conditions. The average relative impacts on maximum 8-hour average ozone is somewhat lower, being ~10% that of the base ROG mixture, with less dependence on conditions. The mass-based ozone impacts were found to be essentially the same as those for ethane, at least to within the uncertainty of atmospheric reactivity calculations and considering the variability of ozone impacts with atmospheric conditions, and very similar to those for acetone. Since ethane has served as the informal standard in regard to deriving “negligible” reactivity for VOC exemption purposes, and since acetone has already been exempted on this basis, these results suggest that exempting methyl pivalate on the same basis may also be appropriate.

REFERENCES

Atkinson, R. (1989): "Kinetics and Mechanisms of the Gas-Phase Reactions of the Hydroxyl Radical with Organic Compounds," J. Phys. Chem. Ref. Data, Monograph no 1.

Atkinson, R. (1991): "Kinetics and Mechanisms of the Gas-Phase Reactions of the NO_3 Radical with Organic Compounds," J. Phys. Chem. Ref. Data, 20, 459-507.

Atkinson, R. (1994): "Gas-Phase Tropospheric Chemistry of Organic Compounds," J. Phys. Chem. Ref. Data, Monograph No. 2.

Atkinson, R. and W. P. L. Carter (1984): "Kinetics and Mechanisms of the Gas-Phase Reactions of Ozone with Organic Compounds under Atmospheric Conditions," Chem. Rev. 84, 437-470.

Baugues, K. (1990): "Preliminary Planning Information for Updating the Ozone Regulatory Impact Analysis Version of EKMA," Draft Document, Source Receptor Analysis Branch, Technical Support Division, U. S. Environmental Protection Agency, Research Triangle Park, NC, January.

Calvert, J. G., and J. N. Pitts, Jr. (1966): "Photochemistry," John Wiley and Sons, New York.

CARB (1999) California Air Resources Board, Proposed Regulation for Title 17, California Code of Regulations, Division 3, Chapter 1, Subchapter 8.5, Article 3.1, sections 94560- 94539.

Carter, W. P. L. (1990): "A Detailed Mechanism for the Gas-Phase Atmospheric Reactions of Organic Compounds," Atmos. Environ., 24A, 481-518.

Carter, W. P. L. (1994a): "Development of Ozone Reactivity Scales for Volatile Organic Compounds," J. Air & Waste Manage. Assoc., 44, 881-899.

Carter, W. P. L. (1994b): "Calculation of Reactivity Scales Using an Updated Carbon Bond IV Mechanism," Report Prepared for Systems Applications International Under Funding from the Auto/Oil Air Quality Improvement Research Program, April 12. Available at http://helium.ucr.edu/~carter/absts.htm#cb4rct.

Carter, W. P. L. (2000): "Documentation of the SAPRC-99 Chemical Mechanism for VOC Reactivity Assessment," Report to the California Air Resources Board, Contracts 92-329 and 95-308, May 8. Available at http://helium.ucr.edu/~carter/absts.htm#saprc99.

Carter, W. P. L. and R. Atkinson (1987): "An Experimental Study of Incremental Hydrocarbon Reactivity," Environ. Sci. Technol., 21, 670-679

Carter, W. P. L. and R. Atkinson (1989): "A Computer Modeling Study of Incremental Hydrocarbon Reactivity", Environ. Sci. Technol., 23, 864.

Carter, W. P. L., and F. W. Lurmann (1990): "Evaluation of the RADM Gas-Phase Chemical Mechanism," Final Report, EPA-600/3-90-001.

Carter, W. P. L. and F. W. Lurmann (1991): "Evaluation of a Detailed Gas-Phase Atmospheric Reaction Mechanism using Environmental Chamber Data," Atm. Environ. 25A, 2771-2806.

Carter, W. P. L., J. A. Pierce, I. L. Malkina, D. Luo and W. D. Long (1993): "Environmental Chamber Studies of Maximum Incremental Reactivities of Volatile Organic Compounds," Report to Coordinating Research Council, Project No. ME-9, California Air Resources Board Contract No. A032-0692; South Coast Air Quality Management District Contract No. C91323, United States Environmental Protection Agency Cooperative Agreement No. CR-814396-01-0, University Corporation for Atmospheric Research Contract No. 59166, and Dow Corning Corporation. April 1. Available at http://helium.ucr.edu/~carter/absts.htm#rct1rept.

Carter, W. P. L., J. A. Pierce, D. Luo, and I. L. Malkina (1995a): "Environmental Chamber Studies of Maximum Incremental Reactivities of Volatile Organic Compounds," Atmos. Environ. 29, 2499-2511.

Carter, W. P. L., D. Luo, I. L. Malkina, and J. A. Pierce (1995b): "Environmental Chamber Studies of Atmospheric Reactivities of Volatile Organic Compounds. Effects of Varying ROG Surrogate and NO_x," Final report to Coordinating Research Council, Inc., Project ME-9, California Air Resources Board, Contract A032-0692, and South Coast Air Quality Management District, Contract C91323. March 24. Available at http://helium.ucr.edu/~carter/absts.htm#rct2rept.

Carter, W. P. L., D. Luo, I. L. Malkina, and D. Fitz (1995c): "The University of California, Riverside Environmental Chamber Data Base for Evaluating Oxidant Mechanism. Indoor Chamber Experiments through 1993," Report submitted to the U. S. Environmental Protection Agency, EPA/AREAL, Research Triangle Park, NC., March 20. Available at http://helium.ucr.edu/~carter/absts.htm#databas.

Carter, W. P. L., D. Luo, I. L. Malkina, and J. A. Pierce (1995d): "Environmental Chamber Studies of Atmospheric Reactivities of Volatile Organic Compounds. Effects of Varying Chamber and Light Source," Final report to National Renewable Energy Laboratory, Contract XZ-2-12075, Coordinating Research Council, Inc., Project M-9, California Air Resources Board, Contract A032-0692, and South Coast Air Quality Management District, Contract C91323, March 26. Available at http://helium.ucr.edu/~carter/absts.htm#explrept.

Carter, W. P. L., D. Luo, and I. L. Malkina (1997): "Environmental Chamber Studies for Development of an Updated Photochemical Mechanism for VOC Reactivity Assessment," Final report to the California Air Resources Board, the Coordinating Research Council, and the National Renewable Energy Laboratory, November 26. Available at http://helium.ucr.edu/~carter/absts.htm#rct3rept.

Carter. W. P. L., D. Luo and I. L. Malkina (2000a): "Investigation of Atmospheric Reactivities of Selected Consumer Product VOCs," Report to California Air Resources Board, May 30. Available at http://helium.ucr.edu/~carter/absts.htm#cpreport.

Chang, T. Y. and S. J. Rudy (1990): "Ozone-Forming Potential of Organic Emissions from Alternative-Fueled Vehicles," Atmos. Environ., 24A, 2421-2430.

Croes, B. E., Technical Support Division, California Air Resources Board, personal communication (1991).

Croes, B. E., et al. (1994): "Southern California Air Quality Study Data Archive," Research Division, California Air Resources Board.

Dasgupta, P. K, Dong, S. and Hwang, H. (1988): "Continuous Liquid Phase Fluorometry Coupled to a Diffusion Scrubber for the Determination of Atmospheric Formaldehyde, Hydrogen Peroxide, and Sulfur Dioxide," Atmos. Environ. 22, 949-963.

Dasgupta, P.K, Dong, S. and Hwang, H. (1990): Aerosol Science and Technology 12, 98-104

Dimitriades, B. (1999): "Scientific Basis of an Improved EPA Policy on Control of Organic Emissions for Ambient Ozone Reduction," J. Air & Waste Manage. Assoc. 49, 831-838

Dodge, M. C. (1984): "Combined effects of organic reactivity and NMHC/NOx ratio on photochemical oxidant formation -- a modeling study," Atmos. Environ., 18, 1657.

EPA (1984): "Guideline for Using the Carbon Bond Mechanism in City-Specific EKMA," EPA-450/4-84-005, February.

Gery, M. W., R. D. Edmond and G. Z. Whitten (1987): "Tropospheric Ultraviolet Radiation. Assessment of Existing Data and Effects on Ozone Formation," Final Report, EPA-600/3-87-047, October.

Gipson, G. L., W. P. Freas, R. A. Kelly and E. L. Meyer (1981): "Guideline for Use of City-Specific EKMA in Preparing Ozone SIPs, EPA-450/4-80-027, March.

Gipson, G. L. and W. P. Freas (1983): "Use of City-Specific EKMA in the Ozone RIA," U. S. Environmental Protection Agency, July.

Johnson, G. M. (1983): "Factors Affecting Oxidant Formation in Sydney Air," in "The Urban Atmosphere -- Sydney, a Case Study." Eds. J. N. Carras and G. M. Johnson (CSIRO, Melbourne), pp. 393-408.

Jeffries, H. E. (1991): "UNC Solar Radiation Models," unpublished draft report for EPA Cooperative Agreements CR813107, CR813964 and CR815779".

Jeffries, H. E., K. G. Sexton, J. R. Arnold, and T. L. Kale (1989): "Validation Testing of New Mechanisms with Outdoor Chamber Data. Volume 2: Analysis of VOC Data for the CB4 and CAL Photochemical Mechanisms," Final Report, EPA-600/3-89-010b.

Jeffries, H. E. and R. Crouse (1991): "Scientific and Technical Issues Related to the Application of Incremental Reactivity. Part II: Explaining Mechanism Differences," Report prepared for Western States Petroleum Association, Glendale, CA, October.

Kwok, E. S. C., and R. Atkinson (1995): "Estimation of Hydroxyl Radical Reaction Rate Constants for Gas-Phase Organic Compounds Using a Structure-Reactivity Relationship: An Update," Atmos. Environ 29, 1685-1695.

Lurmann, F. W. and H. H. Main (1992): "Analysis of the Ambient VOC Data Collected in the Southern California Air Quality Study," Final Report to California Air Resources Board Contract No. A832-130, February.

McBride, S., M. Oravetz, and A.G. Russell. 1997. "Cost-Benefit and Uncertainty Issues Using Organic Reactivity to Regulate Urban Ozone." Environ. Sci. Technol. 35, A238-44.

RRWG (1999): “VOC Reactivity Policy White Paper,” Prepared by the Reactivity Research Work Group Policy Team, October 1. Available at http://www.cgenv.com/Narsto/reactinfo.html.

Tuazon, E. C., S. M. Aschmann, R. Atkinson, and W. P. L. Carter (1998): “The reactions of Selected Acetates with the OH radical in the Presence of NO: Novel Rearrangement of Alkoxy Radicals of Structure RC(O)OCH(O.)R'“, J. Phys. Chem A 102, 2316-2321.

Wang, L, J. B. Milford, and W. P. L. Carter (2000): “Reactivity Estimates for Aromatic Compounds 2. Uncertainty in Incremental Reactivities,” Atmos. Environ. In press.

Wallington, T. J., Y. Ninomiya, M. Mashino, M. Kawasaki, V. L. Orkin, R. E. Huie, M. J. Kurylo and W. P. L. Carter (2000): “Atmospheric Oxidation Mechanism of Methyl Pivalate, $(CH_3)_3CC(O)$-OCH_3,” Manuscript in preparation.

Wollenhaupt, M, S. A. Carl, A. Horowitz, and J. N. Crowley (2000): “Rate Coefficients for Reaction of OH with Acetone between 202 and 395 K,” J. Phys. Chem. A 2000, 104, 2695-2705.

Zafonte, L., P. L. Rieger, and J. R. Holmes (1977): "Nitrogen Dioxide Photolysis in the Los Angeles Atmosphere," Environ. Sci. Technol. 11, 483-487.

APPENDIX A.
MECHANISM LISTING AND TABULATIONS

This Appendix gives a complete listing of the mechanisms used in the model simulations in this report. Table A-1 contains a list of all the model species used in the mechanism, and Table A-2 lists the reactions and rate parameters, and Table A-3 lists the absorption cross sections and quantum yields for the photolysis reactions. In addition, Finally, Table A-4 gives the chamber-dependent parameters used in the model simulations of the chamber experiments.

Table A-1. Listing of the model species in the mechanism used in the model simulations discussed in this report.

Type and Name	Description
	Species used in Base Mechanism
Constant Species.	
O2	Oxygen
M	Air
H2O	Water
H2	Hydrogen Molecules
HV	Light
Active Inorganic Species.	
O3	Ozone
NO	Nitric Oxide
NO2	Nitrogen Dioxide
NO3	Nitrate Radical
N2O5	Nitrogen Pentoxide
HONO	Nitrous Acid
HNO3	Nitric Acid
HNO4	Peroxynitric Acid
HO2H	Hydrogen Peroxide
CO	Carbon Monoxide
SO2	Sulfur Dioxide
Active Radical Species and Operators.	
HO.	Hydroxyl Radicals
HO2.	Hydroperoxide Radicals
C-O2.	Methyl Peroxy Radicals
RO2-R.	Peroxy Radical Operator representing NO to NO2 conversion with HO2 formation.
R2O2.	Peroxy Radical Operator representing NO to NO2 conversion without HO2 formation.
RO2-N.	Peroxy Radical Operator representing NO consumption with organic nitrate formation.
CCO-O2.	Acetyl Peroxy Radicals
RCO-O2.	Peroxy Propionyl and higher peroxy acyl Radicals
BZCO-O2.	Peroxyacyl radical formed from Aromatic Aldehydes
MA-RCO3.	Peroxyacyl radicals formed from methacrolein and other acroleins.
Steady State Radical Species	
O3P	Ground State Oxygen Atoms
O*1D2	Excited Oxygen Atoms
TBU-O.	t-Butoxy Radicals
BZ-O.	Phenoxy Radicals
BZ(NO2)-O.	Nitro-substituted Phenoxy Radical
HOCOO.	Radical formed when Formaldehyde reacts with HO2
PAN and PAN Analogues	
PAN	Peroxy Acetyl Nitrate
PAN2	PPN and other higher alkyl PAN analogues
PBZN	PAN analogues formed from Aromatic Aldehydes
MA-PAN	PAN analogue formed from Methacrolein
Explicit and Lumped Molecule Reactive Organic Product Species	

Table A-1 (continued)

Type and Name	Description
HCHO	Formaldehyde
CCHO	Acetaldehyde
RCHO	Lumped C3+ Aldehydes
ACET	Acetone
MEK	Ketones and other non-aldehyde oxygenated products that react with OH radicals slower than 5 x 10^{-12} cm^3 $molec^{-2}$ sec^{-1}.
MEOH	Methanol
COOH	Methyl Hydroperoxide
ROOH	Lumped higher organic hydroperoxides
GLY	Glyoxal
MGLY	Methyl Glyoxal
BACL	Biacetyl
PHEN	Phenol
CRES	Cresols
NPHE	Nitrophenols
BALD	Aromatic aldehydes (e.g., benzaldehyde)
METHACRO	Methacrolein
MVK	Methyl Vinyl Ketone
ISO-PROD	Lumped isoprene product species
<u>Lumped Parameter Products</u>	
PROD2	Ketones and other non-aldehyde oxygenated products that react with OH radicals faster than 5 x 10^{-12} cm^3 $molec^{-2}$ sec^{-1}.
RNO3	Lumped Organic Nitrates
<u>Uncharacterized Reactive Aromatic Ring Fragmentation Products</u>	
DCB1	Reactive Aromatic Fragmentation Products that do not undergo significant photodecomposition to radicals.
DCB2	Reactive Aromatic Fragmentation Products which photolyze with alpha-dicarbonyl-like action spectrum.
DCB3	Reactive Aromatic Fragmentation Products which photolyze with acrolein action spectrum.
<u>Non-Reacting Species</u>	
CO2	Carbon Dioxide
XC	Lost Carbon
XN	Lost Nitrogen
SULF	Sulfates (SO_3 or H_2SO_4)
<u>Low Reactivity Compounds or Unknown Products Represented as Unreactive</u>	
H2	Hydrogen
HCOOH	Formic Acid
CCO-OH	Acetic Acid
RCO-OH	Higher organic acids
CCO-OOH	Peroxy Acetic Acid
RCO-OOH	Higher organic peroxy acids
NROG	Unspecified Unreactive Carbon

Table A-1 (continued)

Type and Name	Description
	Base ROG VOC Species and Test Compounds Used in the Chamber Simulations
N-C4	n-Butane
N-C6	n-Hexane
N-C8	n-Octane
ETHENE	Ethene
PROPENE	Propene
T-2-BUTE	*Trans*-2-Butene
TOLUENE	Toluene
M-XYLENE	m-Xylene
ME-PVAT	Methyl Pivalate
	Explicit and Lumped VOC Species used in the Ambient Simulations
Primary Organics Represented explicitly	
CH4	Methane
ETHENE	Ethene
ISOPRENE	Isoprene
Example Test VOCs not in the Base Mechanism	
ETHANE	Ethane
Lumped Parameter Species	
ALK1	Alkanes and other non-aromatic compounds that react only with OH, and have kOH < 5 x 10^2 ppm-1 min-1. (Primarily ethane)
ALK2	Alkanes and other non-aromatic compounds that react only with OH, and have kOH between 5 x 10^2 and 2.5 x 10^3 ppm-1 min-1. (Primarily propane and acetylene)
ALK3	Alkanes and other non-aromatic compounds that react only with OH, and have kOH between 2.5 x 10^3 and 5 x 10^3 ppm-1 min-1.
ALK4	Alkanes and other non-aromatic compounds that react only with OH, and have kOH between 5 x 10^3 and 1 x 10^4 ppm-1 min-1.
ALK5	Alkanes and other non-aromatic compounds that react only with OH, and have kOH greater than 1 x 10^4 ppm-1 min-1.
ARO1	Aromatics with kOH < 2x10^4 ppm-1 min-1.
ARO2	Aromatics with kOH > 2x10^4 ppm-1 min-1.
OLE1	Alkenes (other than ethene) with kOH < 7x10^4 ppm-1 min-1.
OLE2	Alkenes with kOH > 7x10^4 ppm-1 min-1.
TERP	Terpenes

Table A-2. Listing of the reactions in the mechanism used in the model simulations discussed in this report. See Carter (2000) for documentation.

Label	Rate Parameters [a] k(298)	A	Ea	B	Reaction and Products [b]
Inorganic Reactions					
1		Phot Set= NO2			NO2 + HV = NO + O3P
2	5.79e-34	5.68e-34	0.00	-2.8	O3P + O2 + M = O3 + M
3	7.96e-15	8.00e-12	4.09		O3P + O3 = #2 O2
4	1.01e-31	1.00e-31	0.00	-1.6	O3P + NO + M = NO2 + M
5	9.72e-12	6.50e-12	-0.24		O3P + NO2 = NO + O2
6	1.82e-12	Falloff, F=0.80			O3P + NO2 = NO3 + M
	0:	9.00e-32	0.00	-2.0	
	inf:	2.20e-11	0.00	0.0	
8	1.81e-14	1.80e-12	2.72		O3 + NO = NO2 + O2
9	3.52e-17	1.40e-13	4.91		O3 + NO2 = O2 + NO3
10	2.60e-11	1.80e-11	-0.22		NO + NO3 = #2 NO2
11	1.95e-38	3.30e-39	-1.05		NO + NO + O2 = #2 NO2
12	1.54e-12	Falloff, F=0.45			NO2 + NO3 = N2O5
	0:	2.80e-30	0.00	-3.5	
	inf:	2.00e-12	0.00	0.2	
13	5.28e-2	Falloff, F=0.45			N2O5 = NO2 + NO3
	0:	1.00e-3	21.86	-3.5	
	inf:	9.70e+14	22.02	0.1	
14	2.60e-22	2.60e-22			N2O5 + H2O = #2 HNO3
15		(Slow)			N2O5 + HV = NO3 + NO + O3P
16		(Slow)			N2O5 + HV = NO3 + NO2
17	6.56e-16	4.50e-14	2.50		NO2 + NO3 = NO + NO2 + O2
18		Phot Set= NO3NO			NO3 + HV = NO + O2
19		Phot Set= NO3NO2			NO3 + HV = NO2 + O3P
20		Phot Set= O3O3P			O3 + HV = O3P + O2
21		Phot Set= O3O1D			O3 + HV = O*1D2 + O2
22	2.20e-10	2.20e-10			O*1D2 + H2O = #2 HO.
23	2.87e-11	2.09e-11	-0.19		O*1D2 + M = O3P + M
24	7.41e-12	Falloff, F=0.60			HO. + NO = HONO
	0:	7.00e-31	0.00	-2.6	
	inf:	3.60e-11	0.00	-0.1	
25		Phot Set= HONO-NO			HONO + HV = HO. + NO
26		Phot Set= HONO-NO2			HONO + HV = HO2. + NO2
27	6.46e-12	2.70e-12	-0.52		HO. + HONO = H2O + NO2
28	8.98e-12	Falloff, F=0.60			HO. + NO2 = HNO3
	0:	2.43e-30	0.00	-3.1	
	inf:	1.67e-11	0.00	-2.1	
29	2.00e-11	2.00e-11			HO. + NO3 = HO2. + NO2
30	1.47e-13	k = k0+k3M/(1+k3M/k2)			HO. + HNO3 = H2O + NO3
	k0:	7.20e-15	-1.56	0.0	
	k2:	4.10e-16	-2.86	0.0	
	k3:	1.90e-33	-1.44	0.0	
31		Phot Set= HNO3			HNO3 + HV = HO. + NO2
32	2.09e-13	k = k1 + k2 [M]			HO. + CO = HO2. + CO2
	k1:	1.30e-13	0.00	0.0	
	k2:	3.19e-33	0.00	0.0	
33	6.63e-14	1.90e-12	1.99		HO. + O3 = HO2. + O2

Table A-2 (continued)

Label	k(298)	A	Ea	B	Reaction and Products [b]
34	8.41e-12	3.40e-12	-0.54		HO2. + NO = HO. + NO2
35	1.38e-12	Falloff, F=0.60			HO2. + NO2 = HNO4
	0:	1.80e-31	0.00	-3.2	
	inf:	4.70e-12	0.00	0.0	
36	7.55e-2	Falloff, F=0.50			HNO4 = HO2. + NO2
	0:	4.10e-5	21.16	0.0	
	inf:	5.70e+15	22.20	0.0	
37		Phot Set= HO2NO2			HNO4 + HV = #.61 {HO2. + NO2} + #.39 {HO. + NO3}
38	5.02e-12	1.50e-12	-0.72		HNO4 + HO. = H2O + NO2 + O2
39	1.87e-15	1.40e-14	1.19		HO2. + O3 = HO. + #2 O2
40A	2.87e-12	k = k1 + k2 [M]			HO2. + HO2. = HO2H + O2
	k1:	2.20e-13	-1.19	0.0	
	k2:	1.85e-33	-1.95	0.0	
40B	6.46e-30	k = k1 + k2 [M]			HO2. + HO2. + H2O = HO2H + O2 + H2O
	k1:	3.08e-34	-5.56	0.0	
	k2:	2.59e-54	-6.32	0.0	
41	4.00e-12	4.00e-12			NO3 + HO2. = #.8 {HO. + NO2 + O2} + #.2 {HNO3 + O2}
42	2.28e-16	8.50e-13	4.87		NO3 + NO3 = #2 NO2 + O2
43		Phot Set= H2O2			HO2H + HV = #2 HO.
44	1.70e-12	2.90e-12	0.32		HO2H + HO. = HO2. + H2O
45	1.11e-10	4.80e-11	-0.50		HO. + HO2. = H2O + O2
S2OH	9.77e-13	Falloff, F=0.45			HO. + SO2 = HO2. + SULF
	0:	4.00e-31	0.00	-3.3	
	inf:	2.00e-12	0.00	0.0	
H2OH	6.70e-15	7.70e-12	4.17		HO. + H2 = HO2. + H2O
Methyl peroxy and methoxy reactions					
MER1	7.29e-12	2.80e-12	-0.57		C-O2. + NO = NO2 + HCHO + HO2.
MER4	5.21e-12	3.80e-13	-1.55		C-O2. + HO2. = COOH + O2
MEN3	1.30e-12	1.30e-12			C-O2. + NO3 = HCHO + HO2. + NO2
MER5	2.65e-13	2.45e-14	-1.41		C-O2. + C-O2. = MEOH + HCHO + O2
MER6	1.07e-13	5.90e-13	1.01		C-O2. + C-O2. = #2 {HCHO + HO2.}
Peroxy Racical Operators					
RRNO	9.04e-12	2.70e-12	-0.72		RO2-R. + NO = NO2 + HO2.
RRH2	1.49e-11	1.90e-13	-2.58		RO2-R. + HO2. = ROOH + O2 + #-3 XC
RRN3	2.30e-12	2.30e-12			RO2-R. + NO3 = NO2 + O2 + HO2.
RRME	2.00e-13	2.00e-13			RO2-R. + C-O2. = HO2. + #.75 HCHO + #.25 MEOH
RRR2	3.50e-14	3.50e-14			RO2-R. + RO2-R. = HO2.
R2NO		Same k as rxn RRNO			R2O2. + NO = NO2
R2H2		Same k as rxn RRH2			R2O2. + HO2. = HO2.
R2N3		Same k as rxn RRN3			R2O2. + NO3 = NO2
R2ME		Same k as rxn RRME			R2O2. + C-O2. = C-O2.
R2RR		Same k as rxn RRR2			R2O2. + RO2-R. = RO2-R.
R2R3		Same k as rxn RRR2			R2O2. + R2O2. =
RNNO		Same k as rxn RRNO			RO2-N. + NO = RNO3
RNH2		Same k as rxn RRH2			RO2-N. + HO2. = ROOH + #3 XC
RNME		Same k as rxn RRME			RO2-N. + C-O2. = HO2. + #.25 MEOH + #.5 {MEK + PROD2} + #.75 HCHO + XC
RNN3		Same k as rxn RRN3			RO2-N. + NO3 = NO2 + O2 + HO2. + MEK + #2 XC

Rate Parameters [a]

Table A-2 (continued)

Label	k(298)	A	Ea	B	Reaction and Products [b]
	Rate Parameters [a]				
RNRR	Same k as rxn RRR2				RO2-N. + RO2-R. = HO2. + #.5 {MEK + PROD2} + O2 + XC
RNR2	Same k as rxn RRR2				RO2-N. + R2O2. = RO2-N.
RNRN	Same k as rxn RRR2				RO2-N. + RO2-N. = MEK + HO2. + PROD2 + O2 + #2 XC
APN2	1.05e-11	Falloff, F=0.30			CCO-O2. + NO2 = PAN
	0:	2.70e-28	0.00	-7.1	
	inf:	1.20e-11	0.00	-0.9	
DPAN	5.21e-4	Falloff, F=0.30			PAN = CCO-O2. + NO2
	0:	4.90e-3	24.05	0.0	
	inf:	4.00e+16	27.03	0.0	
APNO	2.13e-11	7.80e-12	-0.60		CCO-O2. + NO = C-O2. + CO2 + NO2
APH2	1.41e-11	4.30e-13	-2.07		CCO-O2. + HO2. = #.75 {CCO-OOH +O2} + #.25 {CCO-OH + O3}
APN3	4.00e-12	4.00e-12			CCO-O2. + NO3 = C-O2. + CO2 + NO2 + O2
APME	9.64e-12	1.80e-12	-0.99		CCO-O2. + C-O2. = CCO-OH + HCHO + O2
APRR	7.50e-12	7.50e-12			CCO-O2. + RO2-R. = CCO-OH
APR2	Same k as rxn APRR				CCO-O2. + R2O2. = CCO-O2.
APRN	Same k as rxn APRR				CCO-O2. + RO2-N. = CCO-OH + PROD2
APAP	1.55e-11	2.90e-12	-0.99		CCO-O2. + CCO-O2. = #2 {C-O2. + CO2} + O2
PPN2	1.21e-11	1.20e-11	0.00	-0.9	RCO-O2. + NO2 = PAN2
PAN2	4.43e-4	2.00e+15	25.44		PAN2 = RCO-O2. + NO2
PPNO	2.80e-11	1.25e-11	-0.48		RCO-O2. + NO = NO2 + CCHO + RO2-R. + CO2
PPH2	Same k as rxn APH2				RCO-O2. + HO2. = #.75 {RCO-OOH + O2} + #.25 {RCO-OH + O3}
PPN3	Same k as rxn APN3				RCO-O2. + NO3 = NO2 + CCHO + RO2-R. + CO2 + O2
PPME	Same k as rxn APME				RCO-O2. + C-O2. = RCO-OH + HCHO + O2
PPRR	Same k as rxn APRR				RCO-O2. + RO2-R. = RCO-OH + O2
PPR2	Same k as rxn APRR				RCO-O2. + R2O2. = RCO-O2.
PPRN	Same k as rxn APRR				RCO-O2. + RO2-N. = RCO-OH + PROD2 + O2
PPAP	Same k as rxn APAP				RCO-O2. + CCO-O2. = #2 CO2 + C-O2. + CCHO + RO2-R. + O2
PPPP	Same k as rxn APAP				RCO-O2. + RCO-O2. = #2 {CCHO + RO2-R. + CO2}
BPN2	1.37e-11	1.37e-11			BZCO-O2. + NO2 = PBZN
BPAN	3.12e-4	7.90e+16	27.82		PBZN = BZCO-O2. + NO2
BPNO	Same k as rxn PPNO				BZCO-O2. + NO = NO2 + CO2 + BZ-O. + R2O2.
BPH2	Same k as rxn APH2				BZCO-O2. + HO2. = #.75 {RCO-OOH + O2} + #.25 {RCO-OH + O3} + #4 XC
BPN3	Same k as rxn APN3				BZCO-O2. + NO3 = NO2 + CO2 + BZ-O. + R2O2. + O2
BPME	Same k as rxn APME				BZCO-O2. + C-O2. = RCO-OH + HCHO + O2 + #4 XC
BPRR	Same k as rxn APRR				BZCO-O2. + RO2-R. = RCO-OH + O2 + #4 XC
BPR2	Same k as rxn APRR				BZCO-O2. + R2O2. = BZCO-O2.
BPRN	Same k as rxn APRR				BZCO-O2. + RO2-N. = RCO-OH + PROD2 + O2 + #4 XC
BPAP	Same k as rxn APAP				BZCO-O2. + CCO-O2. = #2 CO2 + C-O2. + BZ-O. + R2O2.
BPPP	Same k as rxn APAP				BZCO-O2. + RCO-O2. = #2 CO2 + CCHO + RO2-R. + BZ-O. + R2O2.
BPBP	Same k as rxn APAP				BZCO-O2. + BZCO-O2. = #2 {BZ-O. + R2O2. + CO2}
MPN2	Same k as rxn PPN2				MA-RCO3. + NO2 = MA-PAN
MPPN	3.55e-4	1.60e+16	26.80		MA-PAN = MA-RCO3. + NO2
MPNO	Same k as rxn PPNO				MA-RCO3. + NO = NO2 + CO2 + HCHO + CCO-O2.
MPH2	Same k as rxn APH2				MA-RCO3. + HO2. = #.75 {RCO-OOH + O2} + #.25 {RCO-OH + O3} + XC

Table A-2 (continued)

Label	Rate Parameters [a] k(298)	A	Ea	B	Reaction and Products [b]
MPN3	Same k as rxn APN3				MA-RCO3. + NO3 = NO2 + CO2 + HCHO + CCO-O2. + O2
MPME	Same k as rxn APME				MA-RCO3. + C-O2. = RCO-OH + HCHO + XC + O2
MPRR	Same k as rxn APRR				MA-RCO3. + RO2-R. = RCO-OH + XC
MPR2	Same k as rxn APRR				MA-RCO3. + R2O2. = MA-RCO3.
MPRN	Same k as rxn APRR				MA-RCO3. + RO2-N. = #2 RCO-OH + O2 + #4 XC
MPAP	Same k as rxn APAP				MA-RCO3. + CCO-O2. = #2 CO2 + C-O2. + HCHO + CCO-O2. + O2
MPPP	Same k as rxn APAP				MA-RCO3. + RCO-O2. = HCHO + CCO-O2. + CCHO + RO2-R. + #2 CO2
MPBP	Same k as rxn APAP				MA-RCO3. + BZCO-O2. = HCHO + CCO-O2. + BZ-O. + R2O2. + #2 CO2
MPMP	Same k as rxn APAP				MA-RCO3. + MA-RCO3. = #2 {HCHO + CCO-O2. + CO2}
<u>Other Organic Radical Species</u>					
TBON	2.40e-11	2.40e-11			TBU-O. + NO2 = RNO3 + #-2 XC
TBOD	9.87e+2	7.50e+14	16.20		TBU-O. = ACET + C-O2.
BRN2	3.80e-11	2.30e-11	-0.30		BZ-O. + NO2 = NPHE
BRH2	Same k as rxn RRH2				BZ-O. + HO2. = PHEN
BRXX	1.00e-3	1.00e-3			BZ-O. = PHEN
BNN2	Same k as rxn BRN2				BZ(NO2)-O. + NO2 = #2 XN + #6 XC
BNH2	Same k as rxn RRH2				BZ(NO2)-O. + HO2. = NPHE
BNXX	Same k as rxn BRXX				BZ(NO2)-O. = NPHE
<u>Explicit and Lumped Molecule Organic Products</u>					
FAHV	Phot Set= HCHO_R				HCHO + HV = #2 HO2. + CO
FAVS	Phot Set= HCHO_M				HCHO + HV = H2 + CO
FAOH	9.20e-12	8.60e-12	-0.04		HCHO + HO. = HO2. + CO + H2O
FAH2	7.90e-14	9.70e-15	-1.24		HCHO + HO2. = HOCOO.
FAHR	1.51e+2	2.40e+12	13.91		HOCOO. = HO2. + HCHO
FAHN	Same k as rxn MER1				HOCOO. + NO = HCOOH + NO2 + HO2.
FAN3	5.74e-16	2.00e-12	4.83		HCHO + NO3 = HNO3 + HO2. + CO
AAOH	1.58e-11	5.60e-12	-0.62		CCHO + HO. = CCO-O2. + H2O
AAHV	Phot Set= CCHO_R				CCHO + HV = CO + HO2. + C-O2.
AAN3	2.73e-15	1.40e-12	3.70		CCHO + NO3 = HNO3 + CCO-O2.
PAOH	2.00e-11	2.00e-11			RCHO + HO. = #.034 RO2-R. + #.001 RO2-N. + #.965 RCO-O2. + #.034 CO + #.034 CCHO + #-0.003 XC
PAHV	Phot Set= C2CHO				RCHO + HV = CCHO + RO2-R. + CO + HO2.
PAN3	3.67e-15	1.40e-12	3.52		RCHO + NO3 = HNO3 + RCO-O2.
K3OH	1.92e-13	1.10e-12	1.03		ACET + HO. = HCHO + CCO-O2. + R2O2.
K3HV	Phot Set= ACETONE				ACET + HV = CCO-O2. + C-O2.
K4OH	1.18e-12	1.30e-12	0.05	2.0	MEK + HO. = #.37 RO2-R. + #.042 RO2-N. + #.616 R2O2. + #.492 CCO-O2. + #.096 RCO-O2. + #.115 HCHO + #.482 CCHO + #.37 RCHO + #.287 XC
K4HV	Phot Set= KETONE, qy= 1.5e-1				MEK + HV = CCO-O2. + CCHO + RO2-R.
MeOH	9.14e-13	3.10e-12	0.72	2.0	MEOH + HO. = HCHO + HO2.
MER9	5.49e-12	2.90e-12	-0.38		COOH + HO. = H2O + #.35 {HCHO + HO.} + #.65 C-O2.
MERA	Phot Set= COOH				COOH + HV = HCHO + HO2. + HO.

Table A-2 (continued)

Label	Rate Parameters [a] k(298)	A	Ea	B	Reaction and Products [b]
LPR9	1.10e-11	1.10e-11			ROOH + HO. = H2O + RCHO + #.34 RO2-R. + #.66 HO.
LPRA	Phot Set= COOH				ROOH + HV = RCHO + HO2. + HO.
GLHV	Phot Set= GLY_R				GLY + HV = #2 {CO + HO2.}
GLVM	Phot Set= GLY_ABS, qy= 6.0e-3				GLY + HV = HCHO + CO
GLOH	1.10e-11	1.10e-11			GLY + HO. = #.63 HO2. + #1.26 CO + #.37 RCO-O2. + #-.37 XC
GLN3	9.63e-16	2.80e-12	4.72		GLY + NO3 = HNO3 + #.63 HO2. + #1.26 CO + #.37 RCO-O2. + #-.37 XC
MGHV	Phot Set= MGLY_ADJ				MGLY + HV = HO2. + CO + CCO-O2.
MGOH	1.50e-11	1.50e-11			MGLY + HO. = CO + CCO-O2.
MGN3	2.43e-15	1.40e-12	3.77		MGLY + NO3 = HNO3 + CO + CCO-O2.
BAHV	Phot Set= BACL_ADJ				BACL + HV = #2 CCO-O2.
PHOH	2.63e-11	2.63e-11			PHEN + HO. = #.24 BZ-O. + #.76 RO2-R. + #.23 GLY + #4.1 XC
PHN3	3.78e-12	3.78e-12			PHEN + NO3 = HNO3 + BZ-O.
CROH	4.20e-11	4.20e-11			CRES + HO. = #.24 BZ-O. + #.76 RO2-R. + #.23 MGLY + #4.87 XC
CRN3	1.37e-11	1.37e-11			CRES + NO3 = HNO3 + BZ-O. + XC
NPN3	Same k as rxn PHN3				NPHE + NO3 = HNO3 + BZ(NO2)-O.
BZOH	1.29e-11	1.29e-11			BALD + HO. = BZCO-O2.
BZHV	Phot Set= BZCHO, qy= 5.0e-2				BALD + HV = #7 XC
BZNT	2.62e-15	1.40e-12	3.72		BALD + NO3 = HNO3 + BZCO-O2.
MAOH	3.36e-11	1.86e-11	-0.35		METHACRO + HO. = #.5 RO2-R. + #.416 CO + #.084 HCHO + #.416 MEK + #.084 MGLY + #.5 MA-RCO3. + #-0.416 XC
MAO3	1.13e-18	1.36e-15	4.20		METHACRO + O3 = #.008 HO2. + #.1 RO2-R. + #.208 HO. + #.1 RCO-O2. + #.45 CO + #.117 CO2 + #.2 HCHO + #.9 MGLY + #.333 HCOOH + #-0.1 XC
MAN3	4.58e-15	1.50e-12	3.43		METHACRO + NO3 = #.5 {HNO3 + RO2-R. + CO +MA-RCO3.} + #1.5 XC + #.5 XN
MAOP	6.34e-12	6.34e-12			METHACRO + O3P = RCHO + XC
MAHV	Phot Set= ACROLEIN, qy= 4.1e-3				METHACRO + HV = #.34 HO2. + #.33 RO2-R. + #.33 HO. + #.67 CCO-O2. + #.67 CO + #.67 HCHO + #.33 MA-RCO3. + #-0 XC
MVOH	1.89e-11	4.14e-12	-0.90		MVK + HO. = #.3 RO2-R. + #.025 RO2-N. + #.675 R2O2. + #.675 CCO-O2. + #.3 HCHO + #.675 RCHO + #.3 MGLY + #-0.725 XC
MVO3	4.58e-18	7.51e-16	3.02		MVK + O3 = #.064 HO2. + #.05 RO2-R. + #.164 HO. + #.05 RCO-O2. + #.475 CO + #.124 CO2 + #.1 HCHO + #.95 MGLY + #.351 HCOOH + #-0.05 XC
MVN3	(Slow)				MVK + NO3 = #4 XC + XN
MVOP	4.32e-12	4.32e-12			MVK + O3P = #.45 RCHO + #.55 MEK + #.45 XC
MVHV	Phot Set= ACROLEIN, qy= 2.1e-3				MVK + HV = #.3 C-O2. + #.7 CO + #.7 PROD2 + #.3 MA-RCO3. + #-2.4 XC
IPOH	6.19e-11	6.19e-11			ISO-PROD + HO. = #.67 RO2-R. + #.041 RO2-N. + #.289 MA-RCO3. + #.336 CO + #.055 HCHO + #.129 CCHO + #.013 RCHO + #.15 MEK + #.332 PROD2 + #.15 GLY + #.174 MGLY + #-0.504 XC

Table A-2 (continued)

Label	k(298)	A	Ea	B	Reaction and Products [b]
IPO3	4.18e-18	4.18e-18			ISO-PROD + O3 = #.4 HO2. + #.048 RO2-R. + #.048 RCO-O2. + #.285 HO. + #.498 CO + #.14 CO2 + #.125 HCHO + #.047 CCHO + #.21 MEK + #.023 GLY + #.742 MGLY + #.1 HCOOH + #.372 RCO-OH + #-.33 XC
IPN3	1.00e-13	1.00e-13			ISO-PROD + NO3 = #.799 RO2-R. + #.051 RO2-N. + #.15 MA-RCO3. + #.572 CO + #.15 HNO3 + #.227 HCHO + #.218 RCHO + #.008 MGLY + #.572 RNO3 + #.28 XN + #-.815 XC
IPHV	Phot Set= ACROLEIN, qy= 4.1e-3				ISO-PROD + HV = #1.233 HO2. + #.467 CCO-O2. + #.3 RCO-O2. + #1.233 CO + #.3 HCHO + #.467 CCHO + #.233 MEK + #-.233 XC
Lumped Parameter Organic Products					
K6OH	1.50e-11	1.50e-11			PROD2 + HO. = #.379 HO2. + #.473 RO2-R. + #.07 RO2-N. + #.029 CCO-O2. + #.049 RCO-O2. + #.213 HCHO + #.084 CCHO + #.558 RCHO + #.115 MEK + #.329 PROD2 + #.886 XC
K6HV	Phot Set= KETONE, qy= 2.0e-2				PROD2 + HV = #.96 RO2-R. + #.04 RO2-N. + #.515 R2O2. + #.667 CCO-O2. + #.333 RCO-O2. + #.506 HCHO + #.246 CCHO + #.71 RCHO + #.299 XC
RNOH	7.80e-12	7.80e-12			RNO3 + HO. = #.338 NO2 + #.113 HO2. + #.376 RO2-R. + #.173 RO2-N. + #.596 R2O2. + #.01 HCHO + #.439 CCHO + #.213 RCHO + #.006 ACET + #.177 MEK + #.048 PROD2 + #.31 RNO3 + #.351 XN + #.56 XC
RNHV	Phot Set= IC3ONO2				RNO3 + HV = NO2 + #.341 HO2. + #.564 RO2-R. + #.095 RO2-N. + #.152 R2O2. + #.134 HCHO + #.431 CCHO + #.147 RCHO + #.02 ACET + #.243 MEK + #.435 PROD2 + #.35 XC
Uncharacterized Reactive Aromatic Ring Fragmentation Products					
D1OH	5.00e-11	5.00e-11			DCB1 + HO. = RCHO + RO2-R. + CO
D1HV		(Slow)			DCB1 + HV = HO2. + #2 CO + RO2-R. + GLY + R2O2.
D1O3	2.00e-18	2.00e-18			DCB1 + O3 = #1.5 HO2. + #.5 HO. + #1.5 CO + #.5 CO2 + GLY
D2OH	5.00e-11	5.00e-11			DCB2 + HO. = R2O2. + RCHO + CCO-O2.
D2HV	Phot Set= MGLY_ABS, qy= 3.7e-1				DCB2 + HV = RO2-R. + #.5 {CCO-O2. + HO2.} + CO + R2O2. + #.5 {GLY + MGLY + XC}
D3OH	5.00e-11	5.00e-11			DCB3 + HO. = R2O2. + RCHO + CCO-O2.
D3HV	Phot Set= ACROLEIN, qy= 7.3e+0				DCB3 + HV = RO2-R. + #.5 {CCO-O2. + HO2.} + CO + R2O2. + #.5 {GLY + MGLY + XC}
Base ROG VOCs Used in the Chamber Simulations and Explicit VOCs in the Ambient Simulations					
c1OH	6.37e-15	2.15e-12	3.45		CH4 + HO. = H2O + C-O2.
c2OH	2.54e-13	1.37e-12	0.99	2.0	ETHANE + HO. = RO2-R. + CCHO
c4OH	2.44e-12	1.52e-12	-0.29	2.0	N-C4 + HO. = #.921 RO2-R. + #.079 RO2-N. + #.413 R2O2. + #.632 CCHO + #.12 RCHO + #.485 MEK + #-0.038 XC
c6OH	5.47e-12	1.38e-12	-0.82	2.0	N-C6 + HO. = #.775 RO2-R. + #.225 RO2-N. + #.787 R2O2. + #.011 CCHO + #.113 RCHO + #.688 PROD2 + #.162 XC
c8OH	8.70e-12	2.48e-12	-0.75	2.0	N-C8 + HO. = #.646 RO2-R. + #.354 RO2-N. + #.786 R2O2. + #.024 RCHO + #.622 PROD2 + #2.073 XC
etOH	8.52e-12	1.96e-12	-0.87		ETHENE + HO. = RO2-R. + #1.61 HCHO + #.195 CCHO
etO3	1.59e-18	9.14e-15	5.13		ETHENE + O3 = #.12 HO. + #.12 HO2. + #.5 CO + #.13 CO2 + HCHO + #.37 HCOOH
etN3	2.05e-16	4.39e-13	4.53	2.0	ETHENE + NO3 = RO2-R. + RCHO + #-1 XC + XN

Table A-2 (continued)

Label	Rate Parameters [a]				Reaction and Products [b]
	k(298)	A	Ea	B	
etOA	7.29e-13	1.04e-11	1.57		ETHENE + O3P = #.5 HO2. + #.2 RO2-R. + #.3 C-O2. + #.491 CO + #.191 HCHO + #.25 CCHO + #.009 GLY + #.5 XC
prOH	2.63e-11	4.85e-12	-1.00		PROPENE + HO. = #.984 RO2-R. + #.016 RO2-N. + #.984 HCHO + #.984 CCHO + #-0.048 XC
prO3	1.01e-17	5.51e-15	3.73		PROPENE + O3 = #.32 HO. + #.06 HO2. + #.26 C-O2. + #.51 CO + #.135 CO2 + #.5 HCHO + #.5 CCHO + #.185 HCOOH + #.17 CCO-OH + #.07 INERT + #.07 XC
prN3	9.49e-15	4.59e-13	2.30		PROPENE + NO3 = #.949 RO2-R. + #.051 RO2-N. + #2.693 XC + XN
prOP	3.98e-12	1.18e-11	0.64		PROPENE + O3P = #.45 RCHO + #.55 MEK + #-0.55 XC
t2OH	6.40e-11	1.01e-11	-1.09		T-2-BUTE + HO. = #.965 RO2-R. + #.035 RO2-N. + #1.93 CCHO + #-0.07 XC
t2O3	1.90e-16	6.64e-15	2.10		T-2-BUTE + O3 = #.52 HO. + #.52 C-O2. + #.52 CO + #.14 CO2 + CCHO + #.34 CCO-OH + #.14 INERT + #.14 XC
t2N3	3.91e-13	1.10e-13	-0.76	2.0	T-2-BUTE + NO3 = #.705 NO2 + #.215 RO2-R. + #.08 RO2-N. + #.705 R2O2. + #1.41 CCHO + #.215 RNO3 + #-0.59 XC + #.08 XN
t2OP	2.18e-11	2.18e-11			T-2-BUTE + O3P = MEK
isOH	9.82e-11	2.50e-11	-0.81		ISOPRENE + HO. = #.907 RO2-R. + #.093 RO2-N. + #.079 R2O2. + #.624 HCHO + #.23 METHACRO + #.32 MVK + #.357 ISO-PROD + #-0.167 XC
isO3	1.28e-17	7.86e-15	3.80		ISOPRENE + O3 = #.266 HO. + #.066 RO2-R. + #.008 RO2-N. + #.126 R2O2. + #.192 MA-RCO3. + #.275 CO + #.122 CO2 + #.592 HCHO + #.1 PROD2 + #.39 METHACRO + #.16 MVK + #.204 HCOOH + #.15 RCO-OH + #-0.259 XC
isN3	6.74e-13	3.03e-12	0.89		ISOPRENE + NO3 = #.187 NO2 + #.749 RO2-R. + #.064 RO2-N. + #.187 R2O2. + #.936 ISO-PROD + #-0.064 XC + #.813 XN
isOP	3.60e-11	3.60e-11			ISOPRENE + O3P = #.01 RO2-N. + #.24 R2O2. + #.25 C-O2. + #.24 MA-RCO3. + #.24 HCHO + #.75 PROD2 + #-1.01 XC
tlOH	5.95e-12	1.81e-12	-0.71	0.0	TOLUENE + HO. = #.234 HO2. + #.758 RO2-R. + #.008 RO2-N. + #.116 GLY + #.135 MGLY + #.234 CRES + #.085 BALD + #.46 DCB1 + #.156 DCB2 + #.057 DCB3 + #1.178 XC
mxOH	2.36e-11	2.36e-11	0.00	0.0	M-XYLENE + HO. = #.21 HO2. + #.782 RO2-R. + #.008 RO2-N. + #.107 GLY + #.335 MGLY + #.21 CRES + #.037 BALD + #.347 DCB1 + #.29 DCB2 + #.108 DCB3 + #1.628 XC
<u>Lumped Organic Species used in the Ambient Reactivity Simulations</u>					
t1OH	8.27e-11	1.83e-11	-0.89		TERP + HO. = #.75 RO2-R. + #.25 RO2-N. + #.5 R2O2. + #.276 HCHO + #.474 RCHO + #.276 PROD2 + #5.146 XC
t1O3	6.88e-17	1.08e-15	1.63		TERP + O3 = #.567 HO. + #.033 HO2. + #.031 RO2-R. + #.18 RO2-N. + #.729 R2O2. + #.123 CCO-O2. + #.201 RCO-O2. + #.157 CO + #.037 CO2 + #.235 HCHO + #.205 RCHO + #.13 ACET + #.276 PROD2 + #.001 GLY + #.031 BACL + #.103 HCOOH + #.189 RCO-OH + #4.183 XC
t1N3	6.57e-12	3.66e-12	-0.35		TERP + NO3 = #.474 NO2 + #.276 RO2-R. + #.25 RO2-N. + #.75 R2O2. + #.474 RCHO + #.276 RNO3 + #5.421 XC + #.25 XN
t1OP	3.27e-11	3.27e-11			TERP + O3P = #.147 RCHO + #.853 PROD2 + #4.441 XC
a1OH	2.54e-13	1.37e-12	0.99	2.0	ALK1 + HO. = RO2-R. + CCHO

Table A-2 (continued)

Label	Rate Parameters [a]				Reaction and Products [b]
	k(298)	A	Ea	B	
a2OH	1.04e-12	9.87e-12	1.33		ALK2 + HO. = #.246 HO. + #.121 HO2. + #.612 RO2-R. + #.021 RO2-N. + #.16 CO + #.039 HCHO + #.155 RCHO + #.417 ACET + #.248 GLY + #.121 HCOOH + #0.338 XC
a3OH	2.38e-12	1.02e-11	0.86		ALK3 + HO. = #.695 RO2-R. + #.07 RO2-N. + #.559 R2O2. + #.236 TBU-O. + #.026 HCHO + #.445 CCHO + #.122 RCHO + #.024 ACET + #.332 MEK + #-0.05 XC
a4OH	4.39e-12	5.95e-12	0.18		ALK4 + HO. = #.835 RO2-R. + #.143 RO2-N. + #.936 R2O2. + #.011 C-O2. + #.011 CCO-O2. + #.002 CO + #.024 HCHO + #.455 CCHO + #.244 RCHO + #.452 ACET + #.11 MEK + #.125 PROD2 + #-0.105 XC
a5OH	9.34e-12	1.11e-11	0.10		ALK5 + HO. = #.653 RO2-R. + #.347 RO2-N. + #.948 R2O2. + #.026 HCHO + #.099 CCHO + #.204 RCHO + #.072 ACET + #.089 MEK + #.417 PROD2 + #2.008 XC
b1OH	5.95e-12	1.81e-12	-0.71		ARO1 + HO. = #.224 HO2. + #.765 RO2-R. + #.011 RO2-N. + #.055 PROD2 + #.118 GLY + #.119 MGLY + #.017 PHEN + #.207 CRES + #.059 BALD + #.491 DCB1 + #.108 DCB2 + #.051 DCB3 + #1.288 XC
b2OH	2.64e-11	2.64e-11	0.00		ARO2 + HO. = #.187 HO2. + #.804 RO2-R. + #.009 RO2-N. + #.097 GLY + #.287 MGLY + #.087 BACL + #.187 CRES + #.05 BALD + #.561 DCB1 + #.099 DCB2 + #.093 DCB3 + #1.68 XC
o1OH	3.23e-11	7.10e-12	-0.90		OLE1 + HO. = #.91 RO2-R. + #.09 RO2-N. + #.205 R2O2. + #.732 HCHO + #.294 CCHO + #.497 RCHO + #.005 ACET + #.119 PROD2 + #.92 XC
o1O3	1.06e-17	2.62e-15	3.26		OLE1 + O3 = #.155 HO. + #.056 HO2. + #.022 RO2-R. + #.001 RO2-N. + #.076 C-O2. + #.345 CO + #.086 CO2 + #.5 HCHO + #.154 CCHO + #.363 RCHO + #.001 ACET + #.215 PROD2 + #.185 HCOOH + #.05 CCO-OH + #.119 RCO-OH + #.654 XC
o1N3	1.26e-14	4.45e-14	0.75		OLE1 + NO3 = #.824 RO2-R. + #.176 RO2-N. + #.488 R2O2. + #.009 CCHO + #.037 RCHO + #.024 ACET + #.511 RNO3 + #.677 XC + #.489 XN
o1OP	4.90e-12	1.07e-11	0.47		OLE1 + O3P = #.45 RCHO + #.437 MEK + #.113 PROD2 + #1.224 XC
o2OH	6.33e-11	1.74e-11	-0.76		OLE2 + HO. = #.918 RO2-R. + #.082 RO2-N. + #.001 R2O2. + #.244 HCHO + #.732 CCHO + #.511 RCHO + #.127 ACET + #.072 MEK + #.061 BALD + #.025 METHACRO + #.025 ISO-PROD + #-.054 XC
o2O3	1.07e-16	5.02e-16	0.92		OLE2 + O3 = #.378 HO. + #.003 HO2. + #.033 RO2-R. + #.002 RO2-N. + #.137 R2O2. + #.197 C-O2. + #.137 CCO-O2. + #.006 RCO-O2. + #.265 CO + #.07 CO2 + #.269 HCHO + #.456 CCHO + #.305 RCHO + #.045 ACET + #.026 MEK + #.006 PROD2 + #.042 BALD + #.026 METHACRO + #.073 HCOOH + #.129 CCO-OH + #.303 RCO-OH + #.155 XC
o2N3	7.27e-13	7.27e-13	0.00		OLE2 + NO3 = #.391 NO2 + #.442 RO2-R. + #.136 RO2-N. + #.711 R2O2. + #.03 C-O2. + #.079 HCHO + #.507 CCHO + #.151 RCHO + #.102 ACET + #.001 MEK + #.015 BALD + #.048 MVK + #.321 RNO3 + #.075 XC + #.288 XN
o2OP	2.09e-11	2.09e-11			OLE2 + O3P = #.013 HO2. + #.012 RO2-R. + #.001 RO2-N. + #.012 CO + #.069 RCHO + #.659 MEK + #.259 PROD2 + #.012 METHACRO + #.537 XC

Table A-2 (continued)

Label	Rate Parameters [a] k(298)	A	Ea	B	Reaction and Products [b]
Test Compound Studied for This Project [c]					
	1.18e-12	1.18e-12			ME-PVAT + HO. = #.328 RO2-R. + #.175 RO2-N. + #1.198 R2O2. + #.497 RCO-O2. + #.194 CO + #.619 HCHO + #.034 RCHO + #.497 ACET + #.1 MEK + #.194 RCO-OH + #.07 XC

[a] Except as indicated, the rate constants are given by $k(T) = A \cdot (T/300)^B \cdot e^{-Ea/RT}$, where the units of k and A are $cm^3\ molec^{-1}\ s^{-1}$, Ea are $kcal\ mol^{-1}$, T is ^oK, and R=0.0019872 $kcal\ mol^{-1}\ deg^{-1}$. The following special rate constant expressions are used:

Phot Set = *name*: The absorption cross sections and quantum yields for the photolysis reaction are given in Table A-5, where "*name*" indicates the photolysis set used. If a "qy=*number*" notation is given, the number given is the overall quantum yield, which is assumed to be wavelength independent.

Falloff: The rate constant as a function of temperature and pressure is calculated using $k(T,M) = \{k0(T)\cdot[M]/[1 + k0(T)\cdot[M]/kinf(T)]\} \cdot F^Z$, where $Z = \{1 + [\log_{10}\{k0(T)\cdot[M])/kinf(T)\}]^2\}^{-1}$, [M] is the total pressure in molecules cm^{-3}, F is as indicated on the table, and the temperature dependences of k0 and kinf are as indicated on the table.

(Slow): The reaction is assumed to be negligible and is not included in the mechanism. It is shown on the listing for documentation purposes only.

k = k0+k3M(1+k3M/k2): The rate constant as a function of temperature and pressure is calculated using $k(T,M) = k0(T) + k3(T)\cdot[M]\ \cdot(1 + k3(T)\cdot[M]/k2(T))$, where [M] is the total bath gas (air) concentration in molecules cm^{-3}, and the temperature dependences for k0, k2 and k3 are as indicated on the table.

k = k1 + k2 [M]: The rate constant as a function of temperature and pressure is calculated using $k(T,M) = k1(T) + k2(T)\cdot[M]$, where [M] is the total bath gas (air) concentration in molecules cm^{-3}, and the temperature dependences for k1, and k2 are as indicated on the table.

Same k as Rxn *label*: The rate constant is the same as the reaction with the indicated label.

[b] Format of reaction listing: "=" separates reactants from products; "#*number*" indicates stoichiometric coefficient, "#*coefficient* { *product list* }" means that the stoichiometric coefficient is applied to all the products listed. See Table A-1 for a listing of the model species used.

[c] Best fit or adjusted mechanisms derived as discussed in the text.

Table A-3. Listing of the absorption cross sections and quantum yields for the photolysis reactions.

WL (nm)	Abs (cm^2)	QY	WL (nm)	Abs (cm^2)	QY	WL (nm)	Abs (cm^2)	QY	WL (nm)	Abs (cm^2)	QY	WL (nm)	Abs (cm^2)	QY
							NO2							
205.0	4.31e-19	1.000	210.0	4.72e-19	1.000	215.0	4.95e-19	1.000	220.0	4.56e-19	1.000	225.0	3.79e-19	1.000
230.0	2.74e-19	1.000	235.0	1.67e-19	1.000	240.0	9.31e-20	1.000	245.0	4.74e-20	1.000	250.0	2.48e-20	1.000
255.0	1.95e-20	1.000	260.0	2.24e-20	1.000	265.0	2.73e-20	1.000	270.0	4.11e-20	1.000	275.0	4.90e-20	1.000
280.0	5.92e-20	1.000	285.0	7.39e-20	1.000	290.0	9.00e-20	1.000	295.0	1.09e-19	1.000	300.0	1.31e-19	1.000
305.0	1.57e-19	1.000	310.0	1.86e-19	1.000	315.0	2.15e-19	0.990	320.0	2.48e-19	0.990	325.0	2.81e-19	0.990
330.0	3.13e-19	0.990	335.0	3.43e-19	0.990	340.0	3.80e-19	0.990	345.0	4.07e-19	0.990	350.0	4.31e-19	0.990
355.0	4.72e-19	0.990	360.0	4.83e-19	0.980	365.0	5.17e-19	0.980	370.0	5.32e-19	0.980	375.0	5.51e-19	0.980
380.0	5.64e-19	0.970	385.0	5.76e-19	0.970	390.0	5.93e-19	0.960	395.0	5.85e-19	0.935	400.0	6.02e-19	0.820
405.0	5.78e-19	0.355	410.0	6.00e-19	0.130	411.0	5.93e-19	0.110	412.0	5.86e-19	0.094	413.0	5.79e-19	0.083
414.0	5.72e-19	0.070	415.0	5.65e-19	0.059	416.0	5.68e-19	0.048	417.0	5.71e-19	0.039	418.0	5.75e-19	0.030
419.0	5.78e-19	0.023	420.0	5.81e-19	0.018	421.0	5.72e-19	0.012	422.0	5.64e-19	0.008	423.0	5.55e-19	0.004
424.0	5.47e-19	0.000												
							NO3NO							
585.0	2.89e-18	0.000	586.0	3.32e-18	0.050	587.0	4.16e-18	0.100	588.0	5.04e-18	0.150	589.0	6.13e-18	0.200
590.0	5.96e-18	0.250	591.0	5.44e-18	0.280	592.0	5.11e-18	0.310	593.0	4.58e-18	0.340	594.0	4.19e-18	0.370
595.0	4.29e-18	0.400	596.0	4.62e-18	0.370	597.0	4.36e-18	0.340	598.0	3.67e-18	0.310	599.0	3.10e-18	0.280
600.0	2.76e-18	0.250	601.0	2.86e-18	0.240	602.0	3.32e-18	0.230	603.0	3.80e-18	0.220	604.0	4.37e-18	0.210
605.0	4.36e-18	0.200	606.0	3.32e-18	0.200	607.0	2.40e-18	0.200	608.0	1.85e-18	0.200	609.0	1.71e-18	0.200
610.0	1.77e-18	0.200	611.0	1.91e-18	0.180	612.0	2.23e-18	0.160	613.0	2.63e-18	0.140	614.0	2.55e-18	0.120
615.0	2.26e-18	0.100	616.0	2.09e-18	0.100	617.0	2.11e-18	0.100	618.0	2.39e-18	0.100	619.0	2.56e-18	0.100
620.0	3.27e-18	0.100	621.0	5.24e-18	0.090	622.0	1.02e-17	0.080	623.0	1.47e-17	0.070	624.0	1.21e-17	0.060
625.0	8.38e-18	0.050	626.0	7.30e-18	0.050	627.0	7.53e-18	0.050	628.0	7.37e-18	0.050	629.0	6.98e-18	0.050
630.0	6.76e-18	0.050	631.0	4.84e-18	0.046	632.0	3.27e-18	0.042	633.0	2.17e-18	0.038	634.0	1.64e-18	0.034
635.0	1.44e-18	0.030	636.0	1.69e-18	0.024	637.0	2.07e-18	0.018	638.0	2.03e-18	0.012	639.0	1.58e-18	0.006
640.0	1.23e-18	0.000												
							NO3NO2							
400.0	0.00e+00	1.000	401.0	0.00e+00	1.000	402.0	0.00e+00	1.000	403.0	2.00e-20	1.000	404.0	0.00e+00	1.000
405.0	3.00e-20	1.000	406.0	2.00e-20	1.000	407.0	1.00e-20	1.000	408.0	3.00e-20	1.000	409.0	0.00e+00	1.000
410.0	1.00e-20	1.000	411.0	2.00e-20	1.000	412.0	5.00e-20	1.000	413.0	5.00e-20	1.000	414.0	2.00e-20	1.000
415.0	6.00e-20	1.000	416.0	6.00e-20	1.000	417.0	7.00e-20	1.000	418.0	5.00e-20	1.000	419.0	8.00e-20	1.000
420.0	8.00e-20	1.000	421.0	8.00e-20	1.000	422.0	9.00e-20	1.000	423.0	1.10e-19	1.000	424.0	9.00e-20	1.000
425.0	7.00e-20	1.000	426.0	1.40e-19	1.000	427.0	1.40e-19	1.000	428.0	1.20e-19	1.000	429.0	1.10e-19	1.000
430.0	1.70e-19	1.000	431.0	1.30e-19	1.000	432.0	1.50e-19	1.000	433.0	1.80e-19	1.000	434.0	1.80e-19	1.000
435.0	1.60e-19	1.000	436.0	1.50e-19	1.000	437.0	1.80e-19	1.000	438.0	2.10e-19	1.000	439.0	2.00e-19	1.000
440.0	1.90e-19	1.000	441.0	1.80e-19	1.000	442.0	2.10e-19	1.000	443.0	1.80e-19	1.000	444.0	1.90e-19	1.000
445.0	2.00e-19	1.000	446.0	2.40e-19	1.000	447.0	2.90e-19	1.000	448.0	2.40e-19	1.000	449.0	2.80e-19	1.000
450.0	2.90e-19	1.000	451.0	3.00e-19	1.000	452.0	3.30e-19	1.000	453.0	3.10e-19	1.000	454.0	3.60e-19	1.000
455.0	3.60e-19	1.000	456.0	3.60e-19	1.000	457.0	4.00e-19	1.000	458.0	3.70e-19	1.000	459.0	4.20e-19	1.000
460.0	4.00e-19	1.000	461.0	3.90e-19	1.000	462.0	4.00e-19	1.000	463.0	4.10e-19	1.000	464.0	4.80e-19	1.000
465.0	5.10e-19	1.000	466.0	5.40e-19	1.000	467.0	5.70e-19	1.000	468.0	5.60e-19	1.000	469.0	5.80e-19	1.000
470.0	5.90e-19	1.000	471.0	6.20e-19	1.000	472.0	6.40e-19	1.000	473.0	6.20e-19	1.000	474.0	6.20e-19	1.000
475.0	6.80e-19	1.000	476.0	7.80e-19	1.000	477.0	7.70e-19	1.000	478.0	7.30e-19	1.000	479.0	7.30e-19	1.000
480.0	7.00e-19	1.000	481.0	7.10e-19	1.000	482.0	7.10e-19	1.000	483.0	7.20e-19	1.000	484.0	7.70e-19	1.000
485.0	8.20e-19	1.000	486.0	9.10e-19	1.000	487.0	9.20e-19	1.000	488.0	9.50e-19	1.000	489.0	9.60e-19	1.000
490.0	1.03e-18	1.000	491.0	9.90e-19	1.000	492.0	9.90e-19	1.000	493.0	1.01e-18	1.000	494.0	1.01e-18	1.000
495.0	1.06e-18	1.000	496.0	1.21e-18	1.000	497.0	1.22e-18	1.000	498.0	1.20e-18	1.000	499.0	1.17e-18	1.000
500.0	1.13e-18	1.000	501.0	1.11e-18	1.000	502.0	1.11e-18	1.000	503.0	1.11e-18	1.000	504.0	1.26e-18	1.000
505.0	1.28e-18	1.000	506.0	1.34e-18	1.000	507.0	1.28e-18	1.000	508.0	1.27e-18	1.000	509.0	1.35e-18	1.000
510.0	1.51e-18	1.000	511.0	1.73e-18	1.000	512.0	1.77e-18	1.000	513.0	1.60e-18	1.000	514.0	1.58e-18	1.000
515.0	1.58e-18	1.000	516.0	1.56e-18	1.000	517.0	1.49e-18	1.000	518.0	1.44e-18	1.000	519.0	1.54e-18	1.000
520.0	1.68e-18	1.000	521.0	1.83e-18	1.000	522.0	1.93e-18	1.000	523.0	1.77e-18	1.000	524.0	1.64e-18	1.000
525.0	1.58e-18	1.000	526.0	1.63e-18	1.000	527.0	1.81e-18	1.000	528.0	2.10e-18	1.000	529.0	2.39e-18	1.000
530.0	2.23e-18	1.000	531.0	2.09e-18	1.000	532.0	2.02e-18	1.000	533.0	1.95e-18	1.000	534.0	2.04e-18	1.000
535.0	2.30e-18	1.000	536.0	2.57e-18	1.000	537.0	2.58e-18	1.000	538.0	2.34e-18	1.000	539.0	2.04e-18	1.000
540.0	2.10e-18	1.000	541.0	2.04e-18	1.000	542.0	1.88e-18	1.000	543.0	1.68e-18	1.000	544.0	1.70e-18	1.000
545.0	1.96e-18	1.000	546.0	2.42e-18	1.000	547.0	2.91e-18	1.000	548.0	2.98e-18	1.000	549.0	2.71e-18	1.000
550.0	2.48e-18	1.000	551.0	2.43e-18	1.000	552.0	2.47e-18	1.000	553.0	2.53e-18	1.000	554.0	2.78e-18	1.000
555.0	3.11e-18	1.000	556.0	3.26e-18	1.000	557.0	3.29e-18	1.000	558.0	3.51e-18	1.000	559.0	3.72e-18	1.000
560.0	3.32e-18	1.000	561.0	2.98e-18	1.000	562.0	2.90e-18	1.000	563.0	2.80e-18	1.000	564.0	2.72e-18	1.000
565.0	2.73e-18	1.000	566.0	2.85e-18	1.000	567.0	2.81e-18	1.000	568.0	2.85e-18	1.000	569.0	2.89e-18	1.000
570.0	2.79e-18	1.000	571.0	2.76e-18	1.000	572.0	2.74e-18	1.000	573.0	2.78e-18	1.000	574.0	2.86e-18	1.000
575.0	3.08e-18	1.000	576.0	3.27e-18	1.000	577.0	3.38e-18	1.000	578.0	3.31e-18	1.000	579.0	3.24e-18	1.000
580.0	3.34e-18	1.000	581.0	3.55e-18	1.000	582.0	3.28e-18	1.000	583.0	2.93e-18	1.000	584.0	2.82e-18	1.000
585.0	2.89e-18	1.000	586.0	3.32e-18	0.950	587.0	4.16e-18	0.900	588.0	5.04e-18	0.850	589.0	6.13e-18	0.800
590.0	5.96e-18	0.750	591.0	5.44e-18	0.720	592.0	5.11e-18	0.690	593.0	4.58e-18	0.660	594.0	4.19e-18	0.630
595.0	4.29e-18	0.600	596.0	4.62e-18	0.590	597.0	4.36e-18	0.580	598.0	3.67e-18	0.570	599.0	3.10e-18	0.560
600.0	2.76e-18	0.550	601.0	2.86e-18	0.540	602.0	3.32e-18	0.530	603.0	3.80e-18	0.520	604.0	4.37e-18	0.510
605.0	4.36e-18	0.400	606.0	3.32e-18	0.380	607.0	2.40e-18	0.360	608.0	1.85e-18	0.340	609.0	1.71e-18	0.320

Table A-3 (continued)

WL (nm)	Abs (cm^2)	QY	WL (nm)	Abs (cm^2)	QY	WL (nm)	Abs (cm^2)	QY	WL (nm)	Abs (cm^2)	QY	WL (nm)	Abs (cm^2)	QY
610.0	1.77e-18	0.300	611.0	1.91e-18	0.290	612.0	2.23e-18	0.280	613.0	2.63e-18	0.270	614.0	2.55e-18	0.260
615.0	2.26e-18	0.250	616.0	2.09e-18	0.240	617.0	2.11e-18	0.230	618.0	2.39e-18	0.220	619.0	2.56e-18	0.210
620.0	3.27e-18	0.200	621.0	5.24e-18	0.190	622.0	1.02e-17	0.180	623.0	1.47e-17	0.170	624.0	1.21e-17	0.160
625.0	8.38e-18	0.150	626.0	7.30e-18	0.130	627.0	7.53e-18	0.110	628.0	7.37e-18	0.090	629.0	6.98e-18	0.070
630.0	6.76e-18	0.050	631.0	4.84e-18	0.040	632.0	3.27e-18	0.030	633.0	2.17e-18	0.020	634.0	1.64e-18	0.010
635.0	1.44e-18	0.000												
							<u>O3O3P</u>							
280.0	3.94e-18	0.095	281.0	3.62e-18	0.093	282.0	3.31e-18	0.090	283.0	2.99e-18	0.088	284.0	2.70e-18	0.086
285.0	2.46e-18	0.084	286.0	2.22e-18	0.082	287.0	1.98e-18	0.079	288.0	1.75e-18	0.077	289.0	1.59e-18	0.075
290.0	1.42e-18	0.073	291.0	1.25e-18	0.070	292.0	1.09e-18	0.068	293.0	9.81e-19	0.066	294.0	8.73e-19	0.064
295.0	7.65e-19	0.061	296.0	6.58e-19	0.059	297.0	5.81e-19	0.057	298.0	5.18e-19	0.055	299.0	4.55e-19	0.052
300.0	3.92e-19	0.050	301.0	3.35e-19	0.035	302.0	3.01e-19	0.025	303.0	2.66e-19	0.015	304.0	2.32e-19	0.010
305.0	1.97e-19	0.020	306.0	1.73e-19	0.050	307.0	1.55e-19	0.123	308.0	1.37e-19	0.227	309.0	1.18e-19	0.333
310.0	9.98e-20	0.400	311.0	8.92e-20	0.612	312.0	7.94e-20	0.697	313.0	6.96e-20	0.738	314.0	5.99e-20	0.762
315.0	5.01e-20	0.765	316.0	4.51e-20	0.779	317.0	4.00e-20	0.791	318.0	3.50e-20	0.806	319.0	2.99e-20	0.822
320.0	2.49e-20	0.852	321.0	2.23e-20	0.879	322.0	1.97e-20	0.903	323.0	1.72e-20	0.908	324.0	1.46e-20	0.920
325.0	1.20e-20	0.930	326.0	1.08e-20	0.934	327.0	9.67e-21	0.938	328.0	8.50e-21	0.942	329.0	7.34e-21	0.946
330.0	6.17e-21	0.950	331.0	5.48e-21	0.950	332.0	4.80e-21	0.950	333.0	4.11e-21	0.950	334.0	3.43e-21	0.950
335.0	2.74e-21	0.950	336.0	2.43e-21	0.960	337.0	2.11e-21	0.970	338.0	1.80e-21	0.980	339.0	1.48e-21	0.990
340.0	1.17e-21	1.000	350.0	0.00e+00	1.000	400.0	0.00e+00	1.000	410.0	1.20e-23	1.000	420.0	2.20e-23	1.000
440.0	1.12e-22	1.000	460.0	3.28e-22	1.000	480.0	6.84e-22	1.000	500.0	1.22e-21	1.000	520.0	1.82e-21	1.000
540.0	2.91e-21	1.000	560.0	3.94e-21	1.000	580.0	4.59e-21	1.000	600.0	5.11e-21	1.000	620.0	4.00e-21	1.000
640.0	2.96e-21	1.000	660.0	2.09e-21	1.000	680.0	1.36e-21	1.000	700.0	9.10e-22	1.000	750.0	3.20e-22	1.000
800.0	1.60e-22	1.000	900.0	0.00e+00	1.000									
							<u>O3O1D</u>							
280.0	3.94e-18	0.905	281.0	3.62e-18	0.907	282.0	3.31e-18	0.910	283.0	2.99e-18	0.912	284.0	2.70e-18	0.914
285.0	2.46e-18	0.916	286.0	2.22e-18	0.918	287.0	1.98e-18	0.921	288.0	1.75e-18	0.923	289.0	1.59e-18	0.925
290.0	1.42e-18	0.927	291.0	1.25e-18	0.930	292.0	1.09e-18	0.932	293.0	9.81e-19	0.934	294.0	8.73e-19	0.936
295.0	7.65e-19	0.939	296.0	6.58e-19	0.941	297.0	5.81e-19	0.943	298.0	5.18e-19	0.945	299.0	4.55e-19	0.948
300.0	3.92e-19	0.950	301.0	3.35e-19	0.965	302.0	3.01e-19	0.975	303.0	2.66e-19	0.985	304.0	2.32e-19	0.990
305.0	1.97e-19	0.980	306.0	1.73e-19	0.950	307.0	1.55e-19	0.877	308.0	1.37e-19	0.773	309.0	1.18e-19	0.667
310.0	9.98e-20	0.600	311.0	8.92e-20	0.388	312.0	7.94e-20	0.303	313.0	6.96e-20	0.262	314.0	5.99e-20	0.238
315.0	5.01e-20	0.235	316.0	4.51e-20	0.221	317.0	4.00e-20	0.209	318.0	3.50e-20	0.194	319.0	2.99e-20	0.178
320.0	2.49e-20	0.148	321.0	2.23e-20	0.121	322.0	1.97e-20	0.097	323.0	1.72e-20	0.092	324.0	1.46e-20	0.080
325.0	1.20e-20	0.070	326.0	1.08e-20	0.066	327.0	9.67e-21	0.062	328.0	8.50e-21	0.058	329.0	7.34e-21	0.054
330.0	6.17e-21	0.050	331.0	5.48e-21	0.050	332.0	4.80e-21	0.050	333.0	4.11e-21	0.050	334.0	3.43e-21	0.050
335.0	2.74e-21	0.050	336.0	2.43e-21	0.040	337.0	2.11e-21	0.030	338.0	1.80e-21	0.020	339.0	1.48e-21	0.010
340.0	1.17e-21	0.000												
							<u>HONO-NO</u>							
309.0	0.00e+00	0.410	310.0	1.30e-20	0.410	311.0	1.90e-20	0.411	312.0	2.80e-20	0.421	313.0	2.20e-20	0.432
314.0	3.60e-20	0.443	315.0	3.00e-20	0.454	316.0	1.40e-20	0.464	317.0	3.10e-20	0.475	318.0	5.60e-20	0.486
319.0	3.60e-20	0.496	320.0	4.90e-20	0.507	321.0	7.80e-20	0.518	322.0	4.90e-20	0.529	323.0	5.10e-20	0.539
324.0	7.10e-20	0.550	325.0	5.00e-20	0.561	326.0	2.90e-20	0.571	327.0	6.60e-20	0.582	328.0	1.17e-19	0.593
329.0	6.10e-20	0.604	330.0	1.11e-19	0.614	331.0	1.79e-19	0.625	332.0	8.70e-20	0.636	333.0	7.60e-20	0.646
334.0	9.60e-20	0.657	335.0	9.60e-20	0.668	336.0	7.20e-20	0.679	337.0	5.30e-20	0.689	338.0	1.00e-19	0.700
339.0	1.88e-19	0.711	340.0	1.00e-19	0.721	341.0	1.70e-19	0.732	342.0	3.86e-19	0.743	343.0	1.49e-19	0.754
344.0	9.70e-20	0.764	345.0	1.09e-19	0.775	346.0	1.23e-19	0.786	347.0	1.04e-19	0.796	348.0	9.10e-20	0.807
349.0	7.90e-20	0.818	350.0	1.12e-19	0.829	351.0	2.12e-19	0.839	352.0	1.55e-19	0.850	353.0	1.91e-19	0.861
354.0	5.81e-19	0.871	355.0	3.64e-19	0.882	356.0	1.41e-19	0.893	357.0	1.17e-19	0.904	358.0	1.20e-19	0.914
359.0	1.04e-19	0.925	360.0	9.00e-20	0.936	361.0	8.30e-20	0.946	362.0	8.00e-20	0.957	363.0	9.60e-20	0.968
364.0	1.46e-19	0.979	365.0	1.68e-19	0.989	366.0	1.83e-19	1.000	367.0	3.02e-19	1.000	368.0	5.20e-19	1.000
369.0	3.88e-19	1.000	370.0	1.78e-19	1.000	371.0	1.13e-19	1.000	372.0	1.00e-19	1.000	373.0	7.70e-20	1.000
374.0	6.20e-20	1.000	375.0	5.30e-20	1.000	376.0	5.30e-20	1.000	377.0	5.00e-20	1.000	378.0	5.80e-20	1.000
379.0	8.00e-20	1.000	380.0	9.60e-20	1.000	381.0	1.13e-19	1.000	382.0	1.59e-19	1.000	383.0	2.10e-19	1.000
384.0	2.41e-19	1.000	385.0	2.03e-19	1.000	386.0	1.34e-19	1.000	387.0	9.00e-20	1.000	388.0	5.60e-20	1.000
389.0	3.40e-20	1.000	390.0	2.70e-20	1.000	391.0	2.00e-20	1.000	392.0	1.50e-20	1.000	393.0	1.10e-20	1.000
394.0	6.00e-21	1.000	395.0	1.00e-20	1.000	396.0	4.00e-21	1.000	400.0	0.00e+00	1.000			
							<u>HONO-NO2</u>							
309.0	0.00e+00	0.590	310.0	1.30e-20	0.590	311.0	1.90e-20	0.589	312.0	2.80e-20	0.579	313.0	2.20e-20	0.568
314.0	3.60e-20	0.557	315.0	3.00e-20	0.546	316.0	1.40e-20	0.536	317.0	3.10e-20	0.525	318.0	5.60e-20	0.514
319.0	3.60e-20	0.504	320.0	4.90e-20	0.493	321.0	7.80e-20	0.482	322.0	4.90e-20	0.471	323.0	5.10e-20	0.461
324.0	7.10e-20	0.450	325.0	5.00e-20	0.439	326.0	2.90e-20	0.429	327.0	6.60e-20	0.418	328.0	1.17e-19	0.407
329.0	6.10e-20	0.396	330.0	1.11e-19	0.386	331.0	1.79e-19	0.375	332.0	8.70e-20	0.364	333.0	7.60e-20	0.354
334.0	9.60e-20	0.343	335.0	9.60e-20	0.332	336.0	7.20e-20	0.321	337.0	5.30e-20	0.311	338.0	1.00e-19	0.300
339.0	1.88e-19	0.289	340.0	1.00e-19	0.279	341.0	1.70e-19	0.268	342.0	3.86e-19	0.257	343.0	1.49e-19	0.246
344.0	9.70e-20	0.236	345.0	1.09e-19	0.225	346.0	1.23e-19	0.214	347.0	1.04e-19	0.204	348.0	9.10e-20	0.193
349.0	7.90e-20	0.182	350.0	1.12e-19	0.171	351.0	2.12e-19	0.161	352.0	1.55e-19	0.150	353.0	1.91e-19	0.139
354.0	5.81e-19	0.129	355.0	3.64e-19	0.118	356.0	1.41e-19	0.107	357.0	1.17e-19	0.096	358.0	1.20e-19	0.086
359.0	1.04e-19	0.075	360.0	9.00e-20	0.064	361.0	8.30e-20	0.054	362.0	8.00e-20	0.043	363.0	9.60e-20	0.032

Table A-3 (continued)

WL (nm)	Abs (cm^2)	QY	WL (nm)	Abs (cm^2)	QY	WL (nm)	Abs (cm^2)	QY	WL (nm)	Abs (cm^2)	QY	WL (nm)	Abs (cm^2)	QY
364.0	1.46e-19	0.021	365.0	1.68e-19	0.011	366.0	1.83e-19	0.000						

HNO3

WL (nm)	Abs (cm^2)	QY	WL (nm)	Abs (cm^2)	QY	WL (nm)	Abs (cm^2)	QY	WL (nm)	Abs (cm^2)	QY	WL (nm)	Abs (cm^2)	QY
190.0	1.36e-17	1.000	195.0	1.02e-17	1.000	200.0	5.88e-18	1.000	205.0	2.80e-18	1.000	210.0	1.04e-18	1.000
215.0	3.65e-19	1.000	220.0	1.49e-19	1.000	225.0	8.81e-20	1.000	230.0	5.75e-20	1.000	235.0	3.75e-20	1.000
240.0	2.58e-20	1.000	245.0	2.11e-20	1.000	250.0	1.97e-20	1.000	255.0	1.95e-20	1.000	260.0	1.91e-20	1.000
265.0	1.80e-20	1.000	270.0	1.62e-20	1.000	275.0	1.38e-20	1.000	280.0	1.12e-20	1.000	285.0	8.58e-21	1.000
290.0	6.15e-21	1.000	295.0	4.12e-21	1.000	300.0	2.63e-21	1.000	305.0	1.50e-21	1.000	310.0	8.10e-22	1.000
315.0	4.10e-22	1.000	320.0	2.00e-22	1.000	325.0	9.50e-23	1.000	330.0	4.30e-23	1.000	335.0	2.20e-23	1.000
340.0	1.00e-23	1.000	345.0	6.00e-24	1.000	350.0	4.00e-24	1.000	355.0	0.00e+00	1.000			

HO2NO2

WL (nm)	Abs (cm^2)	QY	WL (nm)	Abs (cm^2)	QY	WL (nm)	Abs (cm^2)	QY	WL (nm)	Abs (cm^2)	QY	WL (nm)	Abs (cm^2)	QY
190.0	1.01e-17	1.000	195.0	8.16e-18	1.000	200.0	5.63e-18	1.000	205.0	3.67e-18	1.000	210.0	2.39e-18	1.000
215.0	1.61e-18	1.000	220.0	1.18e-18	1.000	225.0	9.32e-19	1.000	230.0	7.88e-19	1.000	235.0	6.80e-19	1.000
240.0	5.79e-19	1.000	245.0	4.97e-19	1.000	250.0	4.11e-19	1.000	255.0	3.49e-19	1.000	260.0	2.84e-19	1.000
265.0	2.29e-19	1.000	270.0	1.80e-19	1.000	275.0	1.33e-19	1.000	280.0	9.30e-20	1.000	285.0	6.20e-20	1.000
290.0	3.90e-20	1.000	295.0	2.40e-20	1.000	300.0	1.40e-20	1.000	305.0	8.50e-21	1.000	310.0	5.30e-21	1.000
315.0	3.90e-21	1.000	320.0	2.40e-21	1.000	325.0	1.50e-21	1.000	330.0	9.00e-22	1.000	335.0	0.00e+00	1.000

H2O2

WL (nm)	Abs (cm^2)	QY	WL (nm)	Abs (cm^2)	QY	WL (nm)	Abs (cm^2)	QY	WL (nm)	Abs (cm^2)	QY	WL (nm)	Abs (cm^2)	QY
190.0	6.72e-19	1.000	195.0	5.63e-19	1.000	200.0	4.75e-19	1.000	205.0	4.08e-19	1.000	210.0	3.57e-19	1.000
215.0	3.07e-19	1.000	220.0	2.58e-19	1.000	225.0	2.17e-19	1.000	230.0	1.82e-19	1.000	235.0	1.50e-19	1.000
240.0	1.24e-19	1.000	245.0	1.02e-19	1.000	250.0	8.30e-20	1.000	255.0	6.70e-20	1.000	260.0	5.30e-20	1.000
265.0	4.20e-20	1.000	270.0	3.30e-20	1.000	275.0	2.60e-20	1.000	280.0	2.00e-20	1.000	285.0	1.50e-20	1.000
290.0	1.20e-20	1.000	295.0	9.00e-21	1.000	300.0	6.80e-21	1.000	305.0	5.10e-21	1.000	310.0	3.90e-21	1.000
315.0	2.90e-21	1.000	320.0	2.20e-21	1.000	325.0	1.60e-21	1.000	330.0	1.30e-21	1.000	335.0	1.00e-21	1.000
340.0	7.00e-22	1.000	345.0	5.00e-22	1.000	350.0	4.00e-22	1.000	355.0	0.00e+00	1.000			

HCHO_R

WL (nm)	Abs (cm^2)	QY	WL (nm)	Abs (cm^2)	QY	WL (nm)	Abs (cm^2)	QY	WL (nm)	Abs (cm^2)	QY	WL (nm)	Abs (cm^2)	QY
240.0	6.40e-22	0.270	241.0	5.60e-22	0.272	242.0	1.05e-21	0.274	243.0	1.15e-21	0.276	244.0	8.20e-22	0.278
245.0	1.03e-21	0.280	246.0	9.80e-22	0.282	247.0	1.35e-21	0.284	248.0	1.91e-21	0.286	249.0	2.82e-21	0.288
250.0	2.05e-21	0.290	251.0	1.70e-21	0.291	252.0	2.88e-21	0.292	253.0	2.55e-21	0.293	254.0	2.55e-21	0.294
255.0	3.60e-21	0.295	256.0	5.09e-21	0.296	257.0	3.39e-21	0.297	258.0	2.26e-21	0.298	259.0	5.04e-21	0.299
260.0	5.05e-21	0.300	261.0	5.49e-21	0.308	262.0	5.20e-21	0.316	263.0	9.33e-21	0.324	264.0	8.23e-21	0.332
265.0	4.30e-21	0.340	266.0	4.95e-21	0.348	267.0	1.24e-20	0.356	268.0	1.11e-20	0.364	269.0	8.78e-21	0.372
270.0	9.36e-21	0.380	271.0	1.79e-20	0.399	272.0	1.23e-20	0.418	273.0	6.45e-21	0.437	274.0	6.56e-21	0.456
275.0	2.23e-20	0.475	276.0	2.42e-20	0.494	277.0	1.40e-20	0.513	278.0	1.05e-20	0.532	279.0	2.55e-20	0.551
280.0	2.08e-20	0.570	281.0	1.48e-20	0.586	282.0	8.81e-21	0.602	283.0	1.07e-20	0.618	284.0	4.49e-20	0.634
285.0	3.59e-20	0.650	286.0	1.96e-20	0.666	287.0	1.30e-20	0.682	288.0	3.36e-20	0.698	289.0	2.84e-20	0.714
290.0	1.30e-20	0.730	291.0	1.75e-20	0.735	292.0	8.32e-21	0.740	293.0	3.73e-20	0.745	294.0	6.54e-20	0.750
295.0	3.95e-20	0.755	296.0	2.33e-20	0.760	297.0	1.51e-20	0.765	298.0	4.04e-20	0.770	299.0	2.87e-20	0.775
300.0	8.71e-21	0.780	301.0	1.72e-20	0.780	302.0	1.06e-20	0.780	303.0	3.20e-20	0.780	304.0	6.90e-20	0.780
305.0	4.91e-20	0.780	306.0	4.63e-20	0.780	307.0	2.10e-20	0.780	308.0	1.49e-20	0.780	309.0	3.41e-20	0.780
310.0	1.95e-20	0.780	311.0	5.21e-21	0.764	312.0	1.12e-20	0.748	313.0	1.12e-20	0.732	314.0	4.75e-20	0.716
315.0	5.25e-20	0.700	316.0	2.90e-20	0.684	317.0	5.37e-20	0.668	318.0	2.98e-20	0.652	319.0	9.18e-21	0.636
320.0	1.26e-20	0.620	321.0	1.53e-20	0.585	322.0	6.69e-21	0.550	323.0	3.45e-21	0.515	324.0	8.16e-21	0.480
325.0	1.85e-20	0.445	326.0	5.95e-20	0.410	327.0	3.49e-20	0.375	328.0	1.09e-20	0.340	329.0	3.35e-20	0.305
330.0	3.32e-20	0.270	331.0	1.07e-20	0.243	332.0	2.89e-21	0.216	333.0	2.15e-21	0.189	334.0	1.71e-21	0.162
335.0	1.43e-21	0.135	336.0	1.94e-21	0.108	337.0	4.17e-21	0.081	338.0	2.36e-20	0.054	339.0	4.71e-20	0.027
340.0	2.48e-20	0.000												

HCHO_M

WL (nm)	Abs (cm^2)	QY	WL (nm)	Abs (cm^2)	QY	WL (nm)	Abs (cm^2)	QY	WL (nm)	Abs (cm^2)	QY	WL (nm)	Abs (cm^2)	QY
240.0	6.40e-22	0.490	241.0	5.60e-22	0.490	242.0	1.05e-21	0.490	243.0	1.15e-21	0.490	244.0	8.20e-22	0.490
245.0	1.03e-21	0.490	246.0	9.80e-22	0.490	247.0	1.35e-21	0.490	248.0	1.91e-21	0.490	249.0	2.82e-21	0.490
250.0	2.05e-21	0.490	251.0	1.70e-21	0.490	252.0	2.88e-21	0.490	253.0	2.55e-21	0.490	254.0	2.55e-21	0.490
255.0	3.60e-21	0.490	256.0	5.09e-21	0.490	257.0	3.39e-21	0.490	258.0	2.26e-21	0.490	259.0	5.04e-21	0.490
260.0	5.05e-21	0.490	261.0	5.49e-21	0.484	262.0	5.20e-21	0.478	263.0	9.33e-21	0.472	264.0	8.23e-21	0.466
265.0	4.30e-21	0.460	266.0	4.95e-21	0.454	267.0	1.24e-20	0.448	268.0	1.11e-20	0.442	269.0	8.78e-21	0.436
270.0	9.36e-21	0.430	271.0	1.79e-20	0.419	272.0	1.23e-20	0.408	273.0	6.45e-21	0.397	274.0	6.56e-21	0.386
275.0	2.23e-20	0.375	276.0	2.42e-20	0.364	277.0	1.40e-20	0.353	278.0	1.05e-20	0.342	279.0	2.55e-20	0.331
280.0	2.08e-20	0.320	281.0	1.48e-20	0.312	282.0	8.81e-21	0.304	283.0	1.07e-20	0.296	284.0	4.49e-20	0.288
285.0	3.59e-20	0.280	286.0	1.96e-20	0.272	287.0	1.30e-20	0.264	288.0	3.36e-20	0.256	289.0	2.84e-20	0.248
290.0	1.30e-20	0.240	291.0	1.75e-20	0.237	292.0	8.32e-21	0.234	293.0	3.73e-20	0.231	294.0	6.54e-20	0.228
295.0	3.95e-20	0.225	296.0	2.33e-20	0.222	297.0	1.51e-20	0.219	298.0	4.04e-20	0.216	299.0	2.87e-20	0.213
300.0	8.71e-21	0.210	301.0	1.72e-20	0.211	302.0	1.06e-20	0.212	303.0	3.20e-20	0.213	304.0	6.90e-20	0.214
305.0	4.91e-20	0.215	306.0	4.63e-20	0.216	307.0	2.10e-20	0.217	308.0	1.49e-20	0.218	309.0	3.41e-20	0.219
310.0	1.95e-20	0.220	311.0	5.21e-21	0.236	312.0	1.12e-20	0.252	313.0	1.12e-20	0.268	314.0	4.75e-20	0.284
315.0	5.25e-20	0.300	316.0	2.90e-20	0.316	317.0	5.37e-20	0.332	318.0	2.98e-20	0.348	319.0	9.18e-21	0.364
320.0	1.26e-20	0.380	321.0	1.53e-20	0.408	322.0	6.69e-21	0.436	323.0	3.45e-21	0.464	324.0	8.16e-21	0.492
325.0	1.85e-20	0.520	326.0	5.95e-20	0.548	327.0	3.49e-20	0.576	328.0	1.09e-20	0.604	329.0	3.35e-20	0.632
330.0	3.32e-20	0.660	331.0	1.07e-20	0.650	332.0	2.89e-21	0.640	333.0	2.15e-21	0.630	334.0	1.71e-21	0.620
335.0	1.43e-21	0.610	336.0	1.94e-21	0.600	337.0	4.17e-21	0.590	338.0	2.36e-20	0.580	339.0	4.71e-20	0.570
340.0	2.48e-20	0.560	341.0	7.59e-21	0.525	342.0	6.81e-21	0.490	343.0	1.95e-20	0.455	344.0	1.14e-20	0.420
345.0	3.23e-21	0.385	346.0	1.13e-21	0.350	347.0	6.60e-22	0.315	348.0	1.22e-21	0.280	349.0	3.20e-22	0.245

Table A-3 (continued)

WL (nm)	Abs (cm^2)	QY	WL (nm)	Abs (cm^2)	QY	WL (nm)	Abs (cm^2)	QY	WL (nm)	Abs (cm^2)	QY	WL (nm)	Abs (cm^2)	QY
350.0	3.80e-22	0.210	351.0	1.04e-21	0.192	352.0	7.13e-21	0.174	353.0	2.21e-20	0.156	354.0	1.54e-20	0.138
355.0	6.76e-21	0.120	356.0	1.35e-21	0.102	357.0	3.60e-22	0.084	358.0	5.70e-23	0.066	359.0	5.80e-22	0.048
360.0	8.20e-22	0.000												
							CCHO_R							
262.0	2.44e-20	0.326	266.0	3.05e-20	0.358	270.0	3.42e-20	0.390	274.0	4.03e-20	0.466	278.0	4.19e-20	0.542
280.0	4.50e-20	0.580	281.0	4.69e-20	0.575	282.0	4.72e-20	0.570	283.0	4.75e-20	0.565	284.0	4.61e-20	0.560
285.0	4.49e-20	0.555	286.0	4.44e-20	0.550	287.0	4.59e-20	0.545	288.0	4.72e-20	0.540	289.0	4.77e-20	0.535
290.0	4.89e-20	0.530	291.0	4.78e-20	0.520	292.0	4.68e-20	0.510	293.0	4.53e-20	0.500	294.0	4.33e-20	0.490
295.0	4.27e-20	0.480	296.0	4.24e-20	0.470	297.0	4.38e-20	0.460	298.0	4.41e-20	0.450	299.0	4.26e-20	0.440
300.0	4.16e-20	0.430	301.0	3.99e-20	0.418	302.0	3.86e-20	0.406	303.0	3.72e-20	0.394	304.0	3.48e-20	0.382
305.0	3.42e-20	0.370	306.0	3.42e-20	0.354	307.0	3.36e-20	0.338	308.0	3.33e-20	0.322	309.0	3.14e-20	0.306
310.0	2.93e-20	0.290	311.0	2.76e-20	0.266	312.0	2.53e-20	0.242	313.0	2.47e-20	0.218	314.0	2.44e-20	0.194
315.0	2.20e-20	0.170	316.0	2.04e-20	0.156	317.0	2.07e-20	0.142	318.0	1.98e-20	0.128	319.0	1.87e-20	0.114
320.0	1.72e-20	0.100	321.0	1.48e-20	0.088	322.0	1.40e-20	0.076	323.0	1.24e-20	0.064	324.0	1.09e-20	0.052
325.0	1.14e-20	0.040	326.0	1.07e-20	0.032	327.0	8.58e-21	0.024	328.0	7.47e-21	0.016	329.0	7.07e-21	0.008
							C2CHO							
294.0	5.80e-20	0.890	295.0	5.57e-20	0.885	296.0	5.37e-20	0.880	297.0	5.16e-20	0.875	298.0	5.02e-20	0.870
299.0	5.02e-20	0.865	300.0	5.04e-20	0.860	301.0	5.09e-20	0.855	302.0	5.07e-20	0.850	303.0	4.94e-20	0.818
304.0	4.69e-20	0.786	305.0	4.32e-20	0.755	306.0	4.04e-20	0.723	307.0	3.81e-20	0.691	308.0	3.65e-20	0.659
309.0	3.62e-20	0.627	310.0	3.60e-20	0.596	311.0	3.53e-20	0.564	312.0	3.50e-20	0.532	313.0	3.32e-20	0.500
314.0	3.06e-20	0.480	315.0	2.77e-20	0.460	316.0	2.43e-20	0.440	317.0	2.18e-20	0.420	318.0	2.00e-20	0.400
319.0	1.86e-20	0.380	320.0	1.83e-20	0.360	321.0	1.78e-20	0.340	322.0	1.66e-20	0.320	323.0	1.58e-20	0.300
324.0	1.49e-20	0.280	325.0	1.30e-20	0.260	326.0	1.13e-20	0.248	327.0	9.96e-21	0.236	328.0	8.28e-21	0.223
329.0	6.85e-21	0.211	330.0	5.75e-21	0.199	331.0	4.94e-21	0.187	332.0	4.66e-21	0.174	333.0	4.30e-21	0.162
334.0	3.73e-21	0.150	335.0	3.25e-21	0.133	336.0	2.80e-21	0.117	337.0	2.30e-21	0.100	338.0	1.85e-21	0.083
339.0	1.66e-21	0.067	340.0	1.55e-21	0.050	341.0	1.19e-21	0.033	342.0	7.60e-22	0.017	343.0	4.50e-22	0.000
							ACETONE							
250.0	2.47e-20	0.760	254.0	3.04e-20	0.776	258.0	3.61e-20	0.792	262.0	4.15e-20	0.768	266.0	4.58e-20	0.704
270.0	4.91e-20	0.640	274.0	5.06e-20	0.604	278.0	5.07e-20	0.568	280.0	5.05e-20	0.550	281.0	5.01e-20	0.525
282.0	4.94e-20	0.500	283.0	4.86e-20	0.475	284.0	4.76e-20	0.450	285.0	4.68e-20	0.425	286.0	4.58e-20	0.400
287.0	4.50e-20	0.375	288.0	4.41e-20	0.350	289.0	4.29e-20	0.325	290.0	4.19e-20	0.302	291.0	4.08e-20	0.284
292.0	3.94e-20	0.266	293.0	3.81e-20	0.249	294.0	3.67e-20	0.232	295.0	3.52e-20	0.217	296.0	3.35e-20	0.201
297.0	3.20e-20	0.187	298.0	3.07e-20	0.173	299.0	2.91e-20	0.160	300.0	2.77e-20	0.147	301.0	2.66e-20	0.135
302.0	2.53e-20	0.124	303.0	2.37e-20	0.114	304.0	2.24e-20	0.104	305.0	2.11e-20	0.095	306.0	1.95e-20	0.086
307.0	1.80e-20	0.078	308.0	1.66e-20	0.071	309.0	1.54e-20	0.064	310.0	1.41e-20	0.057	311.0	1.28e-20	0.052
312.0	1.17e-20	0.046	313.0	1.08e-20	0.042	314.0	9.67e-21	0.037	315.0	8.58e-21	0.033	316.0	7.77e-21	0.029
317.0	6.99e-21	0.026	318.0	6.08e-21	0.023	319.0	5.30e-21	0.020	320.0	4.67e-21	0.018	321.0	4.07e-21	0.016
322.0	3.44e-21	0.014	323.0	2.87e-21	0.012	324.0	2.43e-21	0.011	325.0	2.05e-21	0.009	326.0	1.68e-21	0.008
327.0	1.35e-21	0.007	328.0	1.08e-21	0.006	329.0	8.60e-22	0.005	330.0	6.70e-22	0.005	331.0	5.10e-22	0.004
332.0	4.00e-22	0.003	333.0	3.10e-22	0.003	334.0	2.60e-22	0.002	335.0	1.70e-22	0.002	336.0	1.40e-22	0.002
337.0	1.10e-22	0.002	338.0	9.00e-23	0.001	339.0	6.00e-23	0.001	340.0	5.00e-23	0.001	341.0	5.00e-23	0.001
342.0	3.00e-23	0.001	343.0	4.00e-23	0.001	344.0	2.00e-23	0.000						
							KETONE							
198.5	3.95e-19	1.000	199.0	1.61e-19	1.000	199.5	7.75e-20	1.000	200.0	3.76e-20	1.000	200.5	2.51e-20	1.000
201.0	1.83e-20	1.000	201.5	1.36e-20	1.000	202.0	1.16e-20	1.000	202.5	8.97e-21	1.000	203.0	4.62e-21	1.000
203.5	3.18e-21	1.000	204.0	2.42e-21	1.000	204.5	2.01e-21	1.000	205.0	1.77e-21	1.000	205.5	1.64e-21	1.000
206.0	1.54e-21	1.000	206.5	1.52e-21	1.000	207.0	1.54e-21	1.000	207.5	1.62e-21	1.000	208.0	1.64e-21	1.000
208.5	1.60e-21	1.000	209.0	1.57e-21	1.000	209.5	1.49e-21	1.000	210.0	1.47e-21	1.000	210.5	1.52e-21	1.000
211.0	1.50e-21	1.000	211.5	1.62e-21	1.000	212.0	1.81e-21	1.000	212.5	2.10e-21	1.000	213.0	2.23e-21	1.000
213.5	2.06e-21	1.000	214.0	1.69e-21	1.000	214.5	1.49e-21	1.000	215.0	1.42e-21	1.000	215.5	1.42e-21	1.000
216.0	1.42e-21	1.000	216.5	1.48e-21	1.000	217.0	1.48e-21	1.000	217.5	1.53e-21	1.000	218.0	1.56e-21	1.000
218.5	1.67e-21	1.000	219.0	1.68e-21	1.000	219.5	1.78e-21	1.000	220.0	1.85e-21	1.000	220.5	1.92e-21	1.000
221.0	2.01e-21	1.000	221.5	2.11e-21	1.000	222.0	2.23e-21	1.000	222.5	2.33e-21	1.000	223.0	2.48e-21	1.000
223.5	2.60e-21	1.000	224.0	2.74e-21	1.000	224.5	2.85e-21	1.000	225.0	3.04e-21	1.000	225.5	3.15e-21	1.000
226.0	3.33e-21	1.000	226.5	3.55e-21	1.000	227.0	3.73e-21	1.000	227.5	3.93e-21	1.000	228.0	4.11e-21	1.000
228.5	4.34e-21	1.000	229.0	4.56e-21	1.000	229.5	4.75e-21	1.000	230.0	5.01e-21	1.000	230.5	5.27e-21	1.000
231.0	5.53e-21	1.000	231.5	5.83e-21	1.000	232.0	6.15e-21	1.000	232.5	6.45e-21	1.000	233.0	6.73e-21	1.000
233.5	7.02e-21	1.000	234.0	7.42e-21	1.000	234.5	7.83e-21	1.000	235.0	8.11e-21	1.000	235.5	8.45e-21	1.000
236.0	8.82e-21	1.000	236.5	9.21e-21	1.000	237.0	9.65e-21	1.000	237.5	1.00e-20	1.000	238.0	1.05e-20	1.000
238.5	1.10e-20	1.000	239.0	1.15e-20	1.000	239.5	1.20e-20	1.000	240.0	1.23e-20	1.000	240.5	1.28e-20	1.000
241.0	1.32e-20	1.000	241.5	1.38e-20	1.000	242.0	1.44e-20	1.000	242.5	1.50e-20	1.000	243.0	1.57e-20	1.000
243.5	1.63e-20	1.000	244.0	1.68e-20	1.000	244.5	1.75e-20	1.000	245.0	1.81e-20	1.000	245.5	1.88e-20	1.000
246.0	1.96e-20	1.000	246.5	2.03e-20	1.000	247.0	2.11e-20	1.000	247.5	2.19e-20	1.000	248.0	2.25e-20	1.000
248.5	2.33e-20	1.000	249.0	2.40e-20	1.000	249.5	2.48e-20	1.000	250.0	2.56e-20	1.000	250.5	2.64e-20	1.000
251.0	2.73e-20	1.000	251.5	2.81e-20	1.000	252.0	2.88e-20	1.000	252.5	2.98e-20	1.000	253.0	3.07e-20	1.000
253.5	3.16e-20	1.000	254.0	3.25e-20	1.000	254.5	3.34e-20	1.000	255.0	3.43e-20	1.000	255.5	3.51e-20	1.000
256.0	3.59e-20	1.000	256.5	3.67e-20	1.000	257.0	3.75e-20	1.000	257.5	3.84e-20	1.000	258.0	3.94e-20	1.000
258.5	4.03e-20	1.000	259.0	4.13e-20	1.000	259.5	4.22e-20	1.000	260.0	4.28e-20	1.000	260.5	4.33e-20	1.000
261.0	4.41e-20	1.000	261.5	4.49e-20	1.000	262.0	4.57e-20	1.000	262.5	4.65e-20	1.000	263.0	4.72e-20	1.000
263.5	4.78e-20	1.000	264.0	4.85e-20	1.000	264.5	4.92e-20	1.000	265.0	4.99e-20	1.000	265.5	5.04e-20	1.000
266.0	5.12e-20	1.000	266.5	5.22e-20	1.000	267.0	5.28e-20	1.000	267.5	5.34e-20	1.000	268.0	5.41e-20	1.000

Table A-3 (continued)

WL (nm)	Abs (cm^2)	QY	WL (nm)	Abs (cm^2)	QY	WL (nm)	Abs (cm^2)	QY	WL (nm)	Abs (cm^2)	QY	WL (nm)	Abs (cm^2)	QY
268.5	5.46e-20	1.000	269.0	5.51e-20	1.000	269.5	5.55e-20	1.000	270.0	5.59e-20	1.000	270.5	5.63e-20	1.000
271.0	5.66e-20	1.000	271.5	5.70e-20	1.000	272.0	5.74e-20	1.000	272.5	5.78e-20	1.000	273.0	5.81e-20	1.000
273.5	5.86e-20	1.000	274.0	5.90e-20	1.000	274.5	5.93e-20	1.000	275.0	5.96e-20	1.000	275.5	5.97e-20	1.000
276.0	5.98e-20	1.000	276.5	5.98e-20	1.000	277.0	5.99e-20	1.000	277.5	5.99e-20	1.000	278.0	5.98e-20	1.000
278.5	5.96e-20	1.000	279.0	5.96e-20	1.000	279.5	5.95e-20	1.000	280.0	5.94e-20	1.000	280.5	5.92e-20	1.000
281.0	5.90e-20	1.000	281.5	5.88e-20	1.000	282.0	5.86e-20	1.000	282.5	5.83e-20	1.000	283.0	5.79e-20	1.000
283.5	5.75e-20	1.000	284.0	5.71e-20	1.000	284.5	5.67e-20	1.000	285.0	5.61e-20	1.000	285.5	5.56e-20	1.000
286.0	5.51e-20	1.000	286.5	5.45e-20	1.000	287.0	5.41e-20	1.000	287.5	5.37e-20	1.000	288.0	5.33e-20	1.000
288.5	5.27e-20	1.000	289.0	5.21e-20	1.000	289.5	5.15e-20	1.000	290.0	5.08e-20	1.000	290.5	4.99e-20	1.000
291.0	4.89e-20	1.000	291.5	4.82e-20	1.000	292.0	4.73e-20	1.000	292.5	4.62e-20	1.000	293.0	4.53e-20	1.000
293.5	4.41e-20	1.000	294.0	4.32e-20	1.000	294.5	4.23e-20	1.000	295.0	4.15e-20	1.000	295.5	4.11e-20	1.000
296.0	4.01e-20	1.000	296.5	3.94e-20	1.000	297.0	3.88e-20	1.000	297.5	3.77e-20	1.000	298.0	3.69e-20	1.000
298.5	3.63e-20	1.000	299.0	3.54e-20	1.000	299.5	3.46e-20	1.000	300.0	3.36e-20	1.000	300.5	3.24e-20	1.000
301.0	3.16e-20	1.000	301.5	3.06e-20	1.000	302.0	2.95e-20	1.000	302.5	2.82e-20	1.000	303.0	2.70e-20	1.000
303.5	2.59e-20	1.000	304.0	2.49e-20	1.000	304.5	2.42e-20	1.000	305.0	2.34e-20	1.000	305.5	2.28e-20	1.000
306.0	2.19e-20	1.000	306.5	2.11e-20	1.000	307.0	2.04e-20	1.000	307.5	1.93e-20	1.000	308.0	1.88e-20	1.000
308.5	1.80e-20	1.000	309.0	1.73e-20	1.000	309.5	1.66e-20	1.000	310.0	1.58e-20	1.000	310.5	1.48e-20	1.000
311.0	1.42e-20	1.000	311.5	1.34e-20	1.000	312.0	1.26e-20	1.000	312.5	1.17e-20	1.000	313.0	1.13e-20	1.000
313.5	1.08e-20	1.000	314.0	1.04e-20	1.000	314.5	9.69e-21	1.000	315.0	8.91e-21	1.000	315.5	8.61e-21	1.000
316.0	7.88e-21	1.000	316.5	7.25e-21	1.000	317.0	6.92e-21	1.000	317.5	6.43e-21	1.000	318.0	6.07e-21	1.000
318.5	5.64e-21	1.000	319.0	5.19e-21	1.000	319.5	4.66e-21	1.000	320.0	4.36e-21	1.000	320.5	3.95e-21	1.000
321.0	3.64e-21	1.000	321.5	3.38e-21	1.000	322.0	3.17e-21	1.000	322.5	2.80e-21	1.000	323.0	2.62e-21	1.000
323.5	2.29e-21	1.000	324.0	2.13e-21	1.000	324.5	1.93e-21	1.000	325.0	1.70e-21	1.000	325.5	1.58e-21	1.000
326.0	1.48e-21	1.000	326.5	1.24e-21	1.000	327.0	1.20e-21	1.000	327.5	1.04e-21	1.000	328.0	9.51e-22	1.000
328.5	8.44e-22	1.000	329.0	7.26e-22	1.000	329.5	6.70e-22	1.000	330.0	6.08e-22	1.000	330.5	5.15e-22	1.000
331.0	4.56e-22	1.000	331.5	4.13e-22	1.000	332.0	3.56e-22	1.000	332.5	3.30e-22	1.000	333.0	2.97e-22	1.000
333.5	2.67e-22	1.000	334.0	2.46e-22	1.000	334.5	2.21e-22	1.000	335.0	1.93e-22	1.000	335.5	1.56e-22	1.000
336.0	1.47e-22	1.000	336.5	1.37e-22	1.000	337.0	1.27e-22	1.000	337.5	1.19e-22	1.000	338.0	1.09e-22	1.000
338.5	1.01e-22	1.000	339.0	9.09e-23	1.000	339.5	8.22e-23	1.000	340.0	7.66e-23	1.000	340.5	7.43e-23	1.000
341.0	6.83e-23	1.000	341.5	6.72e-23	1.000	342.0	6.04e-23	1.000	342.5	4.78e-23	1.000	343.0	0.00e+00	1.000
							COOH							
210.0	3.12e-19	1.000	215.0	2.09e-19	1.000	220.0	1.54e-19	1.000	225.0	1.22e-19	1.000	230.0	9.62e-20	1.000
235.0	7.61e-20	1.000	240.0	6.05e-20	1.000	245.0	4.88e-20	1.000	250.0	3.98e-20	1.000	255.0	3.23e-20	1.000
260.0	2.56e-20	1.000	265.0	2.11e-20	1.000	270.0	1.70e-20	1.000	275.0	1.39e-20	1.000	280.0	1.09e-20	1.000
285.0	8.63e-21	1.000	290.0	6.91e-21	1.000	295.0	5.51e-21	1.000	300.0	4.13e-21	1.000	305.0	3.13e-21	1.000
310.0	2.39e-21	1.000	315.0	1.82e-21	1.000	320.0	1.37e-21	1.000	325.0	1.05e-21	1.000	330.0	7.90e-22	1.000
335.0	6.10e-22	1.000	340.0	4.70e-22	1.000	345.0	3.50e-22	1.000	350.0	2.70e-22	1.000	355.0	2.10e-22	1.000
360.0	1.60e-22	1.000	365.0	1.20e-22	1.000	370.0	0.00e+00	1.000						
							GLY_R							
230.0	2.87e-21	1.000	235.0	2.87e-21	1.000	240.0	4.30e-21	1.000	245.0	5.73e-21	1.000	250.0	8.60e-21	1.000
255.0	1.15e-20	1.000	260.0	1.43e-20	1.000	265.0	1.86e-20	1.000	270.0	2.29e-20	1.000	275.0	2.58e-20	1.000
280.0	2.87e-20	1.000	285.0	3.30e-20	1.000	290.0	3.15e-20	1.000	295.0	3.30e-20	1.000	300.0	3.58e-20	1.000
305.0	2.72e-20	1.000	310.0	2.72e-20	1.000	312.5	2.87e-20	1.000	315.0	2.29e-20	1.000	320.0	1.43e-20	1.000
325.0	1.15e-20	1.000	327.5	1.43e-20	1.000	330.0	1.15e-20	1.000	335.0	2.87e-21	1.000	340.0	0.00e+00	1.000
345.0	0.00e+00	1.000	350.0	0.00e+00	1.000	355.0	0.00e+00	1.000	360.0	2.29e-21	1.000	365.0	2.87e-21	1.000
370.0	8.03e-21	1.000	375.0	1.00e-20	1.000	380.0	1.72e-20	0.972	382.0	1.58e-20	0.855	384.0	1.49e-20	0.737
386.0	1.49e-20	0.619	388.0	2.87e-20	0.502	390.0	3.15e-20	0.384	391.0	3.24e-20	0.326	392.0	3.04e-20	0.267
393.0	2.23e-20	0.208	394.0	2.63e-20	0.149	395.0	3.04e-20	0.090	396.0	2.63e-20	0.032	397.0	2.43e-20	0.000
398.0	3.24e-20	0.000	399.0	3.04e-20	0.000	400.0	2.84e-20	0.000	401.0	3.24e-20	0.000	402.0	4.46e-20	0.000
403.0	5.27e-20	0.000	404.0	4.26e-20	0.000	405.0	3.04e-20	0.000	406.0	3.04e-20	0.000	407.0	2.84e-20	0.000
408.0	2.43e-20	0.000	409.0	2.84e-20	0.000	410.0	6.08e-20	0.000	411.0	5.07e-20	0.000	411.5	6.08e-20	0.000
412.0	4.86e-20	0.000	413.0	8.31e-20	0.000	413.5	6.48e-20	0.000	414.0	7.50e-20	0.000	414.5	8.11e-20	0.000
415.0	8.11e-20	0.000	415.5	6.89e-20	0.000	416.0	4.26e-20	0.000	417.0	4.86e-20	0.000	418.0	5.88e-20	0.000
							GLY_ABS							
230.0	2.87e-21	1.000	235.0	2.87e-21	1.000	240.0	4.30e-21	1.000	245.0	5.73e-21	1.000	250.0	8.60e-21	1.000
255.0	1.15e-20	1.000	260.0	1.43e-20	1.000	265.0	1.86e-20	1.000	270.0	2.29e-20	1.000	275.0	2.58e-20	1.000
280.0	2.87e-20	1.000	285.0	3.30e-20	1.000	290.0	3.15e-20	1.000	295.0	3.30e-20	1.000	300.0	3.58e-20	1.000
305.0	2.72e-20	1.000	310.0	2.72e-20	1.000	312.5	2.87e-20	1.000	315.0	2.29e-20	1.000	320.0	1.43e-20	1.000
325.0	1.15e-20	1.000	327.5	1.43e-20	1.000	330.0	1.15e-20	1.000	335.0	2.87e-21	1.000	340.0	0.00e+00	1.000
355.0	0.00e+00	1.000	360.0	2.29e-21	1.000	365.0	2.87e-21	1.000	370.0	8.03e-21	1.000	375.0	1.00e-20	1.000
380.0	1.72e-20	1.000	382.0	1.58e-20	1.000	384.0	1.49e-20	1.000	386.0	1.49e-20	1.000	388.0	2.87e-20	1.000
390.0	3.15e-20	1.000	391.0	3.24e-20	1.000	392.0	3.04e-20	1.000	393.0	2.23e-20	1.000	394.0	2.63e-20	1.000
395.0	3.04e-20	1.000	396.0	2.63e-20	1.000	397.0	2.43e-20	1.000	398.0	3.24e-20	1.000	399.0	3.04e-20	1.000
400.0	2.84e-20	1.000	401.0	3.24e-20	1.000	402.0	4.46e-20	1.000	403.0	5.27e-20	1.000	404.0	4.26e-20	1.000
405.0	3.04e-20	1.000	406.0	3.04e-20	1.000	407.0	2.84e-20	1.000	408.0	2.43e-20	1.000	409.0	2.84e-20	1.000
410.0	6.08e-20	1.000	411.0	5.07e-20	1.000	411.5	6.08e-20	1.000	412.0	4.86e-20	1.000	413.0	8.31e-20	1.000
413.5	6.48e-20	1.000	414.0	7.50e-20	1.000	414.5	8.11e-20	1.000	415.0	8.11e-20	1.000	415.5	6.89e-20	1.000
416.0	4.26e-20	1.000	417.0	4.86e-20	1.000	418.0	5.88e-20	1.000	419.0	6.69e-20	1.000	420.0	3.85e-20	1.000
421.0	5.67e-20	1.000	421.5	4.46e-20	1.000	422.0	5.27e-20	1.000	422.5	1.05e-19	1.000	423.0	8.51e-20	1.000
424.0	6.08e-20	1.000	425.0	7.29e-20	1.000	426.0	1.18e-19	1.000	426.5	1.30e-19	1.000	427.0	1.07e-19	1.000
428.0	1.66e-19	1.000	429.0	4.05e-20	1.000	430.0	5.07e-20	1.000	431.0	4.86e-20	1.000	432.0	4.05e-20	1.000

Table A-3 (continued)

WL (nm)	Abs (cm^2)	QY	WL (nm)	Abs (cm^2)	QY	WL (nm)	Abs (cm^2)	QY	WL (nm)	Abs (cm^2)	QY	WL (nm)	Abs (cm^2)	QY
433.0	3.65e-20	1.000	434.0	4.05e-20	1.000	434.5	6.08e-20	1.000	435.0	5.07e-20	1.000	436.0	8.11e-20	1.000
436.5	1.13e-19	1.000	437.0	5.27e-20	1.000	438.0	1.01e-19	1.000	438.5	1.38e-19	1.000	439.0	7.70e-20	1.000
440.0	2.47e-19	1.000	441.0	8.11e-20	1.000	442.0	6.08e-20	1.000	443.0	7.50e-20	1.000	444.0	9.32e-20	1.000
445.0	1.13e-19	1.000	446.0	5.27e-20	1.000	447.0	2.43e-20	1.000	448.0	2.84e-20	1.000	449.0	3.85e-20	1.000
450.0	6.08e-20	1.000	451.0	1.09e-19	1.000	451.5	9.32e-20	1.000	452.0	1.22e-19	1.000	453.0	2.39e-19	1.000
454.0	1.70e-19	1.000	455.0	3.40e-19	1.000	455.5	4.05e-19	1.000	456.0	1.01e-19	1.000	457.0	1.62e-20	1.000
458.0	1.22e-20	1.000	458.5	1.42e-20	1.000	459.0	4.05e-21	1.000	460.0	4.05e-21	1.000	460.5	6.08e-21	1.000
461.0	2.03e-21	1.000	462.0	0.00e+00	1.000									

MGLY_ADJ

219.0	9.84e-21	1.000	219.5	1.04e-20	1.000	220.0	1.06e-20	1.000	220.5	1.11e-20	1.000	221.0	1.15e-20	1.000
221.5	1.18e-20	1.000	222.0	1.22e-20	1.000	222.5	1.24e-20	1.000	223.0	1.26e-20	1.000	223.5	1.26e-20	1.000
224.0	1.25e-20	1.000	224.5	1.24e-20	1.000	225.0	1.25e-20	1.000	225.5	1.27e-20	1.000	226.0	1.27e-20	1.000
226.5	1.29e-20	1.000	227.0	1.31e-20	1.000	227.5	1.32e-20	1.000	228.0	1.35e-20	1.000	228.5	1.37e-20	1.000
229.0	1.40e-20	1.000	229.5	1.42e-20	1.000	230.0	1.48e-20	1.000	230.5	1.53e-20	1.000	231.0	1.57e-20	1.000
231.5	1.59e-20	1.000	232.0	1.61e-20	1.000	232.5	1.62e-20	1.000	233.0	1.61e-20	1.000	233.5	1.68e-20	1.000
234.0	1.74e-20	1.000	234.5	1.80e-20	1.000	235.0	1.84e-20	1.000	235.5	1.87e-20	1.000	236.0	1.89e-20	1.000
236.5	1.91e-20	1.000	237.0	1.93e-20	1.000	237.5	1.94e-20	1.000	238.0	1.96e-20	1.000	238.5	1.96e-20	1.000
239.0	2.01e-20	1.000	239.5	2.04e-20	1.000	240.0	2.08e-20	1.000	240.5	2.10e-20	1.000	241.0	2.14e-20	1.000
241.5	2.16e-20	1.000	242.0	2.19e-20	1.000	242.5	2.20e-20	1.000	243.0	2.23e-20	1.000	243.5	2.26e-20	1.000
244.0	2.28e-20	1.000	244.5	2.29e-20	1.000	245.0	2.30e-20	1.000	245.5	2.32e-20	1.000	246.0	2.33e-20	1.000
246.5	2.35e-20	1.000	247.0	2.38e-20	1.000	247.5	2.41e-20	1.000	248.0	2.46e-20	1.000	248.5	2.51e-20	1.000
249.0	2.57e-20	1.000	249.5	2.61e-20	1.000	250.0	2.65e-20	1.000	250.5	2.67e-20	1.000	251.0	2.69e-20	1.000
251.5	2.69e-20	1.000	252.0	2.71e-20	1.000	252.5	2.72e-20	1.000	253.0	2.73e-20	1.000	253.5	2.74e-20	1.000
254.0	2.76e-20	1.000	254.5	2.78e-20	1.000	255.0	2.82e-20	1.000	255.5	2.87e-20	1.000	256.0	2.93e-20	1.000
256.5	2.98e-20	1.000	257.0	3.07e-20	1.000	257.5	3.12e-20	1.000	258.0	3.17e-20	1.000	258.5	3.21e-20	1.000
259.0	3.26e-20	1.000	259.5	3.28e-20	1.000	260.0	3.29e-20	1.000	260.5	3.31e-20	1.000	261.0	3.33e-20	1.000
261.5	3.34e-20	1.000	262.0	3.36e-20	1.000	262.5	3.38e-20	1.000	263.0	3.42e-20	1.000	263.5	3.44e-20	1.000
264.0	3.48e-20	1.000	264.5	3.54e-20	1.000	265.0	3.59e-20	1.000	265.5	3.65e-20	1.000	266.0	3.73e-20	1.000
266.5	3.80e-20	1.000	267.0	3.87e-20	1.000	267.5	3.95e-20	1.000	268.0	4.02e-20	1.000	268.5	4.08e-20	1.000
269.0	4.13e-20	1.000	269.5	4.17e-20	1.000	270.0	4.20e-20	1.000	270.5	4.22e-20	1.000	271.0	4.22e-20	1.000
271.5	4.22e-20	1.000	272.0	4.23e-20	1.000	272.5	4.24e-20	1.000	273.0	4.27e-20	1.000	273.5	4.29e-20	1.000
274.0	4.31e-20	1.000	274.5	4.33e-20	1.000	275.0	4.37e-20	1.000	275.5	4.42e-20	1.000	276.0	4.48e-20	1.000
276.5	4.56e-20	1.000	277.0	4.64e-20	1.000	277.5	4.71e-20	1.000	278.0	4.78e-20	1.000	278.5	4.83e-20	1.000
279.0	4.87e-20	1.000	279.5	4.90e-20	1.000	280.0	4.92e-20	1.000	280.5	4.93e-20	1.000	281.0	4.94e-20	1.000
281.5	4.92e-20	1.000	282.0	4.90e-20	1.000	282.5	4.86e-20	1.000	283.0	4.83e-20	1.000	283.5	4.79e-20	1.000
284.0	4.76e-20	1.000	284.5	4.72e-20	1.000	285.0	4.70e-20	1.000	285.5	4.68e-20	1.000	286.0	4.66e-20	1.000
286.5	4.65e-20	1.000	287.0	4.65e-20	1.000	287.5	4.68e-20	1.000	288.0	4.73e-20	1.000	288.5	4.78e-20	1.000
289.0	4.84e-20	1.000	289.5	4.89e-20	1.000	290.0	4.92e-20	1.000	290.5	4.92e-20	1.000	291.0	4.90e-20	1.000
291.5	4.86e-20	1.000	292.0	4.81e-20	1.000	292.5	4.75e-20	1.000	293.0	4.70e-20	1.000	293.5	4.65e-20	1.000
294.0	4.58e-20	1.000	294.5	4.48e-20	1.000	295.0	4.38e-20	1.000	295.5	4.27e-20	1.000	296.0	4.17e-20	1.000
296.5	4.07e-20	1.000	297.0	3.99e-20	1.000	297.5	3.94e-20	1.000	298.0	3.88e-20	1.000	298.5	3.82e-20	1.000
299.0	3.76e-20	1.000	299.5	3.72e-20	1.000	300.0	3.69e-20	1.000	300.5	3.68e-20	1.000	301.0	3.70e-20	1.000
301.5	3.72e-20	1.000	302.0	3.74e-20	1.000	302.5	3.74e-20	1.000	303.0	3.75e-20	1.000	303.5	3.71e-20	1.000
304.0	3.62e-20	1.000	304.5	3.51e-20	1.000	305.0	3.38e-20	1.000	305.5	3.25e-20	1.000	306.0	3.15e-20	1.000
306.5	3.04e-20	1.000	307.0	2.92e-20	1.000	307.5	2.80e-20	1.000	308.0	2.71e-20	1.000	308.5	2.63e-20	1.000
309.0	2.52e-20	1.000	309.5	2.43e-20	1.000	310.0	2.34e-20	1.000	310.5	2.25e-20	1.000	311.0	2.19e-20	1.000
311.5	2.12e-20	1.000	312.0	2.06e-20	1.000	312.5	2.02e-20	1.000	313.0	1.96e-20	1.000	313.5	1.92e-20	1.000
314.0	1.91e-20	1.000	314.5	1.88e-20	1.000	315.0	1.86e-20	1.000	315.5	1.85e-20	1.000	316.0	1.86e-20	1.000
316.5	1.87e-20	1.000	317.0	1.87e-20	1.000	317.5	1.87e-20	1.000	318.0	1.83e-20	1.000	318.5	1.75e-20	1.000
319.0	1.69e-20	1.000	319.5	1.60e-20	1.000	320.0	1.50e-20	1.000	320.5	1.41e-20	1.000	321.0	1.34e-20	1.000
321.5	1.27e-20	1.000	322.0	1.21e-20	1.000	322.5	1.18e-20	1.000	323.0	1.14e-20	1.000	323.5	1.08e-20	1.000
324.0	1.01e-20	1.000	324.5	9.62e-21	1.000	325.0	9.28e-21	1.000	325.5	8.75e-21	1.000	326.0	8.49e-21	1.000
326.5	8.21e-21	1.000	327.0	7.71e-21	1.000	327.5	7.38e-21	1.000	328.0	7.18e-21	1.000	328.5	6.86e-21	1.000
329.0	6.71e-21	1.000	329.5	6.63e-21	1.000	330.0	6.46e-21	1.000	330.5	6.29e-21	1.000	331.0	6.21e-21	1.000
331.5	6.18e-21	1.000	332.0	6.20e-21	1.000	332.5	5.49e-21	1.000	333.0	5.21e-21	1.000	333.5	5.38e-21	1.000
334.0	5.35e-21	1.000	334.5	5.04e-21	1.000	335.0	4.94e-21	1.000	335.5	4.90e-21	1.000	336.0	4.52e-21	1.000
336.5	4.26e-21	1.000	337.0	4.11e-21	1.000	337.5	3.76e-21	1.000	338.0	3.61e-21	1.000	338.5	3.58e-21	1.000
339.0	3.47e-21	1.000	339.5	3.32e-21	1.000	340.0	3.22e-21	1.000	340.5	3.10e-21	1.000	341.0	3.00e-21	1.000
341.5	2.94e-21	1.000	342.0	2.89e-21	1.000	342.5	2.86e-21	1.000	343.0	2.88e-21	1.000	343.5	2.88e-21	1.000
344.0	2.89e-21	0.992	344.5	2.91e-21	0.984	345.0	2.95e-21	0.976	345.5	3.00e-21	0.968	346.0	3.08e-21	0.960
346.5	3.18e-21	0.953	347.0	3.25e-21	0.945	347.5	3.30e-21	0.937	348.0	3.39e-21	0.929	348.5	3.51e-21	0.921
349.0	3.63e-21	0.913	349.5	3.73e-21	0.905	350.0	3.85e-21	0.897	350.5	3.99e-21	0.889	351.0	4.27e-21	0.881
351.5	4.47e-21	0.873	352.0	4.63e-21	0.865	352.5	4.78e-21	0.858	353.0	4.92e-21	0.850	353.5	5.07e-21	0.842
354.0	5.23e-21	0.834	354.5	5.39e-21	0.826	355.0	5.56e-21	0.818	355.5	5.77e-21	0.810	356.0	5.97e-21	0.802
356.5	6.15e-21	0.794	357.0	6.35e-21	0.786	357.5	6.56e-21	0.778	358.0	6.76e-21	0.770	358.5	6.95e-21	0.763
359.0	7.20e-21	0.755	359.5	7.44e-21	0.747	360.0	7.64e-21	0.739	360.5	7.89e-21	0.731	361.0	8.15e-21	0.723
361.5	8.43e-21	0.715	362.0	8.71e-21	0.707	362.5	9.02e-21	0.699	363.0	9.33e-21	0.691	363.5	9.65e-21	0.683
364.0	1.00e-20	0.675	364.5	1.04e-20	0.668	365.0	1.08e-20	0.660	365.5	1.11e-20	0.652	366.0	1.15e-20	0.644
366.5	1.19e-20	0.636	367.0	1.23e-20	0.628	367.5	1.27e-20	0.620	368.0	1.31e-20	0.612	368.5	1.35e-20	0.604
369.0	1.40e-20	0.596	369.5	1.44e-20	0.588	370.0	1.47e-20	0.580	370.5	1.51e-20	0.573	371.0	1.55e-20	0.565
371.5	1.59e-20	0.557	372.0	1.64e-20	0.549	372.5	1.70e-20	0.541	373.0	1.73e-20	0.533	373.5	1.77e-20	0.525
374.0	1.81e-20	0.517	374.5	1.86e-20	0.509	375.0	1.90e-20	0.501	375.5	1.96e-20	0.493	376.0	2.02e-20	0.486

Table A-3 (continued)

WL (nm)	Abs (cm^2)	QY	WL (nm)	Abs (cm^2)	QY	WL (nm)	Abs (cm^2)	QY	WL (nm)	Abs (cm^2)	QY	WL (nm)	Abs (cm^2)	QY
376.5	2.06e-20	0.478	377.0	2.10e-20	0.470	377.5	2.14e-20	0.462	378.0	2.18e-20	0.454	378.5	2.24e-20	0.446
379.0	2.30e-20	0.438	379.5	2.37e-20	0.430	380.0	2.42e-20	0.422	380.5	2.47e-20	0.414	381.0	2.54e-20	0.406
381.5	2.62e-20	0.398	382.0	2.69e-20	0.391	382.5	2.79e-20	0.383	383.0	2.88e-20	0.375	383.5	2.96e-20	0.367
384.0	3.02e-20	0.359	384.5	3.10e-20	0.351	385.0	3.20e-20	0.343	385.5	3.29e-20	0.335	386.0	3.39e-20	0.327
386.5	3.51e-20	0.319	387.0	3.62e-20	0.311	387.5	3.69e-20	0.303	388.0	3.70e-20	0.296	388.5	3.77e-20	0.288
389.0	3.88e-20	0.280	389.5	3.97e-20	0.272	390.0	4.03e-20	0.264	390.5	4.12e-20	0.256	391.0	4.22e-20	0.248
391.5	4.29e-20	0.240	392.0	4.30e-20	0.232	392.5	4.38e-20	0.224	393.0	4.47e-20	0.216	393.5	4.55e-20	0.208
394.0	4.56e-20	0.201	394.5	4.59e-20	0.193	395.0	4.67e-20	0.185	395.5	4.80e-20	0.177	396.0	4.87e-20	0.169
396.5	4.96e-20	0.161	397.0	5.08e-20	0.153	397.5	5.19e-20	0.145	398.0	5.23e-20	0.137	398.5	5.39e-20	0.129
399.0	5.46e-20	0.121	399.5	5.54e-20	0.113	400.0	5.59e-20	0.106	400.5	5.77e-20	0.098	401.0	5.91e-20	0.090
401.5	5.99e-20	0.082	402.0	6.06e-20	0.074	402.5	6.20e-20	0.066	403.0	6.35e-20	0.058	403.5	6.52e-20	0.050
404.0	6.54e-20	0.042	404.5	6.64e-20	0.034	405.0	6.93e-20	0.026	405.5	7.15e-20	0.018	406.0	7.19e-20	0.011
406.5	7.32e-20	0.003	407.0	7.58e-20	0.000	407.5	7.88e-20	0.000	408.0	7.97e-20	0.000	408.5	7.91e-20	0.000
409.0	8.11e-20	0.000	409.5	8.41e-20	0.000	410.0	8.53e-20	0.000	410.5	8.59e-20	0.000	411.0	8.60e-20	0.000
411.5	8.80e-20	0.000	412.0	9.04e-20	0.000	412.5	9.45e-20	0.000	413.0	9.34e-20	0.000	413.5	9.37e-20	0.000
414.0	9.63e-20	0.000	414.5	9.71e-20	0.000	415.0	9.70e-20	0.000	415.5	9.65e-20	0.000	416.0	9.69e-20	0.000
416.5	9.89e-20	0.000	417.0	1.00e-19	0.000	417.5	1.02e-19	0.000	418.0	1.00e-19	0.000	418.5	1.02e-19	0.000
419.0	1.01e-19	0.000	419.5	1.01e-19	0.000	420.0	1.03e-19	0.000	420.5	1.01e-19	0.000	421.0	1.04e-19	0.000
							BACL_ADJ							
230.0	1.30e-20	1.000	232.5	1.46e-20	1.000	235.0	1.68e-20	1.000	237.5	1.84e-20	1.000	240.0	2.16e-20	1.000
242.5	2.49e-20	1.000	245.0	2.65e-20	1.000	247.5	2.71e-20	1.000	250.0	3.03e-20	1.000	252.5	3.46e-20	1.000
255.0	3.46e-20	1.000	257.5	3.57e-20	1.000	260.0	3.95e-20	1.000	262.5	4.17e-20	1.000	265.0	4.17e-20	1.000
267.5	4.22e-20	1.000	270.0	4.60e-20	1.000	272.5	4.54e-20	1.000	275.0	4.33e-20	1.000	277.5	4.22e-20	1.000
280.0	4.44e-20	1.000	282.5	4.33e-20	1.000	285.0	3.90e-20	1.000	287.5	3.57e-20	1.000	290.0	3.25e-20	1.000
292.5	2.92e-20	1.000	295.0	2.60e-20	1.000	297.5	2.16e-20	1.000	300.0	1.79e-20	1.000	302.5	1.73e-20	1.000
305.0	1.46e-20	1.000	307.5	1.08e-20	1.000	310.0	9.20e-21	1.000	312.5	7.03e-21	1.000	315.0	6.49e-21	1.000
317.5	5.41e-21	1.000	320.0	5.41e-21	1.000	322.5	5.41e-21	1.000	325.0	4.33e-21	1.000	327.5	3.25e-21	1.000
330.0	3.79e-21	1.000	332.5	3.79e-21	1.000	335.0	4.33e-21	1.000	337.5	4.87e-21	1.000	340.0	5.41e-21	1.000
342.5	5.95e-21	1.000	345.0	6.49e-21	1.000	347.5	7.03e-21	1.000	350.0	8.12e-21	0.995	352.5	7.57e-21	0.960
355.0	9.20e-21	0.925	357.5	9.74e-21	0.890	360.0	1.08e-20	0.855	362.5	1.19e-20	0.820	365.0	1.41e-20	0.785
367.5	1.51e-20	0.750	370.0	1.79e-20	0.715	372.5	2.00e-20	0.680	375.0	2.11e-20	0.645	377.5	2.33e-20	0.610
380.0	2.60e-20	0.575	382.5	2.81e-20	0.540	385.0	3.14e-20	0.505	387.5	3.46e-20	0.470	390.0	3.90e-20	0.435
392.5	4.11e-20	0.399	395.0	4.33e-20	0.364	397.5	4.38e-20	0.329	400.0	4.65e-20	0.294	402.5	4.81e-20	0.259
405.0	5.19e-20	0.224	407.5	5.84e-20	0.189	410.0	6.06e-20	0.154	412.5	6.49e-20	0.119	415.0	6.92e-20	0.084
417.5	6.87e-20	0.049	420.0	6.82e-20	0.014	422.5	6.71e-20	0.000	425.0	6.49e-20	0.000	427.5	5.95e-20	0.000
430.0	5.73e-20	0.000	432.5	6.28e-20	0.000	435.0	6.01e-20	0.000	437.5	5.84e-20	0.000	440.0	5.95e-20	0.000
442.5	6.49e-20	0.000	445.0	5.95e-20	0.000	447.5	4.98e-20	0.000	450.0	3.79e-20	0.000	452.5	2.81e-20	0.000
455.0	1.73e-20	0.000	457.5	1.08e-20	0.000	460.0	5.41e-21	0.000	462.5	3.79e-21	0.000	465.0	2.16e-21	0.000
467.5	1.08e-21	0.000	470.0	1.08e-21	0.000	472.5	0.00e+00	0.000						
							BZCHO							
299.0	1.78e-19	1.000	304.0	7.40e-20	1.000	306.0	6.91e-20	1.000	309.0	6.41e-20	1.000	313.0	6.91e-20	1.000
314.0	6.91e-20	1.000	318.0	6.41e-20	1.000	325.0	8.39e-20	1.000	332.0	7.65e-20	1.000	338.0	8.88e-20	1.000
342.0	8.88e-20	1.000	346.0	7.89e-20	1.000	349.0	7.89e-20	1.000	354.0	9.13e-20	1.000	355.0	8.14e-20	1.000
364.0	5.67e-20	1.000	368.0	6.66e-20	1.000	369.0	8.39e-20	1.000	370.0	8.39e-20	1.000	372.0	3.45e-20	1.000
374.0	3.21e-20	1.000	376.0	2.47e-20	1.000	377.0	2.47e-20	1.000	380.0	3.58e-20	1.000	382.0	9.90e-21	1.000
386.0	0.00e+00	1.000												
							ACROLEIN							
250.0	1.80e-21	1.000	252.0	2.05e-21	1.000	253.0	2.20e-21	1.000	254.0	2.32e-21	1.000	255.0	2.45e-21	1.000
256.0	2.56e-21	1.000	257.0	2.65e-21	1.000	258.0	2.74e-21	1.000	259.0	2.83e-21	1.000	260.0	2.98e-21	1.000
261.0	3.24e-21	1.000	262.0	3.47e-21	1.000	263.0	3.58e-21	1.000	264.0	3.93e-21	1.000	265.0	4.67e-21	1.000
266.0	5.10e-21	1.000	267.0	5.38e-21	1.000	268.0	5.73e-21	1.000	269.0	6.13e-21	1.000	270.0	6.64e-21	1.000
271.0	7.20e-21	1.000	272.0	7.77e-21	1.000	273.0	8.37e-21	1.000	274.0	8.94e-21	1.000	275.0	9.55e-21	1.000
276.0	1.04e-20	1.000	277.0	1.12e-20	1.000	278.0	1.19e-20	1.000	279.0	1.27e-20	1.000	280.0	1.27e-20	1.000
281.0	1.26e-20	1.000	282.0	1.26e-20	1.000	283.0	1.28e-20	1.000	284.0	1.33e-20	1.000	285.0	1.38e-20	1.000
286.0	1.44e-20	1.000	287.0	1.50e-20	1.000	288.0	1.57e-20	1.000	289.0	1.63e-20	1.000	290.0	1.71e-20	1.000
291.0	1.78e-20	1.000	292.0	1.86e-20	1.000	293.0	1.95e-20	1.000	294.0	2.05e-20	1.000	295.0	2.15e-20	1.000
296.0	2.26e-20	1.000	297.0	2.37e-20	1.000	298.0	2.48e-20	1.000	299.0	2.60e-20	1.000	300.0	2.73e-20	1.000
301.0	2.85e-20	1.000	302.0	2.99e-20	1.000	303.0	3.13e-20	1.000	304.0	3.27e-20	1.000	305.0	3.39e-20	1.000
306.0	3.51e-20	1.000	307.0	3.63e-20	1.000	308.0	3.77e-20	1.000	309.0	3.91e-20	1.000	310.0	4.07e-20	1.000
311.0	4.25e-20	1.000	312.0	4.39e-20	1.000	313.0	4.44e-20	1.000	314.0	4.50e-20	1.000	315.0	4.59e-20	1.000
316.0	4.75e-20	1.000	317.0	4.90e-20	1.000	318.0	5.05e-20	1.000	319.0	5.19e-20	1.000	320.0	5.31e-20	1.000
321.0	5.43e-20	1.000	322.0	5.52e-20	1.000	323.0	5.60e-20	1.000	324.0	5.67e-20	1.000	325.0	5.67e-20	1.000
326.0	5.62e-20	1.000	327.0	5.63e-20	1.000	328.0	5.71e-20	1.000	329.0	5.76e-20	1.000	330.0	5.80e-20	1.000
331.0	5.95e-20	1.000	332.0	6.23e-20	1.000	333.0	6.39e-20	1.000	334.0	6.38e-20	1.000	335.0	6.24e-20	1.000
336.0	6.01e-20	1.000	337.0	5.79e-20	1.000	338.0	5.63e-20	1.000	339.0	5.56e-20	1.000	340.0	5.52e-20	1.000
341.0	5.54e-20	1.000	342.0	5.53e-20	1.000	343.0	5.47e-20	1.000	344.0	5.41e-20	1.000	345.0	5.40e-20	1.000
346.0	5.48e-20	1.000	347.0	5.90e-20	1.000	348.0	6.08e-20	1.000	349.0	6.00e-20	1.000	350.0	5.53e-20	1.000
351.0	5.03e-20	1.000	352.0	4.50e-20	1.000	353.0	4.03e-20	1.000	354.0	3.75e-20	1.000	355.0	3.55e-20	1.000
356.0	3.45e-20	1.000	357.0	3.46e-20	1.000	358.0	3.49e-20	1.000	359.0	3.41e-20	1.000	360.0	3.23e-20	1.000
361.0	2.95e-20	1.000	362.0	2.81e-20	1.000	363.0	2.91e-20	1.000	364.0	3.25e-20	1.000	365.0	3.54e-20	1.000
366.0	3.30e-20	1.000	367.0	2.78e-20	1.000	368.0	2.15e-20	1.000	369.0	1.59e-20	1.000	370.0	1.19e-20	1.000

Table A-3 (continued)

WL (nm)	Abs (cm^2)	QY	WL (nm)	Abs (cm^2)	QY	WL (nm)	Abs (cm^2)	QY	WL (nm)	Abs (cm^2)	QY	WL (nm)	Abs (cm^2)	QY
371.0	8.99e-21	1.000	372.0	7.22e-21	1.000	373.0	5.86e-21	1.000	374.0	4.69e-21	1.000	375.0	3.72e-21	1.000
376.0	3.57e-21	1.000	377.0	3.55e-21	1.000	378.0	2.83e-21	1.000	379.0	1.69e-21	1.000	380.0	8.29e-24	1.000
381.0	0.00e+00	1.000												
							IC3ONO2							
185.0	1.79e-17	1.000	188.0	1.81e-17	1.000	190.0	1.79e-17	1.000	195.0	1.61e-17	1.000	200.0	1.26e-17	1.000
205.0	8.67e-18	1.000	210.0	4.98e-18	1.000	215.0	2.47e-18	1.000	220.0	1.17e-18	1.000	225.0	5.80e-19	1.000
230.0	3.10e-19	1.000	235.0	1.80e-19	1.000	240.0	1.10e-19	1.000	245.0	7.00e-20	1.000	250.0	5.70e-20	1.000
255.0	5.20e-20	1.000	260.0	4.90e-20	1.000	265.0	4.60e-20	1.000	270.0	4.10e-20	1.000	275.0	3.60e-20	1.000
280.0	2.90e-20	1.000	285.0	2.30e-20	1.000	290.0	1.70e-20	1.000	295.0	1.20e-20	1.000	300.0	8.10e-21	1.000
305.0	5.20e-21	1.000	310.0	3.20e-21	1.000	315.0	1.90e-21	1.000	320.0	1.10e-21	1.000	325.0	6.10e-22	1.000
330.0	3.70e-22	1.000	335.0	0.00e+00	1.000									
							MGLY_ABS							
219.0	9.84e-21	1.000	219.5	1.04e-20	1.000	220.0	1.06e-20	1.000	220.5	1.11e-20	1.000	221.0	1.15e-20	1.000
221.5	1.18e-20	1.000	222.0	1.22e-20	1.000	222.5	1.24e-20	1.000	223.0	1.26e-20	1.000	223.5	1.26e-20	1.000
224.0	1.25e-20	1.000	224.5	1.24e-20	1.000	225.0	1.25e-20	1.000	225.5	1.27e-20	1.000	226.0	1.27e-20	1.000
226.5	1.29e-20	1.000	227.0	1.31e-20	1.000	227.5	1.32e-20	1.000	228.0	1.35e-20	1.000	228.5	1.37e-20	1.000
229.0	1.40e-20	1.000	229.5	1.42e-20	1.000	230.0	1.48e-20	1.000	230.5	1.53e-20	1.000	231.0	1.57e-20	1.000
231.5	1.59e-20	1.000	232.0	1.61e-20	1.000	232.5	1.62e-20	1.000	233.0	1.61e-20	1.000	233.5	1.68e-20	1.000
234.0	1.74e-20	1.000	234.5	1.80e-20	1.000	235.0	1.84e-20	1.000	235.5	1.87e-20	1.000	236.0	1.89e-20	1.000
236.5	1.91e-20	1.000	237.0	1.93e-20	1.000	237.5	1.94e-20	1.000	238.0	1.96e-20	1.000	238.5	1.96e-20	1.000
239.0	2.01e-20	1.000	239.5	2.04e-20	1.000	240.0	2.08e-20	1.000	240.5	2.10e-20	1.000	241.0	2.14e-20	1.000
241.5	2.16e-20	1.000	242.0	2.19e-20	1.000	242.5	2.20e-20	1.000	243.0	2.23e-20	1.000	243.5	2.26e-20	1.000
244.0	2.28e-20	1.000	244.5	2.29e-20	1.000	245.0	2.30e-20	1.000	245.5	2.32e-20	1.000	246.0	2.33e-20	1.000
246.5	2.35e-20	1.000	247.0	2.38e-20	1.000	247.5	2.41e-20	1.000	248.0	2.46e-20	1.000	248.5	2.51e-20	1.000
249.0	2.57e-20	1.000	249.5	2.61e-20	1.000	250.0	2.65e-20	1.000	250.5	2.67e-20	1.000	251.0	2.69e-20	1.000
251.5	2.69e-20	1.000	252.0	2.71e-20	1.000	252.5	2.72e-20	1.000	253.0	2.73e-20	1.000	253.5	2.74e-20	1.000
254.0	2.76e-20	1.000	254.5	2.78e-20	1.000	255.0	2.82e-20	1.000	255.5	2.87e-20	1.000	256.0	2.93e-20	1.000
256.5	2.98e-20	1.000	257.0	3.07e-20	1.000	257.5	3.12e-20	1.000	258.0	3.17e-20	1.000	258.5	3.21e-20	1.000
259.0	3.26e-20	1.000	259.5	3.28e-20	1.000	260.0	3.29e-20	1.000	260.5	3.31e-20	1.000	261.0	3.33e-20	1.000
261.5	3.34e-20	1.000	262.0	3.36e-20	1.000	262.5	3.38e-20	1.000	263.0	3.42e-20	1.000	263.5	3.44e-20	1.000
264.0	3.48e-20	1.000	264.5	3.54e-20	1.000	265.0	3.59e-20	1.000	265.5	3.65e-20	1.000	266.0	3.73e-20	1.000
266.5	3.80e-20	1.000	267.0	3.87e-20	1.000	267.5	3.95e-20	1.000	268.0	4.02e-20	1.000	268.5	4.08e-20	1.000
269.0	4.13e-20	1.000	269.5	4.17e-20	1.000	270.0	4.20e-20	1.000	270.5	4.22e-20	1.000	271.0	4.22e-20	1.000
271.5	4.22e-20	1.000	272.0	4.23e-20	1.000	272.5	4.24e-20	1.000	273.0	4.27e-20	1.000	273.5	4.29e-20	1.000
274.0	4.31e-20	1.000	274.5	4.33e-20	1.000	275.0	4.37e-20	1.000	275.5	4.42e-20	1.000	276.0	4.48e-20	1.000
276.5	4.56e-20	1.000	277.0	4.64e-20	1.000	277.5	4.71e-20	1.000	278.0	4.78e-20	1.000	278.5	4.83e-20	1.000
279.0	4.87e-20	1.000	279.5	4.90e-20	1.000	280.0	4.92e-20	1.000	280.5	4.93e-20	1.000	281.0	4.94e-20	1.000
281.5	4.92e-20	1.000	282.0	4.90e-20	1.000	282.5	4.86e-20	1.000	283.0	4.83e-20	1.000	283.5	4.79e-20	1.000
284.0	4.76e-20	1.000	284.5	4.72e-20	1.000	285.0	4.70e-20	1.000	285.5	4.68e-20	1.000	286.0	4.66e-20	1.000
286.5	4.65e-20	1.000	287.0	4.65e-20	1.000	287.5	4.68e-20	1.000	288.0	4.73e-20	1.000	288.5	4.78e-20	1.000
289.0	4.84e-20	1.000	289.5	4.89e-20	1.000	290.0	4.92e-20	1.000	290.5	4.92e-20	1.000	291.0	4.90e-20	1.000
291.5	4.86e-20	1.000	292.0	4.81e-20	1.000	292.5	4.75e-20	1.000	293.0	4.70e-20	1.000	293.5	4.65e-20	1.000
294.0	4.58e-20	1.000	294.5	4.48e-20	1.000	295.0	4.38e-20	1.000	295.5	4.27e-20	1.000	296.0	4.17e-20	1.000
296.5	4.07e-20	1.000	297.0	3.99e-20	1.000	297.5	3.94e-20	1.000	298.0	3.88e-20	1.000	298.5	3.82e-20	1.000
299.0	3.76e-20	1.000	299.5	3.72e-20	1.000	300.0	3.69e-20	1.000	300.5	3.68e-20	1.000	301.0	3.70e-20	1.000
301.5	3.72e-20	1.000	302.0	3.74e-20	1.000	302.5	3.74e-20	1.000	303.0	3.75e-20	1.000	303.5	3.71e-20	1.000
304.0	3.62e-20	1.000	304.5	3.51e-20	1.000	305.0	3.38e-20	1.000	305.5	3.25e-20	1.000	306.0	3.15e-20	1.000
306.5	3.04e-20	1.000	307.0	2.92e-20	1.000	307.5	2.80e-20	1.000	308.0	2.71e-20	1.000	308.5	2.63e-20	1.000
309.0	2.52e-20	1.000	309.5	2.43e-20	1.000	310.0	2.34e-20	1.000	310.5	2.25e-20	1.000	311.0	2.19e-20	1.000
311.5	2.12e-20	1.000	312.0	2.06e-20	1.000	312.5	2.02e-20	1.000	313.0	1.96e-20	1.000	313.5	1.92e-20	1.000
314.0	1.91e-20	1.000	314.5	1.88e-20	1.000	315.0	1.86e-20	1.000	315.5	1.85e-20	1.000	316.0	1.86e-20	1.000
316.5	1.87e-20	1.000	317.0	1.87e-20	1.000	317.5	1.87e-20	1.000	318.0	1.83e-20	1.000	318.5	1.75e-20	1.000
319.0	1.69e-20	1.000	319.5	1.60e-20	1.000	320.0	1.50e-20	1.000	320.5	1.41e-20	1.000	321.0	1.34e-20	1.000
321.5	1.27e-20	1.000	322.0	1.21e-20	1.000	322.5	1.18e-20	1.000	323.0	1.14e-20	1.000	323.5	1.08e-20	1.000
324.0	1.01e-20	1.000	324.5	9.62e-21	1.000	325.0	9.28e-21	1.000	325.5	8.75e-21	1.000	326.0	8.49e-21	1.000
326.5	8.21e-21	1.000	327.0	7.71e-21	1.000	327.5	7.38e-21	1.000	328.0	7.18e-21	1.000	328.5	6.86e-21	1.000
329.0	6.71e-21	1.000	329.5	6.63e-21	1.000	330.0	6.46e-21	1.000	330.5	6.29e-21	1.000	331.0	6.21e-21	1.000
331.5	6.18e-21	1.000	332.0	6.20e-21	1.000	332.5	5.49e-21	1.000	333.0	5.21e-21	1.000	333.5	5.38e-21	1.000
334.0	5.35e-21	1.000	334.5	5.04e-21	1.000	335.0	4.94e-21	1.000	335.5	4.90e-21	1.000	336.0	4.52e-21	1.000
336.5	4.26e-21	1.000	337.0	4.11e-21	1.000	337.5	3.76e-21	1.000	338.0	3.61e-21	1.000	338.5	3.58e-21	1.000
339.0	3.47e-21	1.000	339.5	3.32e-21	1.000	340.0	3.22e-21	1.000	340.5	3.10e-21	1.000	341.0	3.00e-21	1.000
341.5	2.94e-21	1.000	342.0	2.89e-21	1.000	342.5	2.86e-21	1.000	343.0	2.88e-21	1.000	343.5	2.88e-21	1.000
344.0	2.89e-21	1.000	344.5	2.91e-21	1.000	345.0	2.95e-21	1.000	345.5	3.00e-21	1.000	346.0	3.08e-21	1.000
346.5	3.18e-21	1.000	347.0	3.25e-21	1.000	347.5	3.30e-21	1.000	348.0	3.39e-21	1.000	348.5	3.51e-21	1.000
349.0	3.63e-21	1.000	349.5	3.73e-21	1.000	350.0	3.85e-21	1.000	350.5	3.99e-21	1.000	351.0	4.27e-21	1.000
351.5	4.47e-21	1.000	352.0	4.63e-21	1.000	352.5	4.78e-21	1.000	353.0	4.92e-21	1.000	353.5	5.07e-21	1.000
354.0	5.23e-21	1.000	354.5	5.39e-21	1.000	355.0	5.56e-21	1.000	355.5	5.77e-21	1.000	356.0	5.97e-21	1.000
356.5	6.15e-21	1.000	357.0	6.35e-21	1.000	357.5	6.56e-21	1.000	358.0	6.76e-21	1.000	358.5	6.95e-21	1.000
359.0	7.20e-21	1.000	359.5	7.44e-21	1.000	360.0	7.64e-21	1.000	360.5	7.89e-21	1.000	361.0	8.15e-21	1.000
361.5	8.43e-21	1.000	362.0	8.71e-21	1.000	362.5	9.02e-21	1.000	363.0	9.33e-21	1.000	363.5	9.65e-21	1.000
364.0	1.00e-20	1.000	364.5	1.04e-20	1.000	365.0	1.08e-20	1.000	365.5	1.11e-20	1.000	366.0	1.15e-20	1.000

Table A-3 (continued)

WL (nm)	Abs (cm^2)	QY	WL (nm)	Abs (cm^2)	QY	WL (nm)	Abs (cm^2)	QY	WL (nm)	Abs (cm^2)	QY	WL (nm)	Abs (cm^2)	QY
366.5	1.19e-20	1.000	367.0	1.23e-20	1.000	367.5	1.27e-20	1.000	368.0	1.31e-20	1.000	368.5	1.35e-20	1.000
369.0	1.40e-20	1.000	369.5	1.44e-20	1.000	370.0	1.47e-20	1.000	370.5	1.51e-20	1.000	371.0	1.55e-20	1.000
371.5	1.59e-20	1.000	372.0	1.64e-20	1.000	372.5	1.70e-20	1.000	373.0	1.73e-20	1.000	373.5	1.77e-20	1.000
374.0	1.81e-20	1.000	374.5	1.86e-20	1.000	375.0	1.90e-20	1.000	375.5	1.96e-20	1.000	376.0	2.02e-20	1.000
376.5	2.06e-20	1.000	377.0	2.10e-20	1.000	377.5	2.14e-20	1.000	378.0	2.18e-20	1.000	378.5	2.24e-20	1.000
379.0	2.30e-20	1.000	379.5	2.37e-20	1.000	380.0	2.42e-20	1.000	380.5	2.47e-20	1.000	381.0	2.54e-20	1.000
381.5	2.62e-20	1.000	382.0	2.69e-20	1.000	382.5	2.79e-20	1.000	383.0	2.88e-20	1.000	383.5	2.96e-20	1.000
384.0	3.02e-20	1.000	384.5	3.10e-20	1.000	385.0	3.20e-20	1.000	385.5	3.29e-20	1.000	386.0	3.39e-20	1.000
386.5	3.51e-20	1.000	387.0	3.62e-20	1.000	387.5	3.69e-20	1.000	388.0	3.70e-20	1.000	388.5	3.77e-20	1.000
389.0	3.88e-20	1.000	389.5	3.97e-20	1.000	390.0	4.03e-20	1.000	390.5	4.12e-20	1.000	391.0	4.22e-20	1.000
391.5	4.29e-20	1.000	392.0	4.30e-20	1.000	392.5	4.38e-20	1.000	393.0	4.47e-20	1.000	393.5	4.55e-20	1.000
394.0	4.56e-20	1.000	394.5	4.59e-20	1.000	395.0	4.67e-20	1.000	395.5	4.80e-20	1.000	396.0	4.87e-20	1.000
396.5	4.96e-20	1.000	397.0	5.08e-20	1.000	397.5	5.19e-20	1.000	398.0	5.23e-20	1.000	398.5	5.39e-20	1.000
399.0	5.46e-20	1.000	399.5	5.54e-20	1.000	400.0	5.59e-20	1.000	400.5	5.77e-20	1.000	401.0	5.91e-20	1.000
401.5	5.99e-20	1.000	402.0	6.06e-20	1.000	402.5	6.20e-20	1.000	403.0	6.35e-20	1.000	403.5	6.52e-20	1.000
404.0	6.54e-20	1.000	404.5	6.64e-20	1.000	405.0	6.93e-20	1.000	405.5	7.15e-20	1.000	406.0	7.19e-20	1.000
406.5	7.32e-20	1.000	407.0	7.58e-20	1.000	407.5	7.88e-20	1.000	408.0	7.97e-20	1.000	408.5	7.91e-20	1.000
409.0	8.11e-20	1.000	409.5	8.41e-20	1.000	410.0	8.53e-20	1.000	410.5	8.59e-20	1.000	411.0	8.60e-20	1.000
411.5	8.80e-20	1.000	412.0	9.04e-20	1.000	412.5	9.45e-20	1.000	413.0	9.34e-20	1.000	413.5	9.37e-20	1.000
414.0	9.63e-20	1.000	414.5	9.71e-20	1.000	415.0	9.70e-20	1.000	415.5	9.65e-20	1.000	416.0	9.69e-20	1.000
416.5	9.89e-20	1.000	417.0	1.00e-19	1.000	417.5	1.02e-19	1.000	418.0	1.00e-19	1.000	418.5	1.02e-19	1.000
419.0	1.01e-19	1.000	419.5	1.01e-19	1.000	420.0	1.03e-19	1.000	420.5	1.01e-19	1.000	421.0	1.04e-19	1.000
421.5	1.05e-19	1.000	422.0	1.06e-19	1.000	422.5	1.04e-19	1.000	423.0	1.05e-19	1.000	423.5	1.05e-19	1.000
424.0	1.01e-19	1.000	424.5	1.01e-19	1.000	425.0	1.05e-19	1.000	425.5	1.03e-19	1.000	426.0	1.02e-19	1.000
426.5	1.01e-19	1.000	427.0	9.77e-20	1.000	427.5	9.81e-20	1.000	428.0	1.00e-19	1.000	428.5	1.02e-19	1.000
429.0	9.89e-20	1.000	429.5	9.85e-20	1.000	430.0	1.04e-19	1.000	430.5	1.08e-19	1.000	431.0	1.05e-19	1.000
431.5	1.02e-19	1.000	432.0	9.64e-20	1.000	432.5	1.01e-19	1.000	433.0	1.06e-19	1.000	433.5	1.09e-19	1.000
434.0	1.04e-19	1.000	434.5	1.03e-19	1.000	435.0	1.07e-19	1.000	435.5	1.16e-19	1.000	436.0	1.09e-19	1.000
436.5	1.11e-19	1.000	437.0	9.81e-20	1.000	437.5	9.71e-20	1.000	438.0	1.06e-19	1.000	438.5	1.16e-19	1.000
439.0	1.08e-19	1.000	439.5	1.05e-19	1.000	440.0	9.70e-20	1.000	440.5	1.01e-19	1.000	441.0	1.04e-19	1.000
441.5	1.07e-19	1.000	442.0	1.02e-19	1.000	442.5	9.68e-20	1.000	443.0	1.00e-19	1.000	443.5	1.14e-19	1.000
444.0	1.13e-19	1.000	444.5	1.03e-19	1.000	445.0	9.74e-20	1.000	445.5	8.46e-20	1.000	446.0	8.70e-20	1.000
446.5	9.97e-20	1.000	447.0	1.01e-19	1.000	447.5	9.15e-20	1.000	448.0	9.41e-20	1.000	448.5	8.99e-20	1.000
449.0	1.10e-19	1.000	449.5	9.12e-20	1.000	450.0	8.56e-20	1.000	450.5	8.28e-20	1.000	451.0	6.15e-20	1.000
451.5	5.56e-20	1.000	452.0	6.47e-20	1.000	452.5	7.27e-20	1.000	453.0	5.75e-20	1.000	453.5	5.08e-20	1.000
454.0	4.38e-20	1.000	454.5	3.81e-20	1.000	455.0	3.61e-20	1.000	455.5	3.61e-20	1.000	456.0	3.13e-20	1.000
456.5	2.72e-20	1.000	457.0	2.44e-20	1.000	457.5	2.22e-20	1.000	458.0	1.82e-20	1.000	458.5	1.43e-20	1.000
459.0	1.32e-20	1.000	459.5	1.05e-20	1.000	460.0	8.95e-21	1.000	460.5	8.90e-21	1.000	461.0	7.94e-21	1.000
461.5	7.04e-21	1.000	462.0	6.46e-21	1.000	462.5	5.63e-21	1.000	463.0	4.78e-21	1.000	463.5	3.94e-21	1.000
464.0	3.26e-21	1.000	464.5	2.97e-21	1.000	465.0	2.65e-21	1.000	465.5	2.46e-21	1.000	466.0	2.27e-21	1.000
466.5	2.08e-21	1.000	467.0	1.86e-21	1.000	467.5	1.76e-21	1.000	468.0	1.60e-21	1.000	468.5	1.44e-21	1.000
469.0	1.34e-21	1.000	469.5	1.20e-21	1.000	470.0	1.07e-21	1.000	470.5	1.02e-21	1.000	471.0	9.92e-22	1.000
471.5	9.97e-22	1.000	472.0	8.87e-22	1.000	472.5	8.27e-22	1.000	473.0	7.76e-22	1.000	473.5	7.15e-22	1.000
474.0	6.71e-22	1.000	474.5	6.67e-22	1.000	475.0	6.10e-22	1.000	475.5	6.17e-22	1.000	476.0	5.54e-22	1.000
476.5	5.22e-22	1.000	477.0	5.10e-22	1.000	477.5	5.17e-22	1.000	478.0	4.80e-22	1.000	478.5	4.71e-22	1.000
479.0	4.60e-22	1.000	479.5	4.35e-22	1.000	480.0	3.90e-22	1.000	480.5	3.71e-22	1.000	481.0	3.62e-22	1.000
481.5	3.52e-22	1.000	482.0	3.05e-22	1.000	482.5	3.05e-22	1.000	483.0	2.86e-22	1.000	483.5	2.53e-22	1.000
484.0	2.75e-22	1.000	484.5	2.59e-22	1.000	485.0	2.47e-22	1.000	485.5	2.36e-22	1.000	486.0	2.12e-22	1.000
486.5	1.89e-22	1.000	487.0	1.93e-22	1.000	487.5	1.86e-22	1.000	488.0	1.82e-22	1.000	488.5	1.75e-22	1.000
489.0	1.74e-22	1.000	489.5	1.72e-22	1.000	490.0	1.66e-22	1.000	490.5	1.75e-22	1.000	491.0	1.54e-22	1.000
491.5	1.74e-22	1.000	492.0	1.63e-22	1.000	492.5	1.53e-22	1.000	493.0	1.52e-22	1.000	493.5	5.85e-23	1.000
494.0	0.00e+00	1.000												

Table A-4. Chamber wall effect and background characterization parameters used in the environmental chamber model simulations for mechanism evaluation.

Cham.	Set [a]	Value	Discussion
RN-I (ppb)			Ratio of the rate of **wall + hν -> HONO** to the NO_2 photolysis rate.
DTC	18	0.066	Average of value of RS-I that gave best fits to n-butane - NOx chamber experiments carried out in this chamber. The initial HONO was optimized at the same time. If a temperature dependence is shown, it was derived from the temperature dependence of the RN-I values that best fit characterization data in outdoor chamber experiments, with the same activation energy used in all cases. If a temperature dependence is not shown, then the temperature variation for experiments in this set is small compared to the run-to-run variability in the best fit RN-I values. Note that the radical source in Sets 3, 12, 13, and 16 runs was anomalously high. Any dependence of apparent radical source on initial NOx levels in Teflon bag chambers was found to be much less than the run-to-run variability.
HONO-F (unitless)			Ratio of the initial HONO concentration to the measured initial NO2. [The initial NO2 in the experiment is reduced by a factor of 1 - (HONO-F)]. Unless the characterization data indicate otherwise, it is assumed that the initial HONO is introduced with the NO2 injection, so is it is assumed to be proportional to the initial NO2 concentration.
DTC	18	0.8%	Average of value of initial HONO to initial NO2 that gave best fits to n-butane - NOx chamber experiments carried out in this chamber. The RN-I parameter was optimized at the same time.
E-NO2/K1 (ppb)			Ratio of rate of NO2 offgasing from the walls to the NO2 photolysis rate.
All Teflon Bag Chambers		0	The NOx offgasing caused by representing the radical source by HONO offgasing appears to be sufficient for accounting for NOx offgasing effects in most cases. RN-I parameters adjusted to fit experiments sensitive to the radical source are consistent with NOx offgasing rates adjusted to fit pure air or aldehyde - air runs, to within the uncertainty and variability.
k(NO2W) (min^{-1})			Rate of unimolecular loss (or hydrolysis) of NO2 to the walls.
All Teflon Bag Chambers		1.6e-4	Based on dark NO2 decay and HONO formation measured in the ETC by Pitts et al. (1984). Assumed to be the same in all Teflon bag chambers, regardless of volume.
YHONO			Yield of HONO in the unimolecular reaction (hydrolysis) of NO2 on the walls.
All Teflon Bag Chambers		0.2	Based on dark NO2 decay and HONO formation measured in the ETC by Pitts et al. (1984). Assumed to be the same in all Teflon bag chambers, regardless of volume.
k(O3W) (min^{-1})			Unimolecular loss rate of O3 to the walls.
DTC	All	1.5e-4	Based on results of O_3 decay in Teflon bag chambers experiments as discussed by Carter et al (1995c).
k(N26I) (min^{-1})			Rate constant for **N2O5 -> 2 Wall-NOx**. This represents the humidity-independent portion of the wall loss of N_2O_5, or the intercept of plots of rates of N_2O_5 loss against humidity.
All Teflon Bag Chambers		2.8e-3	Based on N_2O_5 decay rate measurements made by Tuazon et al (1983) for the ETC. Assumed to be independent of chamber size (Carter et al, 1995c).

Table A-4 (continued)

Cham. Set [a]	Value	Discussion
k(N26S) (ppm^{-1} min^{-1})		Rate constant for **N2O5 + H2O -> 2 Wall-NOx.** This represents the humidity dependent portion of the wall loss of N_2O_5, or the slope of plots of rates of N_2O_5 loss against humidity.
All Teflon Bag Chambers	1.1e-6	Based on N_2O_5 decay rate measurements made by Tuazon et al (1983) for the ETC. Assumed to be independent of chamber size (Carter et al, 1995d).
k(XSHC) (min^{-1})		Rate constant for **OH -> HO2**. This represents the effects of reaction of OH with reactive VOCs in the background air or offgased from the chamber walls. This parameter does not significantly affect model simulations of experiments other than pure air runs.
All Teflon Bag Chambers	250	Estimated from modeling several pure air in the ITC (Carter et al, 1996c), and also consistent with simulations of pure air runs in the ETC (Carter et al, 1997a).
H2O (ppm)		Default water vapor concentration for runs where no humidity data are available.
DTC all	1.0e+3	Experiments in this chamber were carried out using dried purified air. The limited humidity data for such runs indicate that the humidity was less than 5%, probably no more than ~2.5%, and possibly much less than that. The default value corresponds to ~2.5 - 3% RH for the conditions of most experiments.

[a] Set refers to the characterization set, which refers to the group of experiments assumed to have the same run conditions and represented using the same chamber-dependent parameters. See Carter et al (1995) for more discussion. All experiments in this program were in DTC characterization set 18.